CUFFLESS BLOOD PRESSURE MONITORING TECHNOLOGIES BASED ON PULSE TRANSIT TIME

A Dissertation
Presented to
The Academic Faculty

By

Andrew M. Carek

In Partial Fulfillment
of the Requirements for the Degree
Doctor of Philosophy in the
School of Electrical and Computer Engineering

Georgia Institute of Technology

May 2019

CUFFLESS BLOOD PRESSURE MONITORING TECHNOLOGIES BASED ON PULSE TRANSIT TIME

Approved by:

Dr. Omer T. Inan, Advisor
School of Electrical and Computer Engineering
Georgia Institute of Technology

Dr. Hua Wang
School of Electrical and Computer Engineering
Georgia Institute of Technology

Dr. Robert Butera
School of Electrical and Computer Engineering
Georgia Institute of Technology

Dr. Ayazi Farrokh
School of Electrical and Computer Engineering
Georgia Institute of Technology

Dr. Mozziyar Etemadi
Feinberg School of Medicine
Northwestern University

Date Approved: March 21, 2019

To my parents, Peter and Patricia Carek

ACKNOWLEDGEMENTS

I would like to use this section of my dissertation to express my gratitude to the many people who influenced me during my studies.

First and foremost, I would like to express my appreciation for my advisor, Dr. Omer Inan. After being accepted into the ECE Master's program at Georgia Tech, I moved to Atlanta and quickly started looking for a research advisor. Dr. Inan's research immediately stood out to me, and I reached out to set a meeting with him. My interest only grew after that meeting, and to my excitement, he offered me a position in his lab which I gratefully accepted. I am truly blessed for the turn of events that led me to work with Dr. Inan. His guidance, support, and mentorship have sparked my interest in biomedical research, ultimately influencing my decision to continue my research as a Ph.D. candidate. On countless occasions, I came to his office, sent him an email, and even shot him a text message with a problem. Every time, he would promptly help me through the issue, and I would leave with a new perspective and a direction to take. I will be forever thankful for all the support he has given to me.

I would also like to thank Dr. Robert Butera, Dr. Hua Wang, Dr. Ayazi Farrokh, and Dr. Mozziyar Etemadi for taking the time to serve on my committee and provide insightful comments and suggestion regarding my work.

I am incredibly grateful for my lab mates who have been with me during my studies, including Caitlin Teague, Nick Bolus, Oludotun Ode, Sinan Hersek, Venu Ganti, Daniel Whittingslow, Nil Gurel, Samer Mabrouk, Hewon Jung, Brandi Nevius, Hazar Ashouri, Jordan Conant, Md Mobashir Shandhi, Hyeon Ki Jeong, Abdul Javaid, Ozan Bihcen, and Hakan Toreyin. The entire lab has been friendly, helpful, and supportive and has made research truly enjoyable. I would like to thank Nick Bolus for all his contributions to my work. I valued his input and his extensive knowledge of all things related to mechanic and biomedical engineering. Also, I am thankful for the intense and fun rivalry between the

football teams of our two undergraduate universities. May Clemson and Alabama continue to meet in the National Championship for years to come! I would like to thank Oludotun Ode for his help with the embedded systems and computer science sides of my projects. I am grateful to be able to work with Venu Ganti. He has been pivotal in the development of our prototypes and the drafting of this thesis. Additionally, I would like to thank Jordan Conant and Brandi Nevus for their various and meaningful contributions to our prototypes. It was also a pleasure to work with Hazar Ashouri and Hewon Jung during data collection. I would like to thank Daniel Whittingslow for the many one-on-one physiology lessons. I especially would like to thank Caitlin Teague who I've worked closely with during the entirety of my time at Tech and my internships at Microsoft Research and Northwestern Medicine. She has been there for me many times, always willing to hold a brainstorming session or help me think through a problem, whether it pertained to research or something outside of the lab. She is a true friend, and I appreciate everything she had done for me.

Next, I would like to thank Dr. Etemadi for hiring me as an intern in the Etemadi Research Group at Northwestern Medicine during the summer of 2018. Working with Dr. Etemadi and his group has allowed me to gain clinical experience which will be pivotal as I continue to work in this field. I would like to express my thanks for the members of the group who made the experience so great. I would like to thank Alex Heller for his help in developing our prototypes, both while at Northwestern and Georgia Tech. I would also like to thank Flori Garcia-Vicente for managing our group and making sure we would meet our deadlines.

I was fortunate to be accepted as a Microsoft Research intern for the summer of 2017. There, I had the privilege to be mentored by Christian Holz. Christian has made a major impact during my research, introducing me to both the industry and computer science perspectives. Additionally, he has helped refined and grow my skill set, always pushing and motivating me to think outside-the-box. Even after my internship, Christian continued to be a valuable resource in my research, which I am incredibly thankful for.

I would like to thank all my friends, both the ones I met here in Atlanta and the ones that I retained after my studies at Clemson. I am fortunate to make friends at Tech that were always up for a drink or a random adventure. The ones I made outside of Tech, in particular my ultimate Frisbee team, provided me with an athletic outlet that satisfied my competitive nature. Lastly, I am thankful for the friends that I made at Clemson. I am grateful that I still keep up with some great people, and I always look forward to our weekend retreats.

Lastly, but most importantly, I would like to thank my family. I am fortunate to have a support system in place that cares so much about me and my endeavors. My brothers, Bryan and Stephen, both play a significant role in my life. We share an unbreakable bond, and I know that they will always have my back regardless of the situation. Also, I am lucky to have gained an amazing sister-in-law, Amanda, and two precious nieces, Vivian and Olivia. There is nothing that can bring a smile to my face as quickly as those two. I would like to especially thank my parents. I would not be where I am today without their unconditional love and support. My mom has the kindest of heart and purest of souls and has always been someone I could lean on. My dad has shown me wisdom and strength and has been a great role model for me to look up to. I owe both of them my gratitude for their support, inspiration, encouragement, kindness, love, and for always being there for me at every turn. I strive to be half the person either of them are and work every day to make them proud.

TABLE OF CONTENTS

LIST OF TABLES

LIST OF FIGURES

SUMMARY

Hypertension, or high blood pressure, is a cardiovascular disease that affects nearly a third of the US population and is expected to grow by nearly 10% by 2030. Hypertension is a significant contributing factor in cardiovascular diseases such as stroke or heart attacks, and annual medical costs associated with hypertension amount to a staggering $131 billion. As such, the World Health Organization (WHO) has labeled hypertension as a "global public health issue." Therefore, there is great interest to develop novel methods to properly diagnose and monitor this disease. Unfortunately, the current standard for monitoring blood pressure at home involves the use of a cumbersome and inconvenient oscillometric cuff. This method of monitoring blood pressure provides limited insight into heart health, is inconsistently reproduced, and may not capture the daily variations in blood pressure that occur. Less obtrusive systems requiring minimal user effort would enable seamless cardiovascular monitoring in daily life and relieve much of the burden of regular blood pressure monitoring.

Alternative approaches to the cuff are devices that utilize the concept of pulse transit time (PTT). PTT is the time interval for an arterial pulse wave to travel along the arterial wall from a proximal to a distal site, relative to the heart. PTT has been shown in previous works to have an inverse relationship with blood pressure. However, limited techniques exist to conveniently measure PTT in daily life.

This work focuses on developing two techniques for convenient PTT measurements using a scale-based and wearable approach. First, a scale-based approach utilizes full-body vibrations captured based on ballistocardiogram to provide a measurement of the pulse at a proximal location to the heart. We created a custom-made optical sensor on the foot to measure the distal pulse timing. We further refined the measurement of the distal pulse by developing an array-based optical sensor and signal selection techniques to capture a pulse wave while a subject simply stands quietly to obtain a measurement. Using these proximal

and distal sensors, the scale-based approach captures true aortic pulse transit time and provides a superior estimation compared to conventional timing based methods. Second, a watch-based sensor, SeismoWatch, allows the user to sense pulse timings at the chest and the wrist. To acquire two timing references for PTT, an inertial sensor detects the vibrations of the chest associated with opening of the aorta, based on seismocardiography, and an optical sensor at the wrist measures the distal pulse wave. SeismoWatch is non-invasive and compact, allowing for convenient and portable blood pressure tracking.

The systems presented in this work allow for monitoring PTT in a home setting. This work paves the way for methods that are convenient and robust enough for out-of-clinic blood pressure monitoring, potentially improving the management of cardiovascular diseases.

CHAPTER 1
INTRODUCTION

1.1 Motivation

Blood pressure, usually measured in millimeters of Mercury (mmHg), is the pressure exerted by circulating blood on the walls of blood vessels [1]. It is recorded as two values, systolic blood pressure (SP) and diastolic blood pressure (DP), and written as SP/DP. Systolic blood pressure is the intra-arterial pressure when the heart is at full contraction and diastolic blood pressure is the intra-arterial pressure when the heart is fully relaxed. Mean arterial pressure (MAP) is another value which represents the average intra-arterial blood pressure during a cardiac cycle (contraction and relaxation). Elevated blood pressure, or hypertension, is widely known as the leading risk factor for cardiovascular diseases (CVD), such as heart attack and stroke. The impact of hypertension on morbidity and mortality of CVD has been referenced as early as 1959 in a study of nearly 5 million adults that demonstrated a strong and direct relationship between level of BP and risk of complications and death [2]. More recent studies have demonstrated associations between a higher SP and DP and CVD. A meta-analysis of 61-studies showed that increases in SP and DP exponentially increases the risk of CVD, with each increase in 20 mmHg in SP and 10 mmHg above 140/90 in DP doubling the chance of death from stroke, heart disease, or other vascular disease (Figure 1.1) [3].

The first comprehensive guidelines for hypertension, published in 1977, defined hypertension as BP above 140/90 mmHg [4]. However, new guidelines published by the American College of Cardiology and American Heart Association in 2017 redefined hypertension and divided the disease into two stages [5]. Stage I is defined as a SP of 130–139 mmHg or a DP of 80–89 mmHg, and individuals with stage II hypertension have a SP above 140

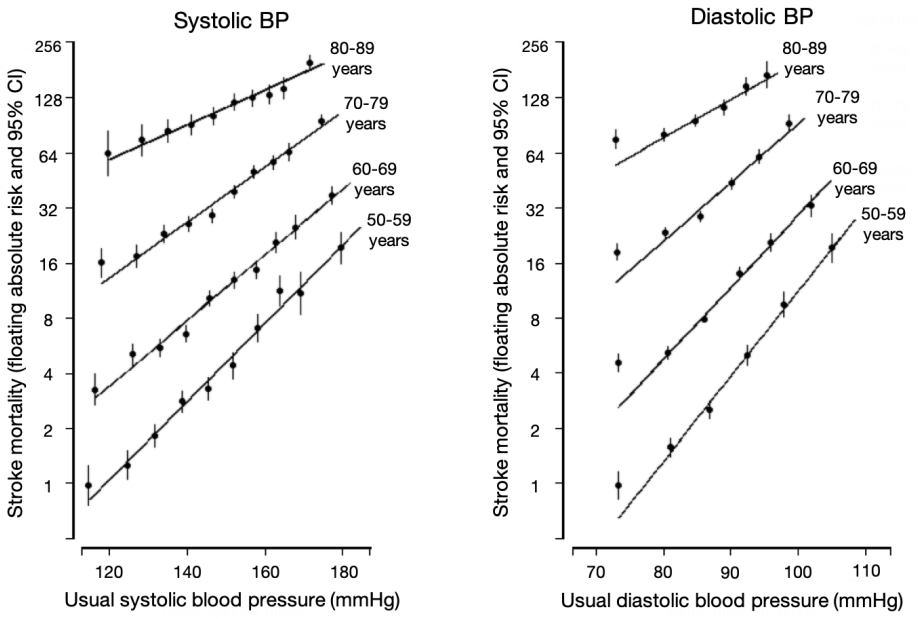

Figure 1.1: Stroke mortality rate associated with systolic and diastolic pressures. Mortality rate increases exponentially with increasing blood pressure. Adapted from [3]

mmHg or a DP above 90 mmHg. The reclassification of hypertension is attributed to the increase in number of studies and meta-analyses reporting higher CVD risk in those patients considered to have stage I hypertension [6]. With these recently established guidelines, it is estimated that 46% of the US population have hypertension, and 32% have stage II hypertension [5]. Aging populations have an increased burden of hypertension as BP progressively increases with age. Depending upon ethnicity, the 40-year risk of adults 45 years of age to develop hypertension is between 84% to 92% [7].

The underlying causes of hypertension are multifactorial, including family history, obesity, and lifestyle [1]. In patients with hypertension, the two factors that dictate BP are altered: the cardiac output (CO) – or amount of blood ejected per heart beat (also known as the stroke volume (SV)) times the heart rate – and the total peripheral vascular resistance (PVR) [8]. The CO depends on the pumping function of the left ventricle, which in turn depends on factors such as preload, afterload, and contractility. The PVR is a function of the smaller smooth-muscle-lined arteries and arterioles (vessels with diameters between

30-300 μm). The diameter of the vessels, which has a profound effect on the PVR, is controlled by the contractile state of the smooth muscle and changes in response to various local and systemic factors.

Patients with chronic or sustained hypertension typically have an increased PVR. The most prominent cause is atherosclerosis, or the thickening of the arterial wall and the narrowing of the vessel. Hypertension damages the inner arterial wall initiating an excessive inflammatory response that thickens the wall and impairs endothelial functions. Atherosclerosis causes an increased strain on the heart and over time damages major organs such as the eyes or kidneys [9]. Ultimately, prolonged hypertension impairs the function of the arteries and leads to end organ damage such as heart failure, kidney failure, vascular aneurysms and retinopathy [10].

In individuals, especially young adults with stage I hypertension (BP = 130-139/80-89 mmHg), the PVR is often normal and the raised hypertension can be attributed to an increase of CO due to an increase in cardiac contractility and heart rate [11]. While the prevalence of CVDs is lower in these patients than patients with established stage II hypertension, patients with stage I hypertension are likely to develop issues involving their vascular system, increasing the PVR and transitioning to stage II hypertension [12]. Based upon an 8-year follow up study, individuals 50 years or younger with stage I hypertension are at a 2.57-fold greater risk of developing stage II hypertension [13]. Thus, monitoring of blood pressure in younger subjects is of particular importance to prevent complications that would arise later in life.

Individuals in low-resource settings are especially vulnerable to issues associated with hypertension and are less likely to partake in interventions to manage hypertension. According to the World Health Organization (WHO), nearly two-thirds of worldwide deaths attributed to hypertension occur in developing countries [14]. The high cost of current technology and the lack of proper training limit the ability to control BP on a wider population basis [15]. Blood pressure monitoring devices need to be inexpensive, easy to use, and

Table 1.1: Comparison of BP Monitoring Techniques

Device	Advantages	Disadvantage
Intra-arterial catheter	• Direct measurement • Continuous	• Invasive • Limited to a clinical setting
CardioMEMs	• Direct measurement • Wirelessly transmits data	• Requires invasive surgery • Expensive
Oscillometric cuff	• Inexpensive • Relatively Portable • Semi-user friendly	• Lengthy measurement procedure • Active sensing
Ultrasound	• Images the artery • Continuous measurement of arterial diameter	• Requires precise placement of probes • Typically expensive
Pulse transit time	• Able to use inexpensive measurement techniques • Near-passive sensing	• Requires two consistent sites • Needs calibration to BP

accurate to be effective and allow for continuous measurements in these areas.

To diagnose and manage hypertension, clinicians rely on both clinic and home readings to properly diagnosis and develop management techniques [16]. While readings are typically limited to semi-regular clinical visits, actual blood pressure is much more dynamic and varies at a much shorter time interval, with the ability to change drastically even within a few heartbeats. In addition to providing a more complete picture of heart health and hemodynamics, providing home measurements has several other benefits. Serial BP monitoring allows for estimates of a drug's efficacy over a short period [17], removes the white-coat effect present only in a clinic [18], and predicts CVD better than clinic based readings [16, 19]. Also, home monitoring systems improve a patient's self-management of hypertension, allowing them to be actively involved in their cardiovascular health [20]. A meta-analysis of 18 controlled trials (1359 patients) showed that those individuals who had home monitoring reduce BP to a greater extent than those who had standard clinic readings [21].

The gold-standard for monitoring BP is through an intra-arterial catheter with an attached strain gauge [22]. This technique measures BP continuously and directly but is invasive and not ideal for longitudinal monitoring. CardioMEMs is a wireless pressure sensor

inserted directly in the pulmonary artery for ubiquitous at-home monitoring. While effective at reducing hospitalization of patients with heart failure, the device is expensive and requires an invasive procedure. Also, CardioMEMs only tracks the pulmonary BP while standardized BP management techniques typically rely on systemic BP measurements [18].

The most common approach to monitoring home BP involves an automatic cuff based on oscillometry. To accurately record BP, a clinician fits a subject with a cuff of the appropriate size and shape. The subject then attaches that cuff to a limb, typically the upper arm, and remains still as the cuff self-inflates and slowly deflates. The device records the arterial pulsations during the deflation to calculate both systolic and diastolic pressures.

For the most part, this form of BP monitoring is relatively inexpensive and accurate [23]; however, limitations do exist. First, an oscillometric device requires a lengthy procedure during which the user must remain in a static position. The cuff inflates to pressure well above occlusion of the artery, potentially troublesome to subjects with high blood pressure or a large arm diameter. Most standards then require multiple readings for an accurate measurement with a suitable amount of time between readings to allow BP in the arm to return to normal levels. To add to the inconvenience, the device itself is cumbersome and bulky, typically limiting the amount of measurements to the home. Omron Healthcare attempted to resolve this issue by incorporating a cuff in a wrist-watch (Heart Guide, Omron Heathcare, Kyoto, Japan). However, wrist-worn devices have significantly lower measurement accuracies compared to upper-arm BP cuffs [24] while monitoring more distal arteries rather than central arteries. Further, both types of oscillometric cuffs rely solely on the pulse amplitude and tend to be inaccurate in subjects with weak pulses from disorders such as atherosclerosis or obesity [25].

Previous works attempt to use ultrasounds to estimate blood pressure. Zakrzewski *et at.* used a combination of an ultrasound and pressure sensors to measure arterial BP [26]. This method applies a well-known method, quantitative ultrasound elastography, to estimate arterial stiffness and thus BP. While the concept is well supported, the ultrasound requires

a skilled operator and may be too expensive for universal use. Wang *et al.* developed a small, flexible, and wearable patch to extract BP changes by measuring the arterial diameter through ultrasound [27]. However, this device does not take into account the effects of smooth muscle contractions and requires precise placement to ensure proper measurement of an artery.

A technique that has recently gained popularity lately uses the concept of pulse transit time (PTT). PTT is the time interval for a pulse wave to travel from two separate locations along the arterial tree and has been shown to be inversely related to BP [28]. This technique requires only the timing of the pulse waves, allowing PTT to be measured using many unobtrusive well-established cardiovascular monitors. As such, systems that monitor PTT have potential to integrate seamlessly in one's life to estimate BP. The work in this thesis focuses on developing techniques for measuring the timing references necessary to calculate BP.

1.2 Major Contributions of this Work

While PTT has been established as a valid technique to estimate BP, it is difficult to conveniently and unobtrusively measure the needed timing references. This work focuses on two techniques to address this need: an at-home bathroom scale and a custom-built watch-based wearable device. Both systems have been extensively evaluated in terms of their robustness and ability to estimate BP.

The weighing scale is able to sense the full-body vibrations associated with the movement of blood, or the ballistocardiogram (BCG). Previous works have used the BCG to estimate the initial ejection of blood but have not used it as a proximal timing reference for PTT calculation. Additionally, there are no known sensors that can conveniently, and without any initial set up, measure a valid distal timing reference during standing. Developing a system in a scale that can gather both timings for PTT calculations would allow for convenient measurement during a basic task: standing. Additionally, there are few devices

that measure true PTT. By incorporating PTT measurement in a wearable, unobtrusive device, BP trend can be estimated throughout the day more easily than with a conventional BP cuff.

The main contributions of this work are given below:

1. Demonstrated that the proximal timing reference for PTT can be measured using the BCG. This work laid the foundation for incorporating a PTT-based monitor in a standard home weighing scale.

2. Utilized an optical sensor, or photoplethysmogram (PPG), to measure the pulse wave at the foot during standing to use as a distal timing reference for PTT calculations. This technique yields more reliable and consistent PPG than commercial optical sensors, particularly in a standing posture.

3. Created an array of PPG sensors to be positioned underneath the sole during standing. The array automatically detects high quality pulse waveforms of larger, more elastic arteries that exhibit a higher correlation to BP. In combination with a scale, PTT is measured without the need for initial setup or attached sensors.

4. Showed that PTT derived from scale-based BCG and foot PPG can estimate BP trends. We compared scaled-based PTT to conventional timing-based methods to estimate BP during varying perturbations. We showed that scale-based PTT is statistically superior at estimating blood pressure, in particular diastolic pressure.

5. Developed a wearable device in a watch form factor to measure PTT while the user performs a simple maneuver. By simultaneously measuring the vibrations of the sternum in response to a heartbeat, or seismocardiography (SCG), and the arrival of the blood at the wrist, PTT can be measured conveniently and unobtrusively during the day.

1.3 Thesis Organization

The rest of the thesis is organized as follows: Chapter 2 discusses the physiological background to PTT and methods for determining the required timing references. Chapter 3 focuses on the scale-based method, and Chapter 4 presents the work related to the watch-based method.

Chapter 3 investigates the potential of a scale-based system to extract PTT. The chapter describes the steps we took to validate the BCG as a proximal timing reference for PTT. Then, we introduce two sensing modalities for the the distal timing reference, one positioned on the dorsum of the foot and one placed below the sole. Finally, both timing references are combined for PTT calculations to estimate BP and then compared to conventional techniques that use timing reference to estimate BP. In Chapter 4, we first introduces SeismoWatch and then describe the study to validate the watch as a method to track BP. Then, an improved version of the device is presented. Finally, Chapter 5 concludes this work and provides directions for future work.

CHAPTER 2

PHYSIOLOGICAL BACKGROUND

2.1 Pulse Transit Time and Its Relationship to BP

As described in Chapter 1, PTT represents the time delay for a pressure wave to travel from a proximal to a distal location along the arterial tree. To estimate BP, PTT leverages the Moens-Korteweg equation that relates the pulse wave velocity (PWV)—defined as PWV = d / PTT, where d is the distance traveled along the arterial tree—to the arterial wall elasticity in terms of Young modulus (E) and compliance (C).

$$PWV = \frac{1}{\sqrt{L * C}} = \sqrt{\frac{Eh}{r\rho}} \tag{2.1}$$

where L is the arterial inertance per unit length, h is the wall thickness, r is the vessel radius, and ρ is the blood density [28]. Furthermore, the compliance of the artery is inversely related to the pressure (P):

$$C(P) = \frac{A_m}{\pi * P_1[1 + (\frac{P-P_0}{P_1}^2)]} \tag{2.2}$$

where A_M, P_0, and P_1 are subject-specific parameters [29]. Popular physical models combine these principles to correlate BP to PWV. By substituting (2.2) into (2.1) and assuming a constant distance, BP follows an inverse relationship with PTT (Figure 2.1).

$$BP = \frac{K_1}{PTT} + K2 \tag{2.3}$$

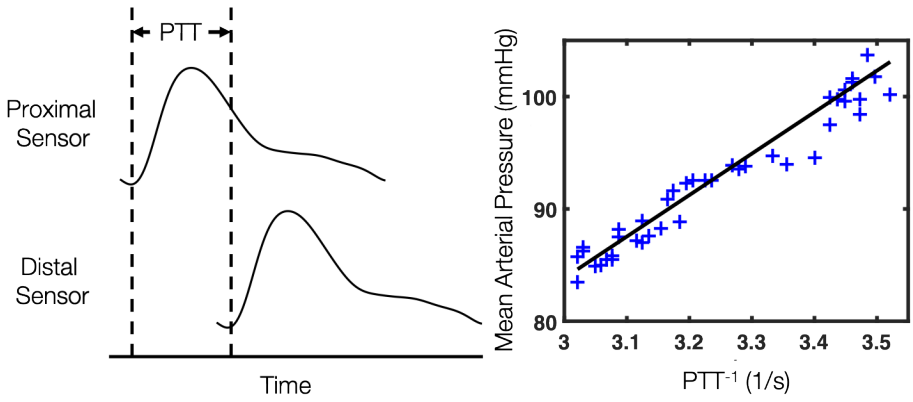

Figure 2.1: PTT is the time delay for a pulse wave to travel from a proximal to distal site in the arterial tree and is inversely related to blood pressure

Replacing the inverse function seen in (2.2) with an exponential arterial model proposed by Hugues, *et al.* [30], a logarithmic model relates PTT and BP,

$$BP = K_3 * \ln(PTT) + K_4 \tag{2.4}$$

where K_1, K_2, K_3, and K_4 are subject-specific parameters that take into account the length of the measurement site, arterial diameter, and the arterial elasticity [28]. Currently, estimation of these parameters is accomplished by taking various PTT and BP readings and using least-squares regression.

Much of the work estimating BP from PTT relies on the correlation between arterial stiffness and BP; however, stiffness can vary due to factors independent of BP. The activation of smooth muscle and the hardening of the arterial wall through aging and diseases both impact the arterial stiffness. The activation of smooth muscle recruits collagen to constrict the artery. Collagen has a higher Young's modulus and can increase the arterial stiffness when the artery is constricted. Arteries that are distally located along the arterial tree, such as arterioles and capillaries, contain larger percentages of collagen and are susceptible to factors that activate smooth muscle such as medication, neurological control systems, or endothelial activation. This effect is mitigated in larger, more central arteries

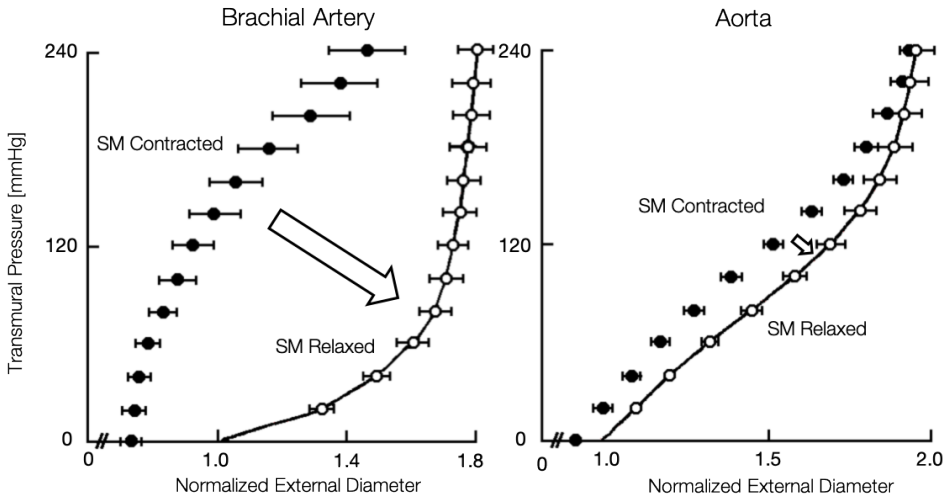

Figure 2.2: Diameter of the brachial artery and aorta in response to external pressure. The state of the smooth muscle (SM) changes the arterial stiffness of the brachial pressure independent to blood pressures. More central arteries, such as the aorta, are less effected by the smooth muscle, allowing for a tighter correlation to blood pressure. Adapted from [32]

that consist of a larger portion of elastin, which reduces the impact of smooth muscle [28]. Thus, the more central arteries, such as the aorta, exhibit a stronger correlation to BP than do peripheral arteries, as is seen in Figure 2.2. PTT-estimated BP techniques will show a higher correlation if the path between the two measurement sites consists of these central arteries.

Aged arteries show a structural difference associated with arteriosclerosis, thickening the wall with exaggerated deposits of collagen, elastin, and proteoglycans. Also, in larger arteries, the continuous strain placed on the wall increases the diameter of the artery over time, changing the relationship between PWV and arterial stiffness shown in (2.1). This structural change affects the speed at which the pulse wave travels through the artery [31]. As such, calibration measurements of PTT estimated BP should be limited to a certain time period, typically a few years in more central arteries and a few months, or even less, in smaller, more peripheral arteries.

2.2 Pulse Arrival Time as a Surrogate for Pulse Transit Time

A common—though physiologically inaccurate—alternative to PTT-estimated BP is through the measurement of the pulse arrival time (PAT), or the timing interval between the R-wave of the electrocardiogram (ECG) and the pulse wave at a distal location. Measuring PAT presents advantages over PTT due to the ease of measurement and high signal quality of the ECG. The ECG can be measured through a wristwatch-based device [33], electronic textiles with integrated electrodes [34], and an armchair with electrodes on the armrests [35].

Researchers pursuing PAT-based approaches argue that the ECG R-wave represents the electrical depolarization of the heart and thus marks the start of the hearts contraction that ejects the blood into the aorta. While the ECG R-wave represents the start of the cardiac cycle, it is not a valid representation of the timing of a forward-going pulse wave. A crucial, often overlooked, time delay occurs between the onset of the R-wave and the ejection of blood, called the pre-ejection period (PEP).

$$PAT = PEP + PTT \tag{2.5}$$

With the electrical depolarization of the left ventricle, an isovolumetric contraction of the heart begins, during which the blood is static and the pressure builds. The ventricular pressure continues to increase until it exceeds the aorta pressure, thus opening the aortic valve and propagating the pulse wave forward [36]. This non-zero, variable time delay changes independent of BP due to shifts in cardiac contractility and after-load [37, 38]. Since PEP represents a non-negligible portion of the PAT (between 12 to 35$\%$ of total PAT as seen in [39]), PAT-based techniques can produce inaccurate estimations of BP. As noted in a previous study [39], subjects injected with a vasoactive drug experienced an increase in peripheral resistance, leading to an increase in BP and a decrease in PTT. PEP, however, increased due to the need to overcome the now-higher aortic pressure in order to open the

aortic valve. By excluding PEP from BP-estimation, the study saw improved correlations to BP.

2.3 Distal and Proximal Timing References for Pulse Transit Time

The main advantage of using PTT over a conventional oscillometric cuff is the ability to use near-passive sensors: in other words, sensors that do not require the user to perform any action, nor be perturbed in any way by the measurement apparatus, for the data to be collected. An oscillometric cuff measures internal pressure by applying an external pressure and measuring the response. To increase the accuracy, the cuff sweeps through a wide range of pressures. While this technique enables one to characterize the arterial pressure during the entire cardiac cycle, providing values of both systolic and diastolic pressure, this intervention makes the cuff bothersome and inconvenient. On the other hand, measuring PTT to estimate BP requires no active systems. With PTT, only the timing reference of the pulse wave is needed and can be obtained by passively sensing a wide range of established cardiovascular signals (Figure 2.3) A downside of PTT is the need for two independent measurements of the pulse wave at different sites, one proximal and one distal in relation to the heart. While clinical measurements typically place either localized pressure sensors—also known as tonometers—or ultrasound probes at the carotid and femoral arteries [40, 41, 42], these are infeasible for at home use due to the high cost and the inconvenience of measurement. To be suitable for home use, techniques to measure PTT must be easily implemented, convenient, and have the ability to measure the two timing references from the same system. This work explores various monitoring techniques and combinations for feasible home PTT monitors.

2.3.1 Photoplethysmogram

A noninvasive measuring technique used extensively in clinics as the basis for pulse oximetry is photoplethysmography (PPG). PPG requires an optical sensing approach composed

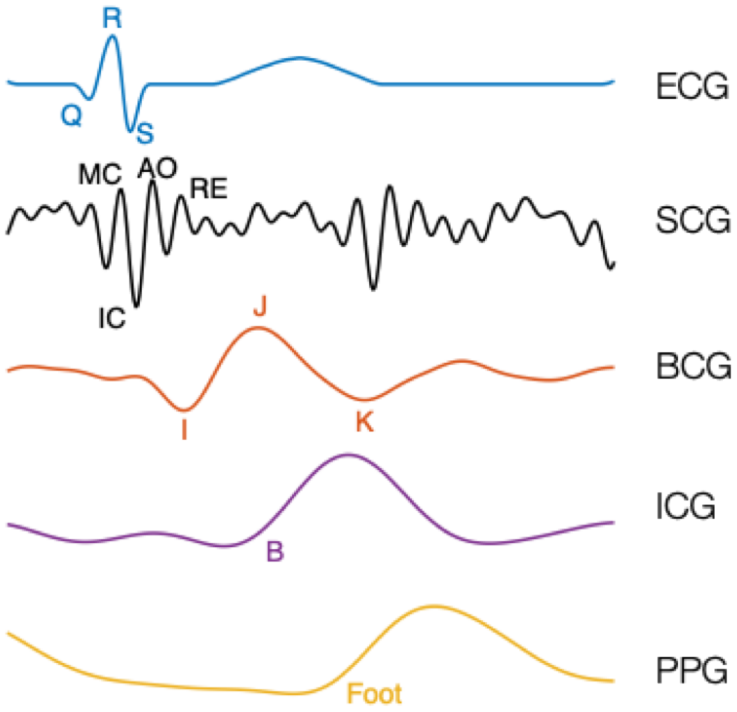

Figure 2.3: Example waveform with labeled physiological markers for electrocardiogram (ECG), seismocardiogram (SCG), ballistocardiogram (BCG), impedance cardiogram (ICG) and photoplethysmogram (PPG)

of a light source and a photosensor. As the volume of arterial blood fluctuates during each cardiac cycle, the artery absorbs varying amounts of light, fluctuating the amount of light transmitted or reflected—depending on the mode—into the photosensor, creating the PPG waveform. The resulting waveform from the photosensor represents the change in arterial blood volume [47]. The BP and PPG waveform look similar and attempts have been made to predict BP using this signal alone, leveraging machine learning techniques to extract features from the PPG [48, 49]. However, this approach may not be valid as PPG depends on intravascular pressure, the distensibility of the vascular wall, and oxygen content of hemoglobin [50].

The PPG waveform depends greatly on the mode of operation and wavelength of the light. PPG can operate either in a transmissive or reflective mode, with both offering certain advantages [43]. Transmissive-mode allows for a majority of the light energy to propagate

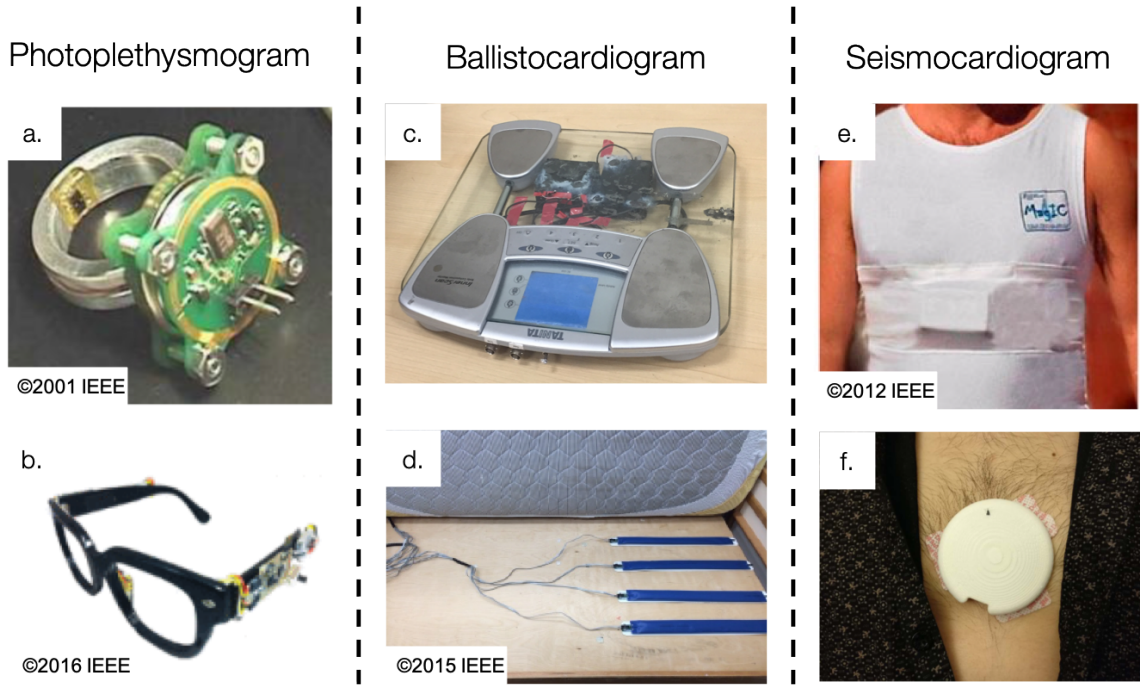

Figure 2.4: Various form factors of at-home cardiovascular sensors. (a) A ring PPG sensor [43]. (b) Glasses with integrated PPG sensors on the frame [44]. (c) A weighing scale with BCG measuring circuit. (d) A bed with force sensors under the mattress, [45] (e) The MagIC vest [46]. (f) A wearable patch that measures the ECG and SCG signals.

through the tissue, increasing the signal quality, but the mechanism behind this mode limits sensing to the toes, fingers, or earlobe. Signal quality of reflective-mode PPGs varies based on sensor location and is typically more susceptible to motion artifacts but can be used in more locations than transmissive mode. In reflective mode, the wavelength of the light varies the penetration depth of the measurement, with longer wavelengths having higher penetration depths [51]. Wearable heart rate monitors typically use green over red or infrared (IR) because of the greater signal amplitude and lower motion artifacts needed for robust peak detection [52, 53]. However, green wavelength mostly senses the cutaneous microvasculature. Longer wavelengths such as red and IR are able to penetrate deeper into the tissue where larger arteries reside and should be used to record valid pulse wave timings for PTT calculations.

2.3.2 Ballistocardiogram

Another waveform of interest in this work is ballistocardiogram (BCG), or the measurement of the reaction force caused by the movement of blood. As the blood ejects out of the left ventricle and travels through the aortic arch, a reactionary force couples into the musculoskeletal system. While this signal was first discovered in the 1800s [54], BCG is not used in the clinic, presumably due to its susceptibility to motion artifacts and the emergence of the ECG to reliably monitor heart rate. Inherently, BCG is a three-dimensional force, though most of the work focuses on the head-to-foot vector [55]. The traditional head-to-foot waveform comprises of three main complexes: the I, J, and K waves as seen in Figure 2.3. Each wave represents the acceleration of blood in various parts of the arterial tree [56]. In particular, the I wave corresponds to the initial movement of blood from the left ventricle during the cardiac ejection. As such, previous work has shown a correlation between the timing of the I wave and the PEP [57].

Measuring the BCG is of benefit because it enables a proximal signal to be captured using a distal sensor. The mechanism produces a full body acceleration and has potential to be measured anywhere on the body as long as the subject remains still. BCG has been recently monitored using various inexpensive and convenient systems such as a weighing scale [57], chair [58], and bed [59]. Furthermore, placing accelerometers on the body, including the wrist, demonstrates the potential of using wearable devices to capture the BCG [60].

2.3.3 Seismocardiogram

In contrast to the BCG, which measures whole-body movements in response to the heartbeat, the seismocardiogram (SCG) measures the local vibrations of the chest wall in response to heart and blood movement. This signal should not be confused with the phonocardiogram (PCG) which is commonly measured in a clinic with a stethoscope. While the PCG contains the higher frequency vibrations (30-150Hz) caused by the closing of the

heart valves [61], the SCG is the low-frequency motion of the heart and blood (less than 25Hz) [62]. The physiological markers that the SCG is believed to represent include the mitral valve closure (MC), isovolumetric contraction (IC), aortic valve opening (AO), rapid ejection (RE), aortic valve closure (AC), mitral valve opening (MO), and rapid filling (RF) [57]. However, subject variability and sensor misplacement can make it difficult to discern the different peaks. For example, the AO point may be mistaken for neighboring peaks or the MC point may be smoothed off and difficult to locate [63].

Typical measurements of the SCG use an accelerometer in contact with the sternum. Chuo *et al.* developed a flexible platform consisting of a MEMS accelerometer with an adhesive backing for SCG monitoring during the day [64]. MagIC is a textile-based wearable device, similar to a shirt, capable of measuring the SCG [46]. Regardless of the form-factor, sensors must be placed consistently on the middle or lower potion of the sternum, where the AO point corresponds closely in time with the cardiac ejection. Misplacement of the sensor distorts the signal and shifts the timing of the various markers of the SCG [65].

2.3.4 Bioimpedance

Other measurements commonly used in PTT calculations include impedance cardiogram (ICG) and impedance plethysmogram (IPG) signals. ICG measures the changing impedance of the blood in the thorax and is typically used to estimate cardiac output [66]. The initiation of the rapid upslope of the ICG towards the maximum—called the b-point—represents the start of the cardiac ejection [67]. Typical measurements of ICG use wet electrodes in two separate locations, one below and one above the heart, making it inconvenient for home use. Previous works measure convenient ICG through textile integration, but is also inconvenient as it requires a custom-made shirt to be continuously worn [68]. IPG uses the same principles as ICG but measures the fluctuations of impedance associated with the pulsation of arterial vessels in a given area of interest [69]. Measurements can be taken at distal locations and have been incorporated in both a scale [70] and a wrist device [71].

However, distal timing can be difficult to extract in certain subjects, as IPG signal quality tends to be low in obese individuals, critically ill patients, patients with heart failure, and other patients with weaker circulation [67, 72].

2.3.5 Techniques Used in this Thesis

After comparing these monitors, we utilized the BCG, SCG, and PPG to develop two form factors for PTT monitoring: a standard weighing scale and a wrist watch. The scale measures both the BCG and PPG at the foot for the proximal and distal timing reference for PTT, respectively. We extensively evaluated this system through human subject testing and validated both the BCG and PPG as effective timing references. While this system provided aortic PTT for BP estimation, the scale is restricted to at-home monitoring. To address this limitation, we developed a watch-based system to allow for mobile PTT measurements. By performing a simple maneuver to capture the SCG at the sternum, the watch measures the proximal timing through the SCG and the distal timing with a PPG sensor on the wrist. This watch-based system significantly outperformed conventional timing-based wearable blood pressure estimations.

CHAPTER 3
WEIGHING SCALE-BASED METHOD FOR UBIQUITOUS PULSE TRANSIT TIME MEASUREMENT

3.1 Introduction

This work in this chapter established weighing scale-based PTT as a potential means for cuffless BP monitoring. Standard weighing scales are widely used to monitor cardiac health, improve weight loss [73] and indicate signs of heart failure [74]. Incorporating a BP monitor in a scale would further improve hemodynamic assessment in a single device.

First, we showed that the BCG could be used as a proximal timing reference. Then, we developed a method of extracting a distal timing reference on the dorsum of the foot that is superior to using commercially available PPG sensors. We further improved distal timing sensing by developing an array of PPG sensors to extract a valid timing reference at the sole automatically. Finally, we combined the BCG and dorsum pulse signal and demonstrated that weighing scale-based PTT is a superior marker of BP than conventional PAT. To the best of our knowledge, this work demonstrates the first application of a weighing scale-based system for BP estimations.

3.2 Ballistocardiogram as a Proximal Timing Reference for PTT

As previously mentioned, BCG is a measurement of the reaction force of the body to the cardiac ejection of blood into the aorta. Since the timing interval between ECG and BCG has been shown to be strongly correlated to the PEP, it may represent a true proximal timing reference for PTT. BCG can provide information of a proximal site at a distal location and be incorporated in common objects such as a weighing scale, chair, or bed. While BCG signals have been shown to be capable of tracking changes in cardiac output [75] and

myocardial contractility [76], the signal has not yet been rigorously explored for measuring PTT and, accordingly, estimating BP.

As such, we tested the hypothesis that the BCG waveform can be a viable proximal timing reference for measuring PTT. We recruited subjects and measured PTT through a modified bathroom scale and a noninvasive finger BP monitor. For comparison, we measured the PAT using the ECG as a proximal timing reference. We determined the correlation between PTT and BP based on various distal timing references and showed an improvement in BCG-based PTT in estimating BP compared to conventional BP measurement devices. The work in this section was a collaborative effort with Dr. Chang-Sei Kim and Dr. Jin-Oh Hahn of the University of Maryland and Dr. Ramakrishna Mukkamala of Michigan State University. The main contributions from the author of this thesis to the work were focused on the development and validation of the hardware, the planning and execution of the human subjects studies, and assistance in the signal processing steps.

3.2.1 Human Subject Studies

The study was conducted under a protocol reviewed and approved by the Georgia Institute of Technology Institutional Review Board. All subjects provided written consent before experimentation. We enrolled fifteen young and healthy volunteers without any history of hypertension or cardiovascular diseases (age: 24 $\pm$ 3 years; gender: 10 males and 5 females; weight 70 $\pm$ 12 kg; height: 175 $\pm$ 10 cm) to participate in the study.

We adapted a customized bathroom scale (BC534, Tanita, Tokyo, Japan) for BCG measurement. The scale is composed of four strain gauges to measure the vertical force placed on the scale. To capture the head-to-foot BCG, we configured the gauges to form a Wheatstone bridge. The output of the bridge connects to a differential amplifier followed by a fourth-order Butterworth band-pass filter in a Sallen-Key topology (G = 81 dB, f_c = 0.1 – 25 Hz). The high-pass filter allows for the removal of the DC component (the weight) and the subsequent amplification of the BCG signal. During the study, each subject wore

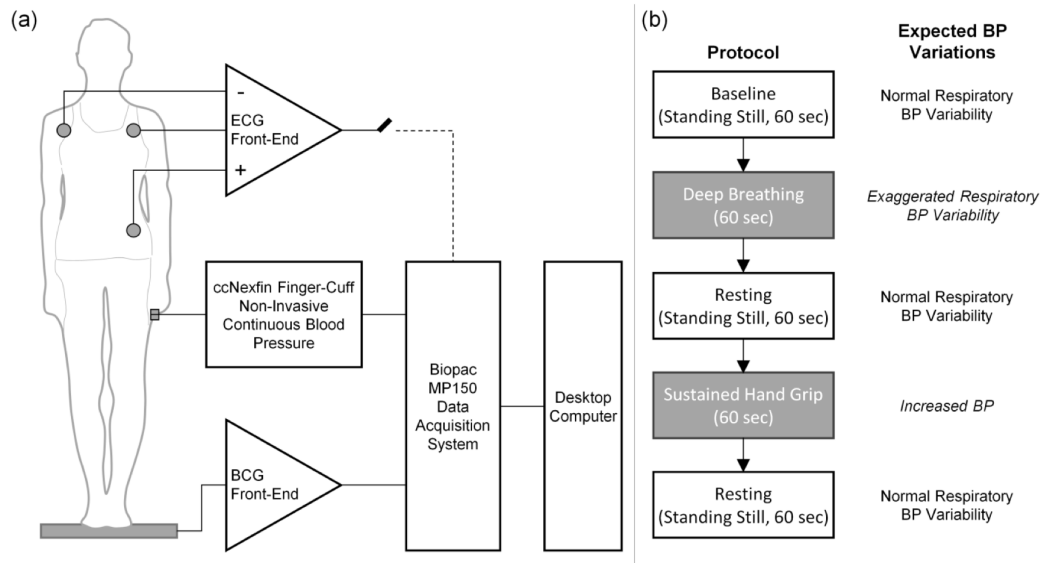

Figure 3.1: (a) Schematic setup for the ECG, BCG, and finger-cuff BP waveform. (b) Overview of the protocol.

standard gel electrodes for Lead II ECG acquisition using a wireless amplifier (BN-EL50, Biopac Systems, Goleta, CA). For BP acquisition, a finger-cuff continuous noninvasive BP sensor based on the volume-clamp method (ccNexfin, Edwards Lifesciences, Irvine, CA) wrapped around the middle finger of the subject. The sensors interfaced to a computer via a data acquisition unit (MP150, Biopac Systems) that collected data at a 1-kHz sample rate and stored for post-processing (see Figure 3.1a).

After placing all the sensors on the subject and instructing the subject stand on the scale, we began the protocol seen in Figure 3.1b. First, a baseline recording was taken while the subject stood still for 60-seconds. We then instructed the subject to breathe deeply and slowly. Finally, we asked the subject to perform a sustained hand grip challenge in which the subject performed an isometric contraction against a fixed resistance using the hand without the attached BP monitor. We chose these perturbations since they are common day-to-day activities, easy to perform, and limited motion artifact coupled into the BCG scale. In between the two perturbations, the subject stood at rest for 60 seconds.

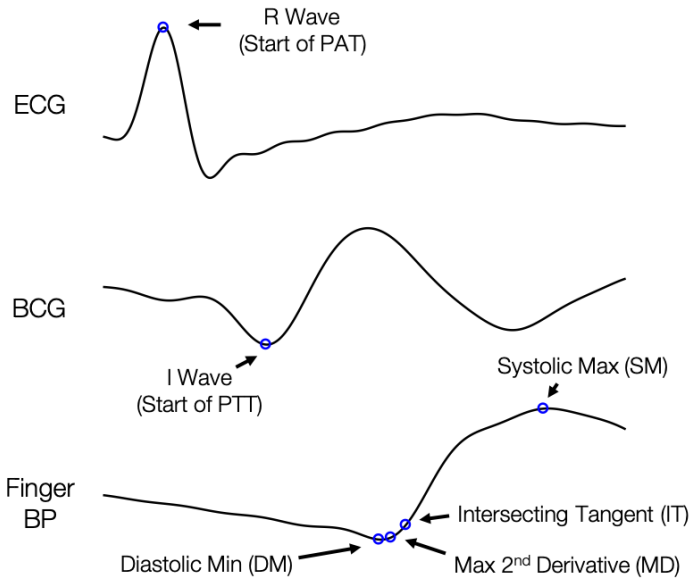

Figure 3.2: Measurement of PTT and PAT using four distal timing references. The BCG I wave and ECG R wave were used as proximal timing references for PTT and PAT, respectively. The four distal timing references included the systolic maximum, intersecting tangent, max second derivative, and diastolic minimum.

3.2.2 Signal Processing

From the data collected, we measured PTT and PAT using the following methods. First, to find the R-wave, a peak detection algorithm determined the local maximum within each ECG beat. Using the R-wave, we partitioned the BP and BCG into individual beats. An exponential-weighted moving-average filtering technique smoothed the BCG beats[77]. We deemed the local minimum that occurred immediately before the J wave (detected by finding the maximum between the R-wave and the maximum of the BP waveform) as the I wave. We extracted four different features from the PPG waveform to use as the distal timing reference: the intersecting tangent, maximum second derivative, diastolic minimum, and systolic maximum. The intersecting tangent is the location of the intersection of a horizontal projection passing through the minimum and a line tangent to the maximum local gradient [78]. Finally, PTT for each beat was the time interval between the BCG I wave

Table 3.1: Correlation of PTT and PAT with BP (Mean $\pm$ SD)

		DP	MAP	SP
Intersecting Tangent	PTT	0.62 ± 0.16	0.65 ± 0.14	0.66 ± 0.14
	PAT	0.51 ± 0.19	0.59 ± 0.17	0.66 ± 0.16
Max 2nd Deriv	PTT	0.54 ± 0.16	0.58 ± 0.14	0.61 ± 0.13
	PAT	0.49 ± 0.18	0.56 ± 0.16	0.63 ± 0.15
Diastolic Min	PTT	0.58 ± 0.20	0.60 ± 0.18	0.61 ± 0.18
	PAT	0.52 ± 0.25	0.60 ± 0.23	0.66 ± 0.22
Systolic Max	PTT	0.66 ± 0.15	0.67 ± 0.14	0.70 ± 0.12
	PAT	0.60 ± 0.14	0.66 ± 0.13	0.72 ± 0.11
All	PTT	0.60 ± 0.17	0.63 ± 0.15	0.65 ± 0.15
	PAT	0.53 ± 0.20	0.60 ± 0.17	0.67 ± 0.17

and the distal timing reference while the PAT was the interval between the ECG R wave and the distal timing reference. In total, there were four different values for PAT and PTT for each beat as seen in Figure 3.2.

Before assessing correlation with BP, a Butterworth low-pass filter (f_c = 0.1 Hz) smoothed the PTT and PAT sequence and prevented the degradation of the PTT to BP correlation due to inadequately measured PTT samples caused by motion artifacts coupled into the BCG. We used the logarithmic model of PTT to formulate a calibration curve for PTT to BP by using the least-squares method. Using the curve, we estimated BP for both PAT and PTT. For each subject, we calculated the correlation between true versus estimated diastolic pressure (DP), mean arterial pressure (MAP), and systolic pressure (SP). Four distal timing references with three different pressure levels resulted in twelve separate r values for each subject.

3.2.3 Use of BCG as a Proximal Timing Reference

The average BP differed greatly across subjects, varying up to 43% $\pm$ 16.5%, 43.8% $\pm$ 14.3%, and 46.2% $\pm$ 15.5% for DP, MAP, and SP, respectively. Table 3.1 summarizes the r values for BP versus PTT as well as compares the r values for the relationship between

BP versus PTT and PAT.

The central hypothesis of this study was that BCG could be a viable proximal timing reference for PTT measurement. To the best of our knowledge, this study is the first intensive investigation to examine the efficacy of BCG, compared with ECG, as a proximal timing reference for measuring PTT and estimating BP.

PTT based on BCG as a proximal timing reference correlated with BP reasonably well and the corresponding confidence intervals were also narrow. The r values between DP and PTT were much higher—ranging between 0.54 and 0.66—than previous studies with ECG and noninvasive wrist/finger BP as proximal and distal arterial waveforms (0.30 and 0.26 - 0.54 in two studies respectively [79, 80]. The r values between SP and PTT which were between 0.61 and 0.70 were comparable to those studies.

Comparing the r values for PTT associated with each distal timing reference, the systolic maximum method resulted in the highest r values consistently for DP, MAP, and SP, followed by the intersecting tangent, diastolic minimum, and maximum second derivative methods. The differences between the systolic maximum and the intersecting tangent methods were not significant while the difference between the systolic maximum and maximum second derivative methods were significant ($p < 0.05$). In general, the systolic maximum is not considered as an ideal timing reference due the potential of corruption caused by the wave reflection phenomena. However, previous studies found a strong correlation between SP and PTT derived from the systolic maximum [79, 81]. A possible explanation is the use of healthy young adults. The efficacy of the systolic maximum method in these subjects may in part be attributed to relatively small wave reflection in these subjects, negligibly corrupting the systolic upstroke waveform. Regardless, the statistical insignificance between the systolic maximum and intersecting tangent supports the later as an adequate distal timing reference for PTT.

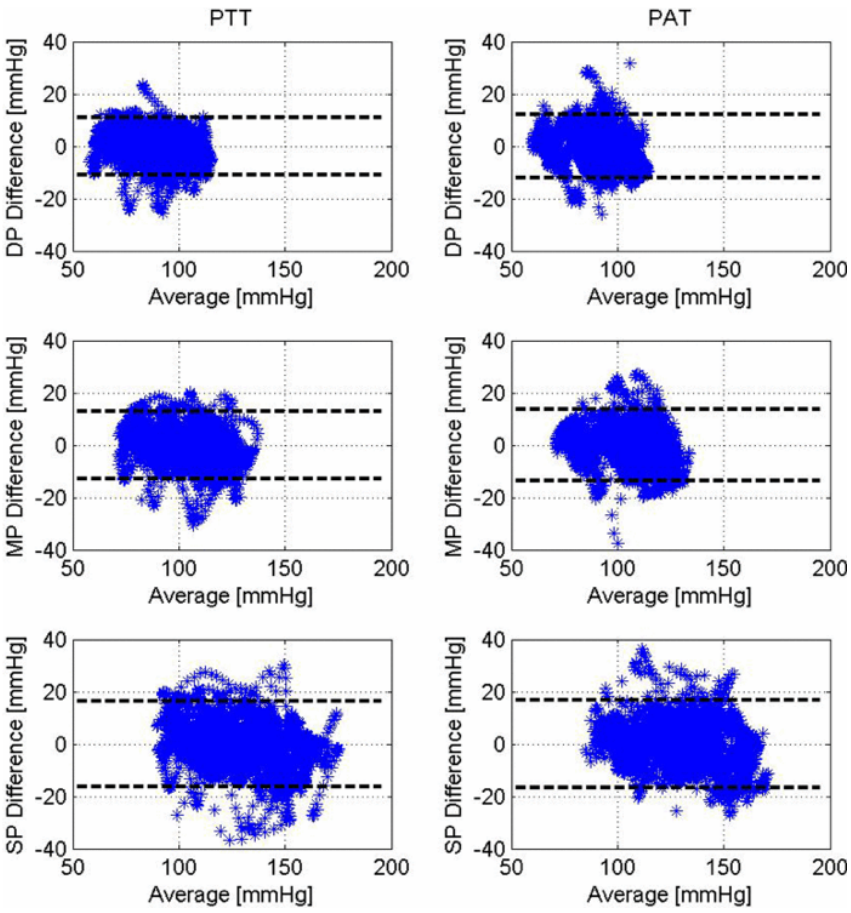

Figure 3.3: Bland-Altman statistics associated with true BP versus PTT- and PAT-estimated BP (all subjects).

3.2.4 Comparison between BCG and ECG as a Proximal Timing Reference

When comparing PTT and PAT, the most notable finding was the improved correlation with DP through PTT rather than PAT regardless of the distal timing reference. By using PTT over PAT, the mean r value increased by 22%, 10%, 12%, and 10% for the intersecting tangent, maximum second derivative, diastolic minimum, and systolic maximum methods, respectively. Additionally, the 95% confidence interval associated with PTT was 8.8%, 5.5%, and 1.0% narrower for DP, MAP, and SP, respectively, when using the intersecting tangent method for the distal timing reference as seen in Figure 3.3. When we combined all methods to find the distal timing together, the difference between PTT and PAT was signif-

icant ($p < 0.05$). The BCG is known to be easily corrupted with motion artifact, temporally skewing the location of the I wave. Nonetheless, PTT with BCG exhibited a stronger correlation to DP and MAP than PAT, supporting the central hypothesis of this work. In contrast, PAT outperformed PTT in estimating SP, though not statistically significant.

3.2.5 Conclusion

We demonstrated that BCG may be used as a proximal timing reference in measuring PTT, and BCG-based PTT may be superior to PAT in estimating DP. To the best of our knowledge, this is the first intensive study to examine the validity of BCG in measuring PTT, and ultimately, in estimating BP. While the results from our study show promise, there are still open challenges before the efficacy of BCG in measuring PTT can be established. Follow-up studies are required to further elucidate the strengths and weaknesses of BCG as a proximal timing reference in measuring PTT and estimating BP.

3.3 Robust Sensing of Distal Pulse Waveform on a Weighing Scale

With the BCG as the proximal timing reference, a robust distal timing reference measurable on the scale is needed for PTT calculations. Ideally, the distal timing reference would allow for aortic PTT over brachial PTT due to the improved correlations to BP. While brachial PTT is simple to obtain using a sensor measuring the finger pulse wave for the distal timing reference, there are limited techniques to measure aortic PTT with measurements limited to a clinical setting only. The most common approach for its measurement involves the use of an arterial tonometer, which is placed by a medical professional first at the carotid artery, then the femoral artery of the patient. This technique, referred to as carotid-femoral pulse wave velocity, is the "gold" standard measurement of aortic stiffness [82] but requires a medical professional and expensive equipment. A commonly used and cheaper measurement for distal pulse timing detection is the PPG. By placing this sensor at the foot, one could detect the pulse wave as it travels through the aorta. However, a previous study by

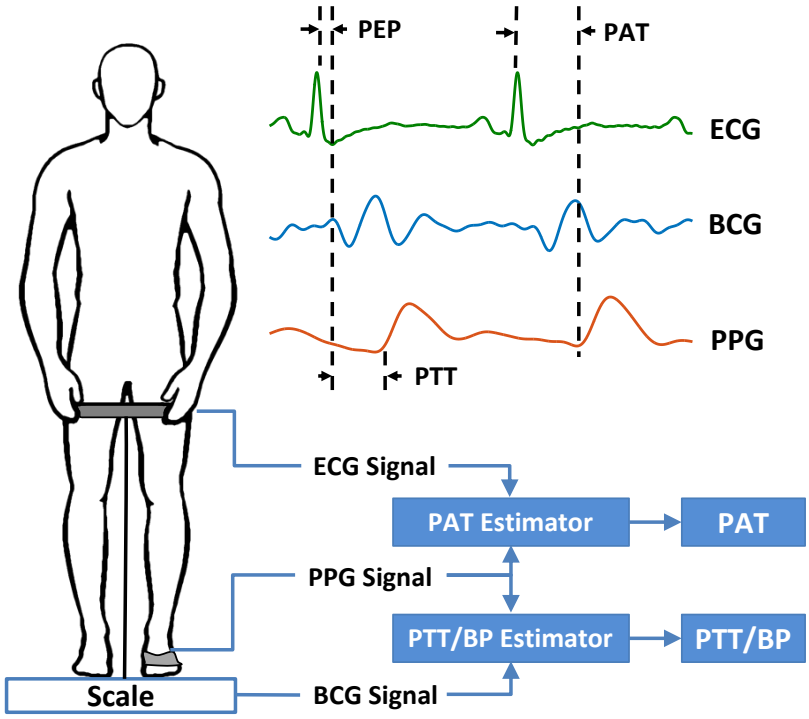

Figure 3.4: Block diagram of the the proposed method of PTT/BP extraction. A representative pair of electrocardiogram (ECG), ballistocardiogram (BCG) and photoplethysmogram (PPG) heartbeats from one subject are shown along with the time points for deriving pre-ejection period (PEP), pulse transit time (PTT), and pulse arrival time (PAT).

Paliakaite *et al.* utilized toe PPG discovered that such an approach does not yield a reliable PPG signal for PTT calculations in standing subjects [83]. They noted that the quality of the measured signal was highly dependent on the subject's motion. These researchers used median filtering over many cardiac cycles to smooth out the motion artifacts corrupting PPG feature detection, suggesting a need for an improved sensor design to facilitate recordings over a shorter time period [83].

To advance the quality of PPG sensing from the foot towards a scale-based PTT measurement system, we developed a custom reflective PPG array to measure the distal pulse wave on the dorsum of the foot (D-PPG), as shown in Figure 3.5a. The object of this study was to assess the reliability and validity by rigorously testing the device and comparing it to multiple existing commercial PPG sensors. We aimed to demonstrate that this method

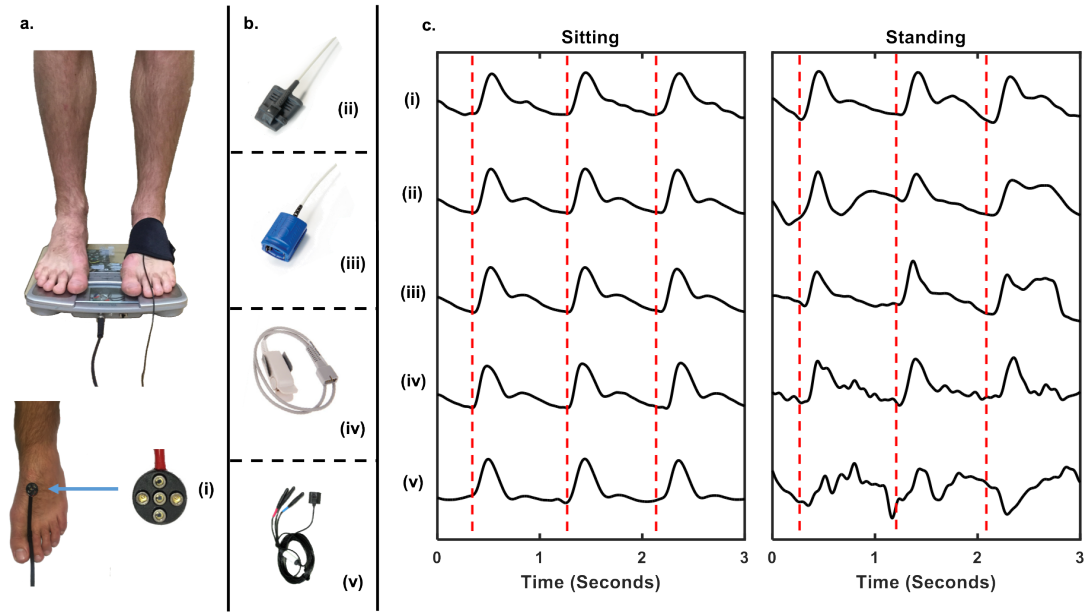

Figure 3.5: (a) Front view of the D-PPG sensor (sensor number (i)) placed under the foot strap, (b) commercially available PPG used, with (ii-iv) being transmissive sensors, and (v) a reflective sensor, and (c) typical normalized signals from each of the sensors while a subject is sitting (left panel) and standing (right panel).

of extracting the pulse can serve as an accurate and repeatable tool for a distal timing reference. With this validation, a convenient weighing-scale based system for measurement of aortic PTT could thus comprise of the proximal timing measurement using BCG and the distal timing using the D-PPG.

3.3.1 Hardware Design

At a high level, the hardware included a D-PPG sensor to obtain a pulse measurement on the foot. The toe sensors comprised of four commercially available LED and photodiode combinations. These sensors connected either to a custom designed analog front-end or a commercially available transducer amplifier.

To obtain a timing reference for cardiac cycles, a wireless amplifier (BN-EL50, Biopac Systems) and standard gel electrodes captured Lead II ECG. The D-PPG sensors have a combination of red light emitting diodes (LEDs) and photodiodes (L1815-02 and S2386-

18k, respectively, Hamamatsu Photonics, Shizuoka, Japan). Red LEDs matched the color emitted from most of the commercial PPG sensors, and thereby ensured a fair comparison. Each of the anodes of the photodiodes on the D-PPG sensors directly connected to a single node. This sums the output current together and assisted in removing zero-mean uncorrelated noise.

We used the 8000 AA and 8000 LS (Nonin) and the DS100A-1 (Medtronic, Minneapolis, MN) as the commercially available transmissive PPG sensors. Additionally, we included the TSD200C (Biopac Systems) in the test to represent a commercial reflective PPG designed to attach to the distal phalanx of the finger or toe. The commercial sensors can be seen in Figure 3.7.

Excluding the PPG100C, all anodes of the photodiodes of the PPGs connected to a transimpedance amplifier configured to act as a high-pass filter (f_c = 1 Hz, G = 100 dB) followed by a gain stage (G = 10 dB). The relatively high cutoff affected the amplitude and phase information for the PPG signal; however, the motion artifacts that could have distorted the signal will be minimized. A following second-order Butterworth Sallen-Key filter (f_c = 20 Hz, G = 20dB) further removed out-of-band noise, including 60 Hz power line interference and 120 Hz light flickers. Each commercial sensor received a comparable amount of power for the LEDs ($\sim$10 mW) with the D-PPG receiving equal to or lower amounts of power.

The TSD200C interfaced to the PPG100C amplifier (G = 100 dB, BW = 0.01 Hz - 10 Hz). The TSD200C consisted of a matched photodiode and an infrared LED. Though the PPG sensors of various waveforms may have produced different SNR values, we deemed an IR LED acceptable due to the study focusing on the relative changes in PAT detection rate for standing versus sitting.

The contact pressure has been shown to affect the SNR value of PPG signal [84]. To provide an estimate of the pressure, a force sensor measured the orthogonal force vector of the D-PPG sensor applied to the surface of the skin (FS20-0000-1500-G, Measurement

Specialities, Hampton, Virginia). The sensor's output has a 1V to 3V range corresponding to a linear force range between 0 and 7.36N. The output of the force sensor connected to a third-order Butterworth Sallen-Key low-pass filter (f_c = 10 Hz) with unity gain.

The MP150 DAQ and its corresponding software, Acquknowledge (Biopac Systems), sampled the sensors at 2 kHz and stored on a desktop computer for further signal processing.

3.3.2 Human Subject Studies

The Georgia Institute of Technology Institutional Review Board approved this study. We enrolled twelve young and healthy subjects (age: 25 $\pm$ 4 years; gender: seven males and five females; weight: 70 $\pm$ 10 kg; height 175 $\pm$ 15 cm). Due to the levels of melanin influencing the PPG signal [85], we recruited subjects of varying race and ethnicity (seven Caucasian and five non-Caucasian).

We tested various aspects of the D-PPG sensors to optimize the design: (1) location on the dorsal surface, (2) applied pressure, and (3) LED and photodiode configuration. The final test (4) compared the D-PPG sensor to the commercially-available sensors previously mentioned during both seated and standing positions. For each transition between position, we asked the subject to remain still until the cardiovascular system reached homeostasis. We then conducted the following tests:

1) Effects of Sensor Location

We partitioned the dorsum of the foot into seven regions, as seen in Figure 3.7c, to map out the space of convenient surfaces that could be instrumented and placed the sensor sequentially at each of the seven positions. To ensure constant contact pressure at each site, we placed the force sensor on top of the D-PPG. A strap wrapped around the foot held both sensors in place and minimized the amount of light that could reach the photodiodes. We tightened the strap to a certain pressure using the force sensor as feedback. After correct

placement of the sensors, the subject remained seated for twenty-seconds to take measurements. At the end of each measurement, we removed the D-PPG and placed it in a new location with the correct contact pressure.

2) Effects of Contact Pressure

We placed the D-PPG on the dorsal side of the foot, near the most distal end of the first metatarsal with the pressure sensor on top. The strap wrapped around the foot in a similar manner to the previous test. We adjusted the strap to vary the pressure through the entire range of the force sensor (0 mmHg to 195 mmHg) in eight equal intervals. While this range may seem at first to be high, since typical aortic systolic BP values are less than 140 mmHg for healthy subjects and any higher contact pressure would occlude the artery, the BP at the foot during standing is significantly higher than brachial artery pressure due to gravity-induced hydrostatic pressure. Specifically, an additive pressure of ρgh must be added where ρ is the density of blood, g in acceleration due to gravity, and h is the height difference between the foot and the heart. Thus, systolic pressure at the foot can regularly exceed 200 mmHg in a healthy subject, preventing the largest pressure applied at 200 mmHg from occluding the artery. As with the previous test, the subject remained still for twenty seconds per contact pressure to take measurements.

3) Various LED and Photodiode Configurations

We constructed five different combinations of LEDs and photodiodes as seen in Figure 3.7a. For each configuration, we recorded twenty seconds measurement at a constant pressure on the same location as the previous test.

4) Performance Comparison to Commercial PPG Sensors

The subject wore each of the commercial sensors on either the first or second toe after inspection of the signal amplitude to determine the best possible location. Again, we placed

the D-PPG in configuration I near the larger toe on the dorsum and tightened it to a constant pressure 98 mmHg, a comfortable level of tightness for all subjects. The subject then remained still for twenty seconds while we took measurements. Without moving their feet, the subjects transitioned from a seated to a standing position and stood as naturally as possible. After a brief period to reach homeostasis, the subject remained standing for 20 seconds for measurements.

3.3.3 Signal Processing

We used the following model to quantify the quality of the timing references extracted from the various PPG waveforms. The approach leveraged the arrival of the pulse on a beat-by-beat basis and determined if that timing was physiologically possible and therefore reliable. Using the full recording, we calculated a term we deemed the detection ratio (DR) to give an approximation of the reliability of the sensor the given subject,

$$DR = \frac{1}{M} \sum_{i=1} 1_{|PAT_{\mu|} - PAT_i| \leq 13ms} \tag{3.1}$$

where PAT_{μ} was the ensemble averaged—or sample-by-sample mean with respect to fiducial points—PAT for all beats in a single measurement and M was the total number of beats. Similar to previous studies, the R-waves were used as the fiducial points [60, 77].

The first step was to partition the signal into individual beats using the ECG. A digital band-pass filter (f_{pass} = 0.8 - 25 Hz) applied to the ECG helped extract the QRS complex. An automatic beat detection algorithm detected the timing of the R-waves. For the foot of the PPG, we used the intersecting tangent method due to its robustness to morphological artifacts and its effectiveness in extracting PTT as seen in the previous study.

When measuring beat-by-beat fluctuations in PAT for a person at rest in a short-term recording, the only change that would be expected is one associated with respiration. During inspiration, systolic blood pressure decreases leading to an increase in PTT [86]. Addi-

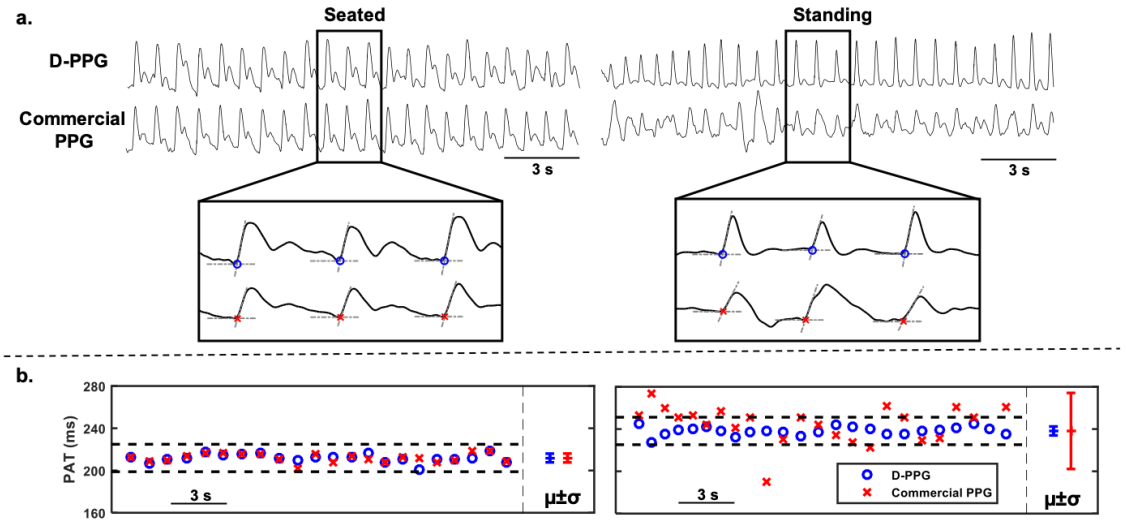

Figure 3.6: (a) Filtered PPG waveforms from the D-PPG and a commercially available PPG while the subject is sitting and standing. A zoomed-in window shows the arrival of the pulse wave using the intersecting tangent method. (b) Extracted PAT for the complete recording. The horizontal black line represents the range of possible PAT values centered on the PAT for the ensemble averaged beat. The D-PPG values were able to stay within the range for both seated and standing while the PAT for the commercial sensor regularly showed values outside of the range during standing. The commercial sensor's PAT was shifted to have equal means with the D-PPG

tionally, the isovolumetric contraction time (PEP) lengthens [87]. Therefore, PAT increases with inspiration. Previous works have shown the variation in PAT due to respiration should be no more the ± 13 ms [88, 89, 90]. Thus, computing the ensemble averaged PPG beats (PPG_μ) and determining the PAT for that beat allowed for the formation of a range of physiologically possible PAT values. Beats within 13 ms of PPG_μ were acceptable while we assumed those outside the range to be detected incorrectly and corrupted with motion artifacts. The number of acceptable beats to the total number of beats formed the DR (thus, a DR of 1 is ideal while a DR of 0 means the section had no acceptable beats). Figure 3.6 showed an example of a clean waveform with a high DR and a noisy waveform with unreliable distal timing references.

Theoretically, the preferred metric would be a direct method of assessing the robustness of PAT timing based on the D-PPG to an ideal pulse wave measurement. However, there are

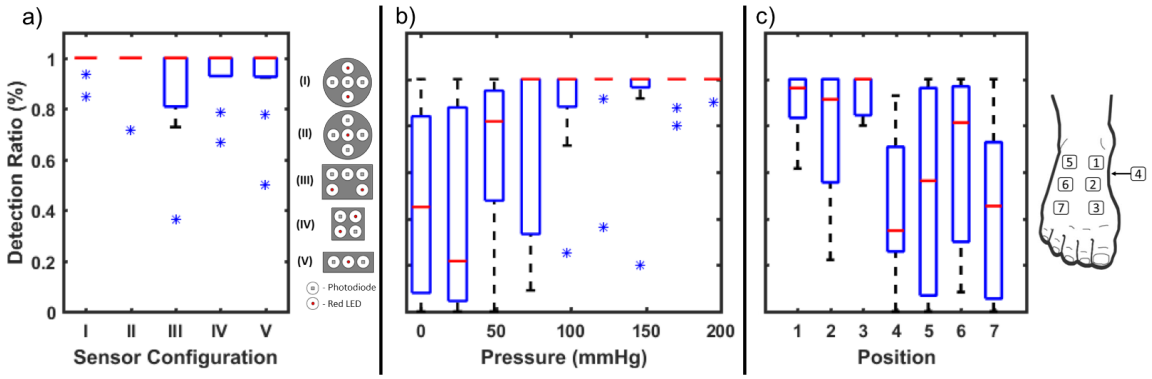

Figure 3.7: Results from the three separate optimization tests along with error bars. (a) Applied pressure to the dorsum, (b) position on the surface of the foot, and c) LED/photodiode configuration.

no methods short of intra-arterial catheterization that could yield a "gold standard" distal pulse timing reference for a standing subject. Accordingly, we have decided to use the DR metric as a means of gauging the overall acceptability of various sensing methods for beat-by-beat PAT detection from the scale.

3.3.4 Results

Figure 3.7 summarizes the results from changing the location, applied pressure, and sensor layout. Figure 3.7a shows a box plot of the DR values at different pressures. The larger pressures generally correlated with the larger DR. Figure 3.7b presents a box plot of the DR values at each position. The area of the largest mean DR was position 3 followed by position 1 and 2. These three positions had a cumulative mean of $82.7\% \pm 26.5\%$ compared to a cumulative mean of $60\% \pm 31.5\%$ for the other positions. Figure 3.7c shows a box plot for each of the five LED and photodiode configuration test. The best sensor was the two-LED, three-photodiode combination (98.2 $\%$).

The average DR of each sensor during sitting and standing is seen in Figure 3.8 with a statistically summary provided in Table 1. The average DR for each sensor in the seated position was sufficiently high for all sensors to facilitate heartbeat detection, though the

Table 3.2: Comparison Between Custom and Commercial Sensors

	Standing				Standing			
	μ	σ	max	min	μ	σ	max	min
i	0.95	0.15	1.00	0.47	0.93	0.14	1.00	0.53
ii	0.83	0.34	1.00	0.00	0.43	0.39	1.00	0.00
iii	0.82	0.30	1.00	0.00	0.41	0.33	1.00	0.00
iv	0.71	0.33	1.00	0.04	0.40	0.40	0.93	0.00
v	0.73	0.32	1.00	0.10	0.46	0.46	1.00	0.00

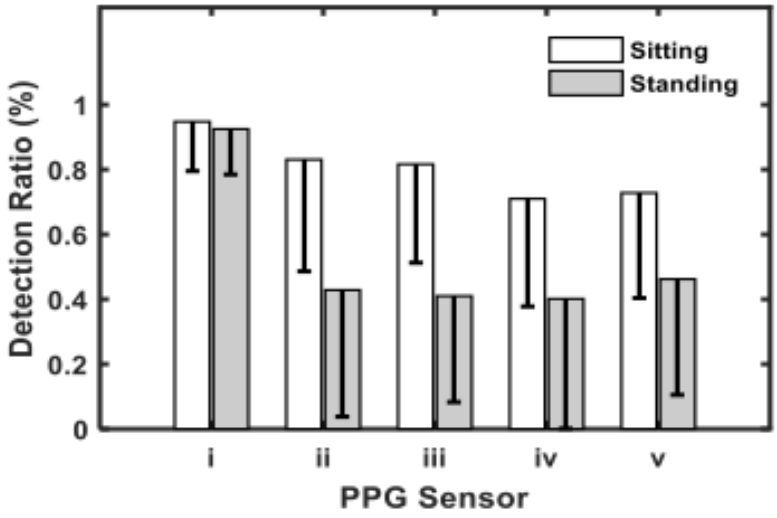

Figure 3.8: Comparison of sitting and standing DR values for each sensor seen in Figure 3.5. The custom reflected sensor we designed achieves the highest DR for both the seated and standing postures.

D-PPG sensor did provide an approximately 15% improvement in DR. Additionally, the inter-subject variability in waveform quality was substantially lower for the D-PPG sensor. The results of measurements during the standing position better showed the difference between the D-PPG and the commercial PPGs. The average DR for the D-PPG sensor was 92.8% ($\pm$14.0%) while the commercial sensors average 42.9% ($\pm$39.1%), 41.0% ($\pm$32.7%), 40.1% ($\pm$40.0%), and 46.3% ($\pm$35.7%), respectively. For the D-PPG, the waveform quality was sufficient for readily extracting signal peaks and the waveform foot for pulse arrival detection. For the commercial sensors, the motion artifacts and changes in the

waveform associated with contact pressure variations from standing corrupted the signal such that the peaks and the foot timings were not discernible.

3.3.5 Optimization of the D-PPG Sensor

An exciting result from this study was the robustness and repeatability of the D-PPG sensors to external factors such as body weight, skin tone, and standing posture. While the DR retained a high value, two of the subjects with high levels of melanin exhibited less than 20% DR regardless of posture for the commercially available sensors. For the D-PPG sensor, eleven of the twelve subjects achieved a DR above 90% while seated or standing. Using an array of sensors along with placing the sensors in a well-perfused region of the foot rather than the toe, contributed to the improvement in performance.

As a quick comparison between reflective sensors, we placed the TSD200C reflective PPG to the dorsum of the foot in each of seven locations and compared the results to the D-PPG sensor. The D-PPG showed a significant increase in DR with a mean increase of 46% ($p < 0.05$). These results support the D-PPG sensor as an improved method to capture the pulse waveform.

3.3.6 Comparison Between D-PPG and Commercial Sensors

The average DR for each sensor in the seated posture was greater than 70%, and visually, the peak and foot locations were readily discernible. The DR decreased substantially for the commercial sensors when the subject transitioned from a seated to a standing posture, decreasing by an average of 34.6% ($p < 0.01$ for all sensors). The only sensor to exhibit a high-quality PPG waveform during a standing position was the D-PPG. Though the change of position did result in a decrease in DR, the mean standing DR remained at an acceptable level and was a significant improvement over the commercially available sensors ($p < 0.005$).

For most of the subjects in the study, standing appeared to have caused variations in the

contact pressure placed on the commercial sensors associated with normal postural sway during standing and resulted in a decrease in DR. The strong effects of contact pressure variations on PPG signal amplitude are known for finger-based PPG sensors. Based on our findings, motion artifacts coupled into the commercial sensors to a greater extent than to the D-PPG, corrupting the commercial sensors signals while preserving the D-PPG signal. Additionally, as the added weight placed on the artery increased contact pressure to or above systolic pressure, the artery stiffened and the pulse wave became smaller. The pressure placed on the D-PPG sensor was minimal during standing and the signal remained intact.

3.3.7 Conclusion

In this study, we demonstrated that the D-PPG yields a more reliable and consistent pulse waveform than commercial PPG sensors, particularly in a standing position. The results are consistently better than commercially available sensor packing options in terms of DR. Overall, the weighing-scale based approach for PTT measurement with the BCG as a proximal timing reference and the D-PPG as the distal timing reference may provide a convenient and accurate means of extracting aortic PTT for arterial stiffness and BP assessment.

3.4 A Reflective Photoplethysmogram Array and Channel Selection Algorithm for Weighing Scale Based Blood Pressure Measurement

Our previous method was based on the use of the BCG as the proximal timing reference and the use of the D-PPG as the distal timing reference, with a strap placed over the foot to apply needed pressure for the D-PPG. While this method was demonstrated to be accurate in our study with healthy, young adult subjects, the requirement of a foot strap limited the convenience of the approach. If a subject could simply stand on a scale, and if the distal pulse could be extracted accurately, no setup would be required, increasing the convenience of a PTT measurement.

Distal pulse detection from the bottom of the foot, without a strap, was first demonstrated through IPG by Gonzalex-Landaeta, *et al.*, using aluminum foil squares placed under the subject's foot and Inan, *et al.*, using electrodes embedded in a modified electronic weighing scale. While this method is more convenient than a foot strap, IPG signals have some disadvantages that must be taken into consideration. As mentioned in Chapter 2, IPG signal quality is low in waveforms taken from certain subjects, such as obese individuals, critically ill patients, patients with heart failure, and other patients with weak circulation [67, 72]. Additionally, skin-electrode impedance while using dry electrodes may be high at the bottom of the feet for some subjects, depending on body composition.

In this section, we present an array of PPG sensors positioned under the foot with associated electronics and signal detection algorithms for convenient PPG-based distal pulse detection on a scale. With the proximal timing detected through the BCG, the sole PPG array was also able to detect the distal timing. The overall system was evaluated in healthy, young adult subjects to assess the accuracy with which blood pressure can be estimated from PTT derived from these two measurements.

3.4.1 Hardware Design

Figure 3.9 depicts the proposed method to extract PTT. Proximal and distal timing references relied on the combination of a high-resolution force plate and an array of PPG sensors placed on the top of the plate. Both sensors were connected to custom-built analog front-end (AFE) circuits followed by a data acquisition unit (DAQ) for post-processing and PTT extraction. This system allowed subjects to stand on the scale to obtain a measurement, with minimal to no initial setup required.

To obtain the proximal timing reference, we used a high-resolution force plate (Type 9260AA6, Kistler Group, Winterthur, Switzerland) for a BCG waveform. The force plate has three-component sensors, one for each dimension, on each of the four legs. Each of the z-direction sensors, which provide the head-to-foot component of the BCG, connect to

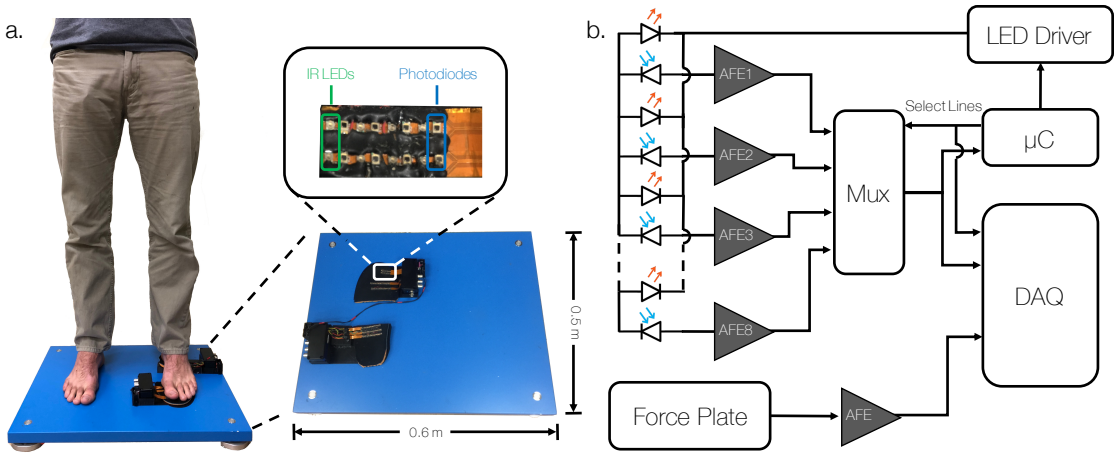

Figure 3.9: (a) Force plate measured the BCG while an array of PPG sensors measured the pulse wave at the sole. The subject simply has to stand on the force plate and PPG array to measure PTT. (b) Each of a total of forty-eight photodiodes for PPG sensing passes through a custom analog front-end (AFE) circuit. All output signals were then multiplexed and sent to a data acquisition (DAQ) unit for further processing on a laptop.

an AFE composed of a gain and low-pass filter stage (G = 20dB, f_c = 20Hz) followed by an adder circuit to combine all four signals. The study uses this force plate rather than a cheaper and more common home-bathroom because of the improved detection of PEP in the BCG waveform.

A custom-built PPG array measured the distal timing reference. For the PPG array, we placed flexible PCB strips with pairs of IR LEDs (Vishay Intertechnology Inc, PA, USA) and photodiodes (SD040-101-411, Advance Photonix Inc, MI, USA) on a common shoe insert. The array included five strips of eight IR LED and PD pairs and two strips of four IR and PD pairs allowing for a total of forty-eight PPG measurements. We surrounded the IR LEDs and PDs with a thin layer of hot melt adhesive to insulate the conductive pads from the body, reducing the light leaking from the LEDs to the PDs, and increasing the comfort for the subject as they place their body weight on the sensors. The strips of IR LED and PD pairs were placed in three sections of the insert: three six-PPG strips on the lower middle to measure the midfoot PPG, two six-PPG strips on the upper middle for forefoot PPG measurements, and finally, two four-PPG strips on the upper portion to measure the toe

PPG. The top half of the insert containing just the forefoot and toe sensors was separated from the bottom half to adjust for different foot sizes.

As shown in Figure 3.9, we connected the cathode of each PD to a transimpedance amplifier configured to operate as a low-pass filter (G = 109dB, f_c = 24Hz) with an additional gain stage further amplifying and low-pass filtering the signal (G = 47dB, f_c = 12Hz). The outputs of eight PPG AFEs were connected to the inputs of an eight-channel multiplexer (MAX4617, Maxim Integrated, San Jose, CA). In total, there were six multiplexers to read all forty-eight PPG channels. Three digital channels of a Teensy 3.2 (PJRC.com LLC, OR, USA) controlled the three select lines, stepping through the lines at a rate of 10kHz. Following the overflow of the select lines every 1600 nanoseconds, a pause of 400 nanoseconds occurred to fix the sample rate of individual channels to 500Hz and to create a notable event to indicate an overflow without an additional line. The Teensy 3.2 was also used to set the current of an LED driver to 4mA per IR LED.

3.4.2 Human Subject Studies

This study was approved by the Georgia Institute of Technology IRB. We enrolled 16 young and healthy subjects for the study (age: 26 $\pm$ 3; gender: 12 males, 4 female; weight: 70kg $\pm$ 14kg; height: 172 $\pm$ 10).

To obtain a timing reference, gel electrodes in a Lead II configuration measured the electrocardiogram (ECG) using a wireless amplifier (BN-EL50, Biopac Systems). The ECG was solely used in this study to indicate the start of the cardiac cycle for the initial assessment of the PPG waveform and not for calculating PTT. The ccNexfin (Edwards Lifesciences) continuous blood pressure monitor measured the reference BP waveform against which the PTT-based estimates were compared. The MP150 DAQ (Biopac Systems) recorded the outputs of the six multiplexers, the output of the force plate AFE, the blood pressure waveform, and the ECG at 12.5kHz. The DAQ also recorded the least significant bit of the select lines from the Teensy for partitioning the multiplexed PPG signals.

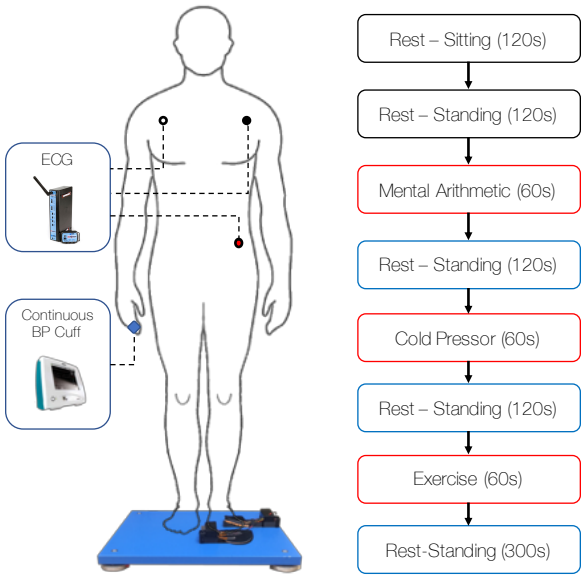

Figure 3.10: Block diagram of the protocol. The black boxed portion of the protocol was used to determine the PPG reliability in standing compared to seated postures. To compare PTT estimated BP to measured BP, waveforms were recorded during three interventions (red) and three rest periods (blue). Data collected during exercise were not analyzed, due too the fact that the subject could not stand on the scale during the stepping exercise; however, data from the exercise recovery period were analyzed.

The protocol involved two sections to test: (1) the ability of the PPG array to measure an accurate distal pulse timing and (2) the correlation between (i) the PTT derived from a combination of a force plate (BCG) and PPG foot array and (ii) blood pressure measured by the ccNexfin. The full protocol, as well as the experimental setup, can be seen in Figure 3.10.

1) Determining the PPG Reliability

Prior to evaluating the accuracy with which the BCG-to-PPG array derived PTT can estimate blood pressure, we validated the quality of the distal pulse timing delivered by the PPG signal measured from the sole. The goal was to first independently assess the distal pulse timing quality, then combine the distal pulse with the BCG for examining the ability to measure blood pressure via PTT. The main challenge associated with measuring PPG

signals from the foot is due to the variations in contact quality between the subject and the sensor due to the inability of the subject to stand still, thus creating variations in contact pressure between the foot and the platform. When the subject is sitting with the foot on the sensor array, nearly any PPG sensing approach – including simple toe-clip approaches using conventional sensors – can deliver a high-quality PPG waveform and thus an accurate distal pulse timing. However, as seen in the previous work with the D-PPG sensor, once the subject stands upright, the conventional approaches to sensing PPG waveforms have difficulty producing high-quality waveforms, and the custom PPG sensing techniques must be evaluated carefully.

We conducted an experimental protocol similar to that described in the D-PPG evaluation, yielding a comparison between PPG timings from a subject in seated and standing postures successively. Each subject first sat in a chair for two minutes with the left foot fixed to the top of the PPG array; then, without changing the position of his / her feet, the subject stood for another two minutes while the system obtained measurements. The actual measurement of PTT for blood pressure estimation would require the subject to stand on the scale since BCG signals cannot be measured from a user if he / she is not standing on the scale platform. The seated posture allowed us to determine the optimal high-quality PPG waveform morphology for the subject from the bottom of the feet and then to compare against this morphology once the subject stands. This allowed us to quantify the performance degradation once the subject stands on the PPG sensor array. The metric we used for this comparison is the detection ratio, as described in previous sections.

2) Correlating Scale PTT to Finger-Cuff Blood Pressure

To quantify the best-case ability of PTT measured with this system to estimate BP, we used a human subjects protocol similar to our previous studies. Specifically, both PTT and blood pressure were measured continuously as the subjects underwent different hemodynamic perturbations to increase blood pressure temporarily. A linear fit was then determined

using least-square regression between PTT^{-1} and BP.

Each subject underwent three different hemodynamic perturbations. While standing on the force plate and PPG foot array, the subject first performed a mental arithmetic (MA) exercise by adding digits of a three-digit number, then adding the result to the original number [91]. The subject repeated this procedure with the newly calculated number for sixty seconds. A period of rest allowed the subject to return to hemodynamic homeostasis. We then obtained a cold pressor recording by having the subject immerse the hand without the ccNexfin in cold water for sixty seconds [92]. After another rest period, the subject stepped off of the force place and performed a high-intensity box jump exercise for sixty seconds. The subject then returned to the force plate for the final resting period, during which the blood pressure recovered from the elevated state during exercise back to the resting value. This combination of physiological perturbations for varying blood pressure employed a variety of mechanisms for modifying blood pressure, including increased cardiac output (mental arithmetic, exercise), increased total peripheral resistance (cold pressor), and increased cardiac contractility (exercise). Thus, a more comprehensive assessment of the accuracy with which blood pressure can be estimated was obtained as compared to using only one perturbation, such as only exercise recovery.

3.4.3 Signal Processing

1) Extracting Clean PPG Waveforms from the Sensor Array

We used the following steps to transform the multiplexed PPG signals to "clean" waveforms for distal timing calculations. First, the least significant bit of the select lines allowed for partitioning of the individual PPG signals. The 400 ns digital low periods indicated the start of the eight channel sweep. Each consecutive toggle of the line specified the selection of the next PPG connected to the multiplexer. After using this information to partition the data into individual PPG signals, a digital FIR band-pass filter (f_{pass} = 0.5 - 8 Hz) further removed out-of-band noise.

We then separated the data based on the section of the protocol, excluding exercise as the subject was not on the scale—the post-exercise data during recovery was analyzed, however. For each section, we determined the signal-to-noise (SNR) of each PPG signal using a technique in [93] and removed those signals with low SNR. To find the SNR, we first extracted the individual PPG beats using a peak detection algorithm. We then formed an upper peak envelope smoothed over a two-second window and located all local maximums greater than 60% of the envelope. Since the anacrotic or dicrotic notch could occur in close proximity to the forward going wave, consecutive peaks within 300 ms were identified, and we removed the peak with a lower amplitude. With the remaining peaks, we captured individual PPG beats by extracting a window 300ms before and 500ms after the peak. Ideally, the PPG beats within a short time-window are consistent with only amplitude variations caused by slowly-varying effects such as respiration. Assuming the noise to be uncorrelated and zero-mean, the ensemble average of the PPG beats represented the cardiac component (the signal). The non-cardiac components (the noise) were the differences between the individual beats and a best fit scaled version of the signal.

To formulate the SNR of a given PPG signal, we divided the beats of the PPG into an array X of M beats. Each beat was a scaled version of the ensemble averaged beat $\vec{s}$ with additive noise.

$$X = \vec{s} * \vec{a} + V \tag{3.2}$$

where

$$X = [\vec{x_1} \quad \vec{x_2} \quad \dots \quad \vec{x_M}] \tag{3.3}$$

The scaling factor of each kth beats of X described the relative amplitude of the projection of each measured PPG beat, $\vec{x_k}$ onto $\vec{s}$.

$$a_k = \frac{\vec{s}^T * \vec{x}_k}{||\vec{s}||} \tag{3.4}$$

Thus, the noise of each beat was calculated using:

$$\vec{v_k} = \vec{x_k} - \vec{s} * a_k \tag{3.5}$$

The NSR for each kth beat was estimated directly

$$NSR_k = \frac{\sigma^2_{\vec{v_k}}}{\sigma^2_{\vec{s}}} \tag{3.6}$$

Finally, the SNR of the signal was computed

$$SNR = 10 \log_{10} \frac{1}{M} \sum_{k=0}^{M} \frac{1}{NSR_k} \tag{3.7}$$

2) Segmenting PPG Waveforms into Groups and Calculating DR and PTT

For each section of the protocol, we separated the PPG signals into three groups: the toe PPG, forefoot PPG, and midfoot PPG as is seen in Figure 3.11. The three groups represented different locations on the arterial tree with varying depths below the skin surface and differing arterial diameters. For each group, we removed the signals with an SNR below 0dB or with an SNR 10 dB below the max SNR of that group. This effectively removed signals deemed too noisy that could corrupt the distal timing reference. This included noisy beats that produced unreliable peaks when using our proposed peak detection algorithm. The ensemble average of the remaining signals represented the "clean" PPG waveform of that group.

We first determined the consistency of the PPG as a measurement of the distal timing by calculating the detection ratio (DR). As mentioned in greater extent in the previous section, the DR effectively determines the consistency of the calculated distal timing by computing the percentage of PATs that are within a physiologically possible range for a subject at rest. Since PAT is the time interval between the R-wave of ECG and the arrival of the pulse,

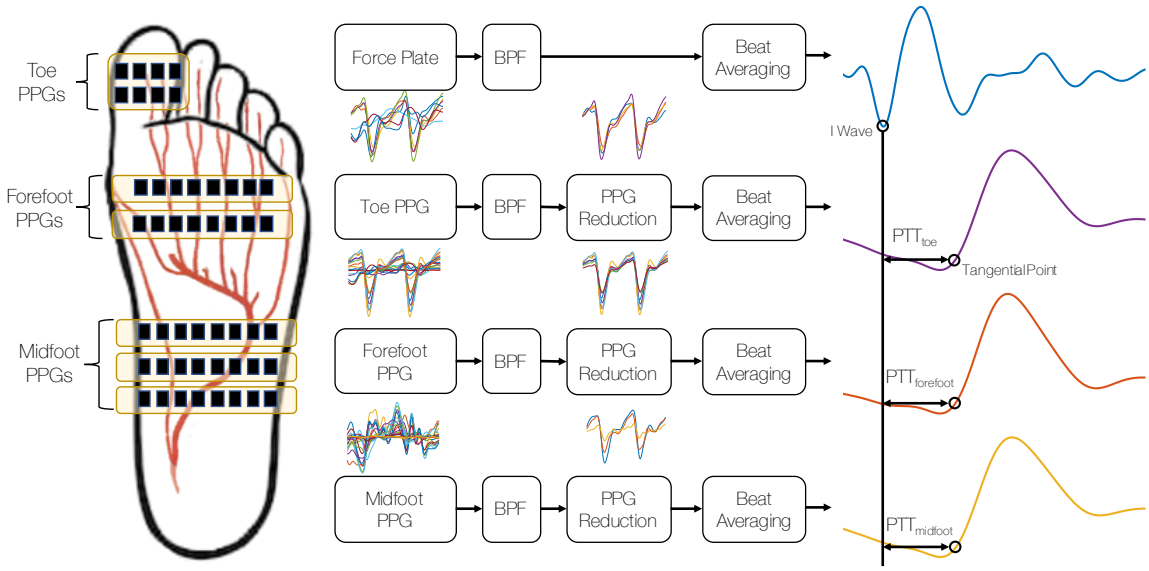

Figure 3.11: The PPG sensors were divided into three groups based on the location on the foot: the toe, forefoot, and midfoot. After digital filtering, the SNR of the PPG sensors was calculated. Those with relatively low SNR, below 0 dB or 10 dB less than the max, were removed from further processing. Using the peaks of the PPG signal, individual beats of the PPG and BCG were extracted and ensemble averaged together. The I-wave of the BCG and the distal pulse arrival (computed based on the intersecting tangents approach) of each group's PPG represented the proximal and distal timing reference for PTT calculations.

we used the ECG to separate the PPG signal into individual peaks. We ignored the first sixty seconds of sitting and standing to account for hemodynamic changes that occurred during transitions between sitting and standing. To find the distal reference in the PPGs, the intersecting tangent method was applied.

We determined PTT for the remaining sections of the protocol and formulated a calibration curve to BP. First, we used the peaks of the PPG found using our peak detection algorithm to separate the "clean" PPG, the blood pressure waveform, and a digitally filtered version of the BCG (f_{pass} = 0.5 - 20 Hz) into individual beats and then ensemble averaged the beats of each waveform. The local minimum immediately before the maximum of the BCG signal was denoted the I wave and used as the proximal timing reference. To find the distal reference in the three PPGs, we again used the intersecting tangent method. We computed PTT using the difference between these proximal and distal timing points.

3.11 shows a block diagram describing the steps involved in calculating PTT from the raw PPG signals. Lastly, the minimum and maximum of the ensemble averaged BP waveforms indicated the diastolic and systolic pressure, respectively.

3) Selecting Optimal PPG Waveforms for PTT Calculation

The simplest approach to estimating a distal pulse timing from an array of 48 PPG signals obtained from the foot would be to average all the waveforms together and obtain one distal timing from this averaged "sole" PPG. However, this simple approach has many theoretical flaws that would result in low-quality PTT—and subsequently blood pressure—estimation. Most importantly, the PPG signals captured from the different portions of the foot arrive at different times based on the proximity to the heart and the superficiality of the interrogated arterial blood volume; thus, simply averaging them together would smear the distal timing by conflating the diastolic portions of multiple different PPG signals that are not synchronized in time. An important contribution of the work presented in this thesis was the investigation of *physiology-driven* methods for determining the optimal PPG waveform set for each subject to estimate PTT and blood pressure.

The principle upon which we operated to determine such an optimal PPG waveform set for each subject was based on the fact that distal timing measurements from larger arteries should provide PTT estimates that are modulated by less confounding factors besides BP compared to smaller arteries in the microvasculature. Thus, the more likely that a PPG waveform set is derived from larger arteries, the better the PTT estimate derived from that waveform set should relate to BP.

We defined three methods for quantitatively determining which PPG signals were primarily capturing blood volume pulse from the larger arteries in the foot: selecting PPG waveforms with (1) the earliest average distal timing, (2) highest average SNR, and (3) highest average augmentation index (AIx). The first method, finding the earliest distal timing, may indicate that the PPG originates from larger arteries since the pulse arrives at the

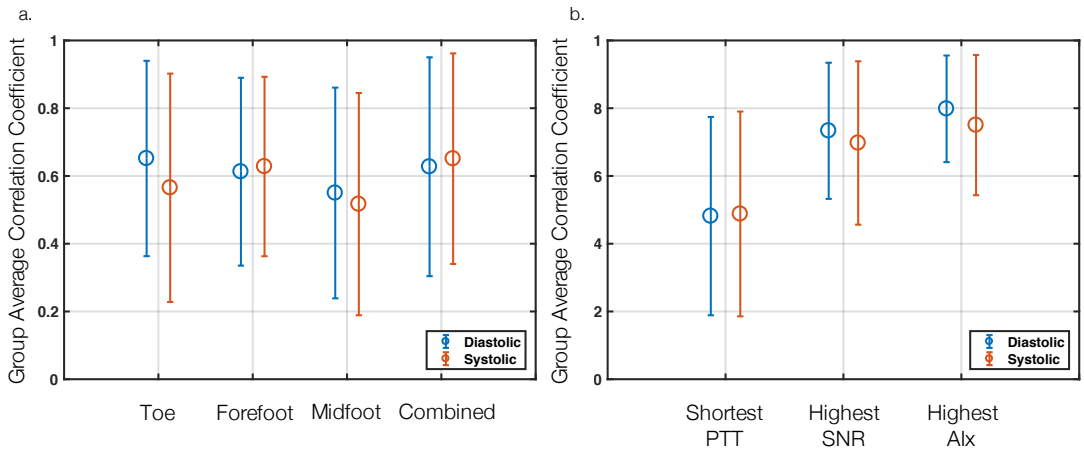

Figure 3.12: (a) Best case correlation between PTT^{-1} and BP based on the section of the foot. (b) Correlations based on the sections of the foot selected to have the larger arteries based on the shortest PTT, highest SNR, and highest augmentation index (AIx).

larger arteries first, then continues to propagate along the arterial tree to the microvasculature. The second method, finding the highest average SNR PPG signals, may indicate origination from the larger arteries due to the fact the vessels in the microvasculature are more susceptible to motion artifact and pressure-induced occlusion and thus would yield lower SNR signals. The third method, selection based on highest AIx is based on the fact that AIx is the difference between the max peak of the PPG and the dicrotic notch, expressed as a fraction of the total pulse amplitude, and is typically a marker of arterial stiffness [94]. However, it may indicate the size of the artery due to the damping of the pressure pulse that occurs with the decreasing size of the artery [95].

We compared the inverse of the PTTs to both the systolic and diastolic pressures. For each group, we computed the correlation coefficient (r) between the time delay and the pressure levels. We also calculated the root-mean-squared error (RMSE), the RMS difference between the measured and a best-case PTT estimated BP.

3.4.4 Results

1. Comparison of Seated to Standing PPG Waveforms using DR

The DRs of the PPGs supports the sensor array as a method of extracting a reliable distal timing reference. While seated, the toe PPG, forefoot PPG, and midfoot PPG had a DR of $64\% \pm 29\%$, $92\% \pm 15\%$, and $96\% \pm 10\%$, respectively. Both the toe PPG DR and midfoot PPG DR changed significantly ($p<0.05$) when the subject moved from seated to standing. The toe PPG DR increased to $85\% \pm 26\%$, and the midfoot PPG DR decreased to $62\% \pm 32\%$. Though insignificant ($p>0.05$), the forefoot PPG DR decreased to $81\% \pm 25\%$.

2. Assessing PTT Based Blood Pressure Estimation

Figure 3.12 shows the average correlation between PTT^{-1} and diastolic BP for each of the sections of the foot as well as each method to select the largest artery previously proposed. With regards to the sections of the foot, the highest correlation to diastolic BP was found at the forefoot, followed by the toe and then the midfoot (r=0.65$\pm$0.29, 0.61$\pm$0.28, 0.55$\pm$0.31). When we combined all signals on the foot, there was no significant change in the r values (r=0.63$\pm$0.32). Correlations decreased when fitting PTT^{-1} to systolic BP with r=0.57$\pm$0.33 and 0.51$\pm$0.33 when using the toe PPG and midfoot PPGs, respectively, but slightly increased when using the forefoot PPG (0.63$\pm$0.26) or all PPGs combined (0.65$\pm$0.31). Both the forefoot and the toe PPGs performed significantly better than the midfoot PPGs ($p<0.05$). We found no significant differences between the correlations found using the midfoot and forefoot PPGs ($p>0.05$).

Figure 3.12b shows a comparison between the three previously mentioned methods attempting to extract the PPG waveform from larger arteries. Extracting the signals with the highest average AIx resulted in the highest correlation to diastolic BP (r=0.80$\pm$0.16) compared to the highest average SNR (r=0.73$\pm$0.20) and the shortest average PTT (r=0.48$\pm$0.29). Correlation to systolic pressure was lower in all three methods, though the highest average

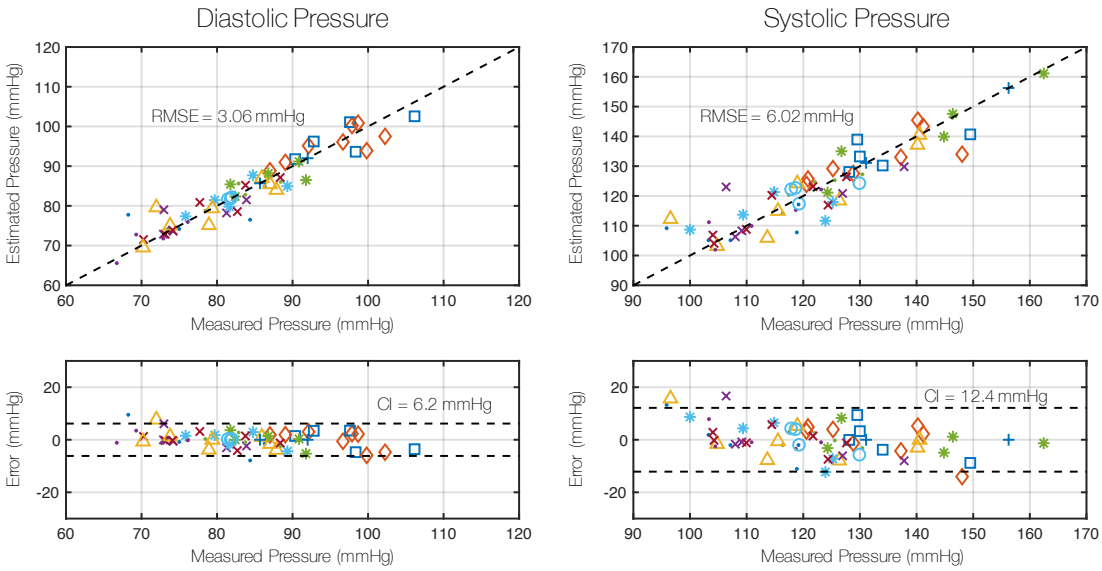

Figure 3.13: Correlation and Bland-Altman plots for diastolic and systolic pressure using the best-case estimation of BP based on PTT derived from the BCG and the PPG with the highest augmentation index.

AIx still performed the best (r=0.75$\pm$0.21) followed by highest average SNR (r=0.70$\pm$0.24) and shortest PTT (0.49$\pm$0.30).

Using the PPG waveforms with the largest AIx, we estimated BP using a best-case correlation curve and compared this to the measured BP as shown in Figure 3.13. The average RMSE between the estimated and measured BP, was 2.6$\pm$1.6 mmHg for diastolic pressure and 5.2$\pm$3.1 mmHg for systolic pressure. The group RMSE for diastolic and systolic were 3.06 mmHg and 6.02 mmHg, respectively. Figure 3.13 also shows a Bland-Atman plot comparing the BP cuff's measurement to the difference between BP cuff's measurement and the PTT-based estimate of BP. Diastolic estimations had the narrowest 95% confidence interval (CI) at 6.2 mmHg with systolic estimations at 12.4 mmHg.

3.4.5 Detection Ratio of the PPG Array

In our previous study, we demonstrated that foot strap-enabled sensing of PPG signals from the dorsum of the foot outperformed commercially available toe-clip PPG sensors. For the

most part, the effectiveness of the PPG array presented in this work in capturing the distal pulse timing not only exceeded the toe-clip based sensors but also performed comparably to the D-PPG without requiring the foot wrap. However, both the toe PPG while sitting and the midfoot PPG while standing performed significantly worse than the other sections. An interesting result was the change in DR in both sections when the subject changed posture from sitting to standing, presumably due to the change in weight distribution on the sole. When the subject was in a seated position, only the weight of the toe was on the PPG which was unable to create a high enough force to apply adequate contact pressure, corrupting the signal quality. As the weight transferred entirely to the feet when the subject stood, the contact pressure increased on the toe, and the signal quality improved. Regarding the midfoot PPGs, the pressure placed on the midfoot increased to a level that may be too high in some subjects for a reliable distal timing reference.

3.4.6 Effect of Sensor Location on Correlation

Similarly to the DR results, the midfoot had the weakest performance overall in terms of correlation to BP out of the three sections. The low DR and correlation provided evidence that PPGs sensing the midfoot were more likely to be measuring vessels in the microvasculature than the other PPGs, or that they were sensing from a portion of the foot that has lowest amount of perfusion. An increase in blood pressure and prevalence of adjacent supporting muscle and bone make larger arteries less susceptible to external pressures [96].

Compared to the midfoot, the remaining two sections both had higher correlations, though not significant, while also having a high DR during standing. The forefoot has the advantage of being highly perfused with vessels from the deep plantar arteries or the plantar metatarsal arteries. These arteries fan across the forefoot, increasing the probability that a PPG sensor was in an ideal location to sense an artery with optimal contact pressure. Similarly to the forefoot, the toe is a heavily perfused region, increasing the chances of capturing an artery within the volume being interrogated optically.

It is important to note that these assessments do not represent the overall results, and there was substantial variability across subjects that should be considered. In three of the sixteen subjects, PTT derived from the midfoot PPG resulted in the highest correlation coefficient. The anatomical structure of the foot slightly differs among subjects, depending on various factors such as muscle tone, the thickness of calluses, and melanin levels, each affecting optical penetration depth and signal quality.

3.4.7 Assessing Proposed Methods to Select Optimal PPG Signal for PTT

While the locations allowed for independent calibration curves to be formed, the site of the highest correlation varied across subjects, presumably due to the various types of vessels measured as the distal timing. The three methods proposed—shortest average PTT, highest average SNR, and highest average AIx—attempted to select the best PPG to use in PTT calculations based on physiological expectations. Shortest average PTT performed the worse, presumably due to the different positions of the sensors having a more significant effect of PTT than the location along the arterial tree. The midfoot was most likely to be selected using this method, due to its proximity to the heart compared to the other sections. Highest SNR provided an improved correlation to blood pressure than the shortest average PTT. Increasing the pressure applied to the measurement region limited the blood flow to the smaller arteries and microvasculature. Larger arteries were less susceptible to occlusion during high external pressure, preserving signal quality and increasing the SNR. However, there could be issues with using the SNR to determine the larger arteries as the microvasculature has been shown to provide increased signal quality in scenarios where the pressure is low enough to prevent occlusion [97, 53]. The distribution of weight on the sole was non-uniform and subject-dependent causing the contact force of the PPG sensors to vary. While an area of low SNR indicated the measurement of smaller occluded vessels, high SNR could have been either from the sensing of a larger artery or of smaller vessels from a sensor with low contact pressure. The toe might be particularly sensitive to this

effect due to the high perfusion and the minimal involvement in weight-bearing [98, 99].

The highest correlation occurred from the PPGs with the highest AIx. As the pulse moved from a larger to a smaller artery, the increase in arterial resistance caused the vessel to act as a mechanical low-pass filter, dampening the pulse wave and removing the high-frequency components [95]. The pulse wave smoothed off, removing the steep drop after the initial forward-going pulse wave. When the reflected wave that created the dicrotic notch arrived at the site, the pulse wave was at a higher initial level in the smaller arteries. As a result, measurements of the microvasculature had a dicrotic notch higher in amplitude – thus a lower AIx – than more proximal, larger arteries. The use of the AIx to determine which PPG waveforms to use in the PTT based blood pressure estimation is an important contribution, as this step allowed the correlation to blood pressure to be substantially improved over combining waveforms directly without any physiologically-driven down-selection step.

3.4.8 PPG Array Advantages and Limitations

Using the PPG with the highest AIx, this setup was able to track blood pressure trends simply by standing, without the need for a strap or additional sensors. The array of PPG sensors had a large enough spread of sensors on the sole to pick up pulse waveforms from larger arteries. Using these waveforms and the BCG, the calculated PTT exhibited a strong correlation to both diastolic and systolic BP, comparable to our previous study that used a PPG sensor on the dorsum of the foot. While estimations of systolic blood pressure did have a higher error than diastolic, this is not surprising since PTT tends to have a higher correlation with diastolic pressure.

While the study presents a method to reliably and accurately track changes in blood pressure, several limitations should be noted. As with our previous studies, only young and healthy subjects participated in the study; older subjects could have difficulty standing balanced for a reliable BCG and PPG measurement. Additionally, age increases arterial

stiffness, potentially affecting the measurement of the PPG at the sole or the calculation of AIx. With regard to the hardware, the system does require small alterations for each subject to adjust for varying foot sizes. Future work can increase the number of sensors and total sensing area and automatically map the sole upon placement of the foot. Only the sensors in areas of interest would record the PPG for PTT calculations. Finally, the significant limitation for the device, as with all PTT-based BP monitors, is the need for calibration. The current state of the device only tracks trends in blood pressure and not absolute values. Further calibration techniques will need to be developed to convert PTT to a standardized metric such as blood pressure. The calibration curve will then need to be tested on subjects over an extended period of time to assess the accuracy for long-term monitoring.

3.4.9 Conclusion

This work attempted to increase the convenience of monitoring through an unobtrusive system by using PTT. A combination of a scale and an array of PPG sensors measures both the proximal and distal timing reference for PTT during standing without the need for user involvement or a wearable external sensor. We conducted a study to test the reliability of this method and the ability for PTT to track changes in blood pressure. We tested various methods to down-select from the array for PPG measures to determine the optimal PPG waveforms to use as the distal timing reference. By using the PPG associated with larger arteries through examining the augmentation index, the system showed a high correlation to blood pressure. To the best of our knowledge, this work is the first of its kind to automatically select high-quality signals and utilize physiology-driven methods for determining optimal PPG waveform sets for PTT calculations.

3.5 Weighing Scale-Based PTT is a Superior Marker of BP than PAT

In the previous study, we developed a system in a form similar to a bathroom weighing scale for convenient measurement of PTT through larger, more elastic arteries including the

aorta. The weighing scale comprised of a ballistocardiogram sensor to measure a proximal waveform indicative of the mechanical timing of aortic ejection when the subject stands. The D-PPG sensor simultaneously acquired a distal blood volume waveform from the foot to act as the second timing reference.

In this section, we ran a human study using the weighing scale and D-PPG sensor to calculate PTT during multiple interventions used to change BP through different physiological mechanisms. We compared these estimations to those produced through conventional measurements and showed significant improvements. This work was in collaboration with Stephanie Martin, Dr. Chang-Sei Kim and Dr. Jin-Oh Hahn of the University of Maryland and Dr. Ramakrishna Mukkamala of Michigan State University. The main contributions from the author of this thesis to the work were focused on the development and validation of the hardware, the planning and execution of the human subjects studies, and assistance in the signal processing steps.

3.5.1 Human Subject Studies

We studied human subjects under a protocol approved by the Georgia Institute of Technology and Michigan State University Institutional Review Boards and performed procedures following the guidelines and regulation of both IRBs. We recruited 22 young and healthy adults (age: 25 $\pm$ 3.5 years, gender: 19 males, 3 females; height 177 $\pm$ 11 cm; weight 75 $\pm$ 15 kg) for the study and obtained written, informed consent.

Sensor placement can be seen in Figure 3.14. For Lead II ECG, each subject wore gel electrodes on the chest interfaced to a wireless transmitter (BN-EL50, Biopac Systems). Eight gel electrodes on the neck and thorax in standard impedance cardiography configuration interfaced to a wireless bioimpedance module (BN-NICO, Biopac Systems) to provide ICG. We placed a transmission-mode PPG clip (8000AA, Nonin Medica) on an index finger and interfaced the sensor to a wired PPG module (PPG100C, Biopac Systems). The ccNexfin (Edwards Lifesciences) on the middle finger of the same hand provided contin-

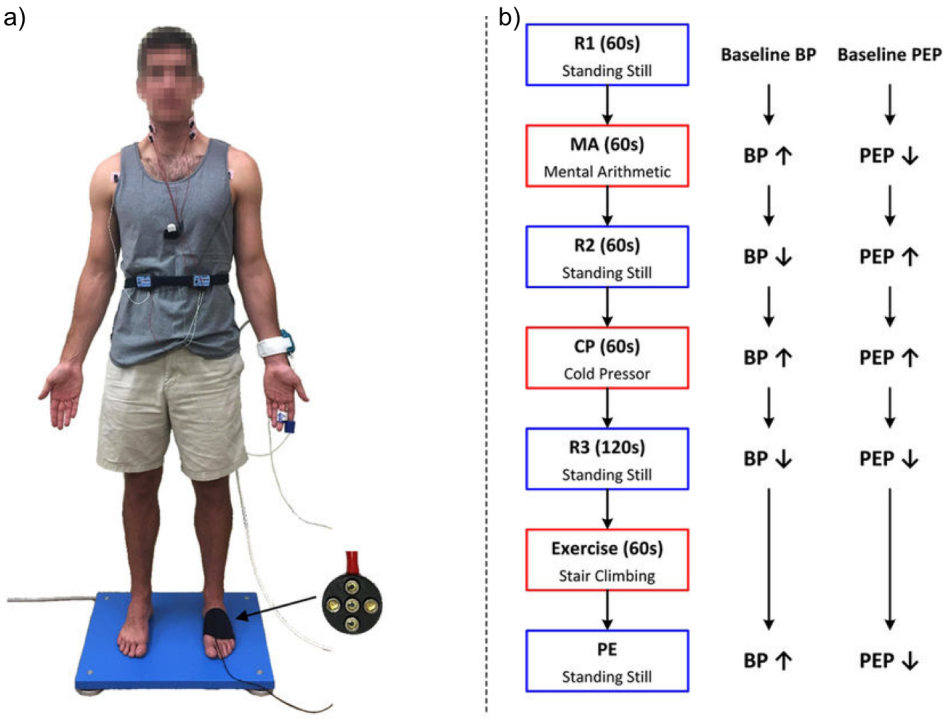

Figure 3.14: Data collection for comparing scale PTT to conventional PAT. (a) For scale PTT, a force place measured the BCG while a foot strap measured the PPG. Standard sensors measured the ECG, finger PPG, and ICG waveforms. (b) The subjects underwent three baseline periods (R1, R2, R3) along with performing three perturbations to increase BP but vary the PEP: mental arithmetic (MA), cold pressor (CP) and post-exercise (PE).

uous BP. During the study, the volunteer stood on the custom weighing scale-like system described earlier in this chapter (Type 9260AA6, Kistler Group). We placed the D-PPG sensor with the adjustable strap for pulse measurements at the foot. We interfaced all of the measurements to a laptop computer via a data acquisition unit (MP150, Biopac Systems) and recorded the waveform at 2kHz sampling rate. Note that we obtained the ICG as an additional benchmark for comparison.

We collected the data during three hemodynamic interventions similar to the protocol described earlier in this chapter. First, after standing still for 60 seconds to obtain a baseline recording, the subject performed the same mental arithmetic challenge by repeatedly continuously adding digits of a three-digit number and then added the sum to the original amount. Second, the subject immersed the hand without the blood pressure cuff and PPG

clip in a bucket of cold water for 60 seconds to get a cold pressor recording. Finally, after resting for 120 seconds to obtain a third baseline recording, the subject got off the scale, performed a stair-climbing exercise for 60 seconds and then returned on the scale to obtain a post-exercise recording.

3.5.2 Signal Processing

For each subject record, we selected segments from the three baseline periods and interventions yielding six sets of six waveforms for each subject. We first band-pass filtered the BCG, PPG, and ICG waveform segments using a first-order Butterworth high-pass filter (f_{pass} = 0.5 - 10 Hz). A simple peak detection algorithm located the R-wave of the ECG. We considered the I-wave of the BCG to be the local minimum between the ECG R-wave and the J-wave—the highest peak within 100 ms to 300 ms after the R-wave. The ICG B-point was the maximum of the first derivative between consecutive R-waves. The intersecting tangent method used previously found the foot of the PPGs, and the minimum and maximum of the BP waveform were the diastolic and systolic BP references. We then averaged the time delays and BP references over five beat intervals. To maximize the BP range for the subject, we selected the interval wherein average diastolic BP was minimum during the rests and maximum during the interventions.

We determined the following values: scale PTT as the delay between the I-wave and the foot of the D-PPG, conventional PAT as the time delay between the R-wave and the foot of the finger PPG, PEP as the time delay between the R-wave and the I-wave, arm PTT as the time delay between the I-wave and foot of the finger PPG, and ICG-foot PPG PTT was the time delay between the ICG B-point and the foot of the D-PPG. We then assessed and compared the time delays as markers of BP. Each time delay was calibrated to the BP references using least-square regression and computed the correlation coefficient. Then, we compared the RMSE between the predicted and BP reference levels per subject as an indication of the best-case BP measurement accuracy offered by the time delay.

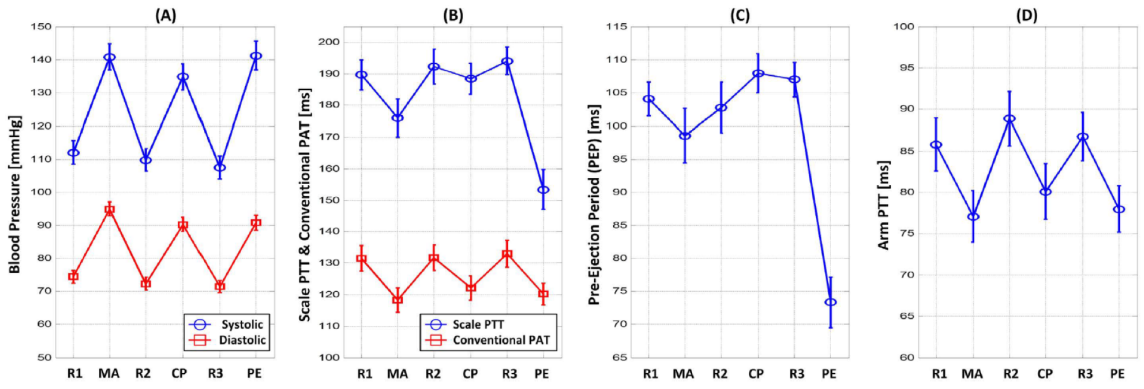

Figure 3.15: Group average ($\mu \pm \sigma$) of (a) diastolic and systolic pressures, (b) scale PTT and Conventional PAT, (c) PEP, and (d) arm PTT for each baseline period and perturbation.

3.5.3 Results

Figure 3.15a shows the group average and standard deviation of DP and SP for three rest and three intervention periods. Each intervention successfully altered BP, increasing by about 20 mmHg for DP and 30 mmHg for SP. Figure 3.15b shows the corresponding group averages of scale PTT and conventional PAT. While both time delays changed in opposite directions, the magnitude of change varied. Scale PTT decreased by similar amounts during each intervention while conventional PAT appeared to under-respond to cold pressor and over-respond to exercise. As seen in Figure 3.15c, PEP may be responsible for the inconsistent changes in conventional PAT. PEP decreased in response to mental arithmetic but increased in response to cold pressor and decreased considerably in response to exercise. Figure 3.15d shows the group average arm PTT. This result indicated that PEP is not singularly responsible for the inconsistent changes in PAT relative to BP, as the arm PTT component did not increase enough from cold pressor to the thirst rest. Smooth muscle contraction occurring during cold pressor could explain why arm PTT under-responded to the third rest since cold pressor is known to cause smooth muscle contraction. However, arm PTT did not over-respond to cold pressor to support the cold pressor hypothesis, though a delayed onset of contraction would explain this finding.

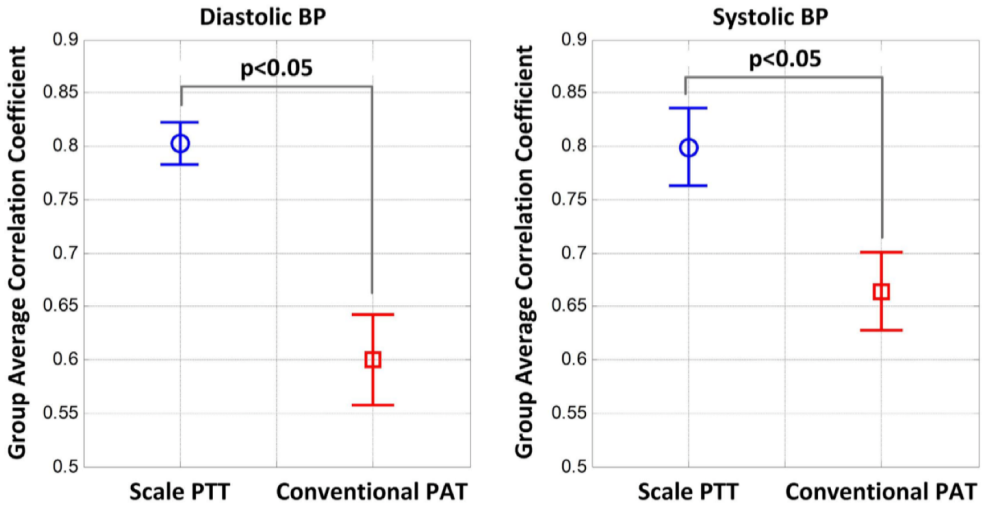

Figure 3.16: Group average correlation coefficients between scale PTT/conventional PAT and BP for diastolic and systolic pressures.

Figure 3.16 shows group average correlations coefficients for scale PTT and conventional PAT when correlated to diastolic and systolic BP. Figure 3.17 shows correlation plots of the best-case calibrated BP predicted by scale PTT and conventional PAT verses cc-Nexfin BP levels and Bland-Altman plots of the errors between the estimated BP and measured BP of all subjects. Scale PTT yielded a good diastolic tracked the diastolic BP changes well with a correlation coefficient of 0.80 $\pm$ 0.02 and a best-case RMSE of 5.7 $\pm$ 0.4 mmHg after calibration. Conventional PTT performed well with a correlation coefficient of 0.60 $\pm$ 0.04 and an RMSE of 7.1 $\pm$ 0.6 mmHg. The elimination of the PEP mitigated the effect of the smooth muscle contraction in scale PTT to improve estimates by 20-33$\%$. With regard to systolic pressure, scale PTT tracked pressure fairly well and better than PAT by 15-20$\%$, though the RMSE only improved by 1.5 mmHg. However, due to the significant improvement in the correlation coefficient when using PTT, the difference between the methods may be more substantial in larger BP ranges. In sum, scale PTT tracked the BP changes with a level of accuracy that was good overall and better than conventional PAT.

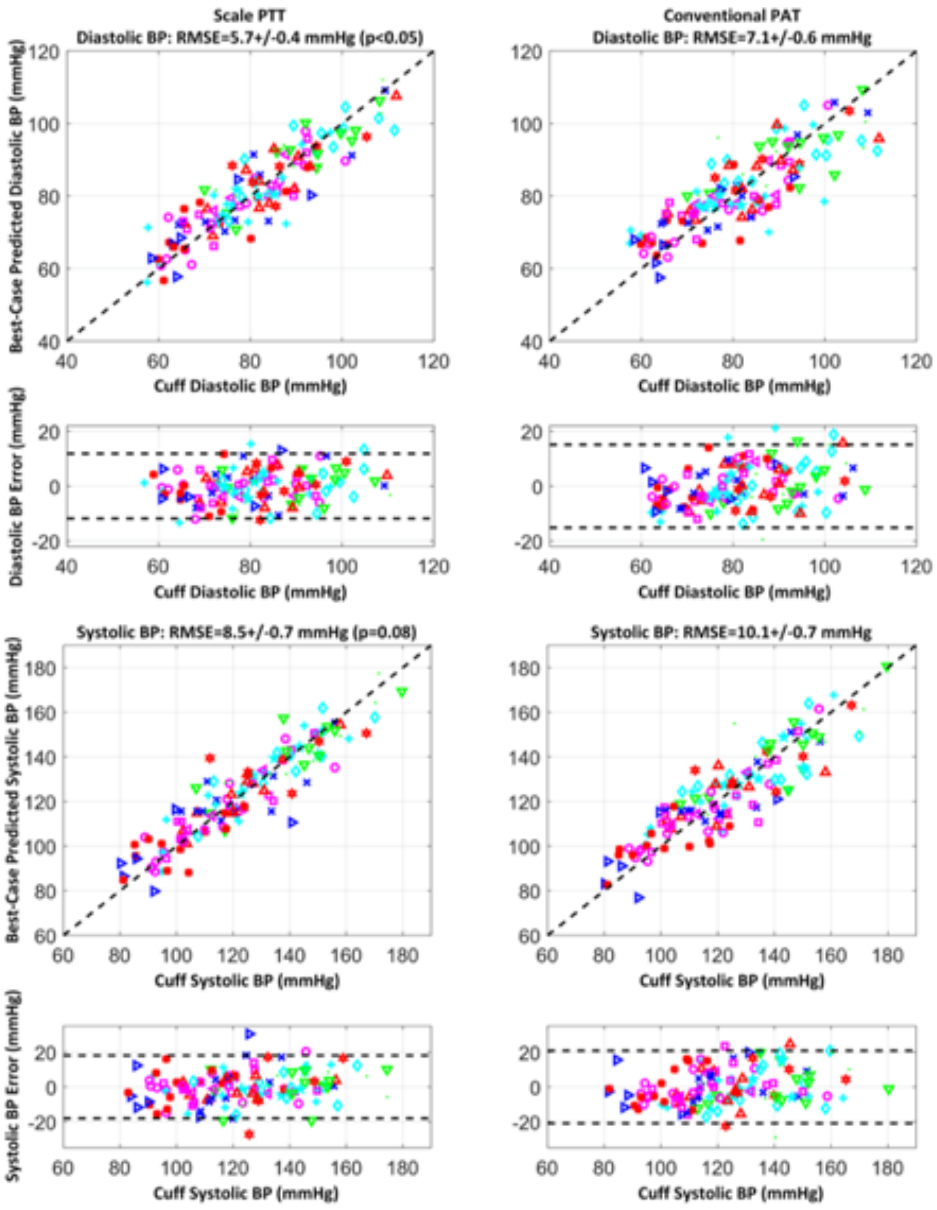

Figure 3.17: Correlation plots of scale PTT and conventional PAT based estimations versus measured BP and Bland-Altman plots of errors.

Finally, scale PTT tended to track BP changes better than arm PTT and similarly to the less convenient ICG-to-foot PPG PTT. Arm PTT and ICG-to-foot PPG PTT yielded a group average correlation coefficient of 0.71 ± 0.04 and 0.79 ± 0.05 with diastolic BP, respectively.

3.5.4 Comparison Between Scale PTT and Conventional PAT

During this study, we measured scale PTT using the BCG from a weighing scale and the PPG from the D-PPG. We compared scale PTT to conventional PAT—the time delay between the ECG and the finger PPG—as markers of BP during a set of interventions that increase BP while changing PEP. The results show a significant increase in correlation when using scale PTT over conventional PAT. When comparing estimations of BP between the two time delays, the elimination of PEP improved BP estimations by 30-50%. As seen in previous sections, scale PTT estimated diastolic BP better than systolic BP, though scale PTT was still an improvement over conventional PAT for both BP references. In sum, scale PTT proved a good tracking of diastolic BP changes whereas PAT did not track diastolic or systolic BP with acceptable accuracy.

Despite wide acknowledgement of its shortcomings, conventional PAT has been employed in most studies of cuff-less BP monitoring due to its convenient nature. However, the convenience of a scale may be comparable to standard measurements recording PAT involving gel electrodes and a finger PPG clip. While many form factors could be more convenient than a scale, such as a wristwatch requiring the placement of the opposite hand on the watch, the substantial improvement in tracking BP may offset any convenience trade-off. Note that, scale PTT can track BP changes similarly to PTT derived with ICG while providing a higher level of convenience.

3.5.5 Conclusion

With such successful future efforts, the system as implemented in the form of an actual bathroom weighing scale could be used for cuff-less BP monitoring at home to facilitate hypertension control. Additionally, PTT measurement could potentially be used for monitoring large arterial stiffness, without the need for calibration. While arterial stiffness is a proven cardiovascular risk factor, current measurement techniques require a tonometer or ultrasound measurement preventing it from becoming a routine clinical measurement. The

convenient scale could thus allow for large artery stiffness monitoring in both a clinic and at home.

3.6 Conclusion and Future Work

We first showed that features extracted from the BCG could be the proximal timing reference for PTT calculations. Unlike the ECG, the BCG indicated the start of the pulse wave propagation through the arterial tree, and thus BCG-based PTT provided superior blood pressure estimation compared to ECG-based PAT methods. We then developed a sensor (D-PPG) to measure the pulse wave at the bottom of the foot to enable scale-based PTT measurements. We showed that this method was superior to commercially available sensors at detecting the arrival of the pulse wave. We further refined the measurement of the pulse wave at the foot by developing an array of sensors in contact with the sole. The array used signal quality and physiological markers to extract the optimal pulse measurements for PTT. Finally, we combined the BCG with the D-PPG to measure *aortic* PTT. We showed significant improvements in BP estimations when compared to conventional PAT methods.

This work demonstrates for the first time the practicality of a scale-based system to track changes in BP. A scale-based system provides many benefits over current timing-based BP monitors. By incorporating monitors in a standard bathroom scale, PTT measurement can occur in conjunction with weight measurements. This could make BP measurements very convenient, especially in subjects with heart failure or in obese subjects where both weight and BP tracking are beneficial for management. Additionally, measuring the BCG and foot PPG allows for aortic PTT measurements, minimizing the impact of smooth muscle activation on PTT and improving the estimations of BP.

Future work should improve the home scale to assess the quality of PTT-based BP estimation in a broader population of subjects with varying demographics. In our studies, we tested the approach in only young and healthy subjects; further testing in older subjects is

needed. Older subjects may have difficulty standing still enough for a valid BCG or PPG measurement. Furthermore, age increases the arterial stiffness, potentially affecting the ability to measure a reliable distal pulse at the foot. Potentially, additional efforts could utilize similar measurement techniques but explore different form factors, such as a shoe. This would allow for measurements to be taken during all still standing activities throughout the day, and remove the requirement to be barefoot.

CHAPTER 4
SEISMOWATCH: A WEARABLE CUFFLESS BLOOD PRESSURE MONITORING

4.1 Introduction

This chapter discusses the device and corresponding study shown in [100]. The method uses a wristwatch form factor, similar to that of fitness monitoring wearable devices currently in the market (Fitbit, Apple Watch, etc.). Our method measures PTT when the user places the face of the watch onto the sternum for a short period of time ($<$ 15 seconds). An accelerometer inside the watch measures the SCG for the proximal timing reference, and PPG sensors facing the wrist measure the distal timing reference. Though the required user input is not conducive for continuous measurements, the device can provide episodic BP estimation as a more convenient alternative to the conventional BP oscillometric cuffs.

4.2 Recording Seismocardiogram and Photoplethysmogram Signals in a Wrist Watch Form Factor for PTT Measurements

4.2.1 Hardware Design

Our prototype system focused on obtaining SCG and PPG measurements to simultaneously detect both the proximal and distal timing reference, respectively. This proposed system was able to obtain, for the first time, both references from the same convenient wearable device and can be used in an at-home setting by performing a simple maneuver. All parts are commercially available, with similar devices being used in current smart watches.

To measure the SCG, we chose the ADXL354 accelerometer (Analog Devices, Norwood, MA) due to its ultra-low noise floor (20 $\mu g/\sqrt{Hz}$). A low noise floor accelerometer was needed since the SCG signal amplitude is small, typically around 10mg to 50mg peak

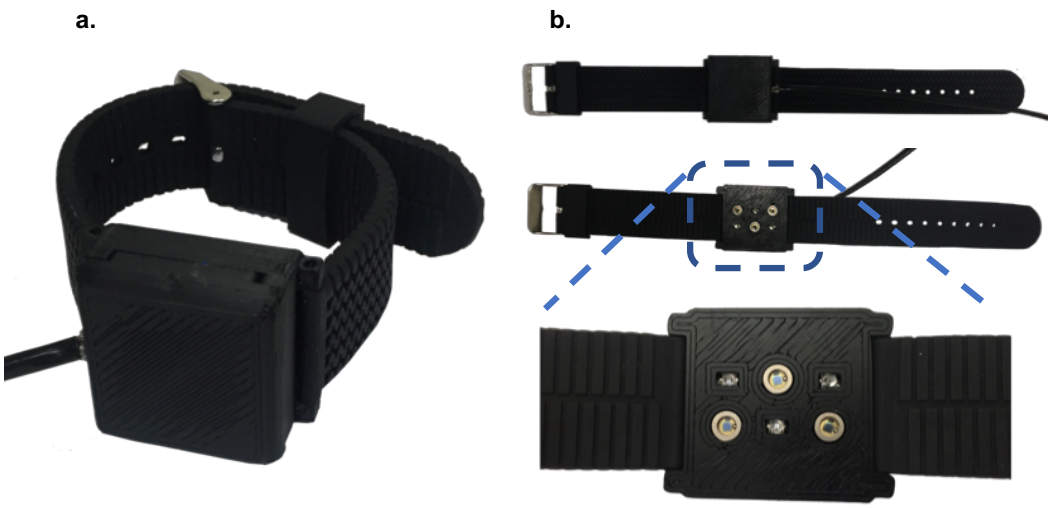

Figure 4.1: (a) Isometric view of the watch. (b) Views of the watch showing positions of the accelerometer, photodiodes and IR LEDs.

to peak. The Apple Watch (Apple Inc, Cupertino, CA) uses the BMA 280 (Bosch, Stuttgart, Germany) with a noise level of 120 $\mu g/\sqrt{Hz}$ or an average peak to peak of 5 mg peak to peak. This noise would couple into the SCG and make feature extraction difficult. The ADXL354 limits the noise to only 0.8 mg peak to peak and reduces the noise in the SCG signal.

SeismoWatch consisted of an array of three IR LED and photodiode pairs. While most wrist-based heart rate monitors (including the Apple Watch) use green LEDs to maximize signal quality for heart rate extraction, IR LEDs allowed for deeper penetration into the skin and for the capture of the arterial pulse wave from the larger arteries. We biased the cathode of the photodiode to 5V to increase the sensor's linearity and connected the anodes to a transimpedance amplifier configured to act as a first-order low-pass filter (f_c = Hz, G = 110 dB) followed by a band-pass filter (BW = 0.7 - 8Hz, G = 20 dB). A potentiometer in series with the LEDs allowed for manual subject-specific calibration of the LEDs light intensity. After visual inspection of the signal during the study, we altered the light intensity, accounting for differing melanin levels or arterial depths.

We designed a custom 3D printed watch to house the accelerometer, photodiodes, and

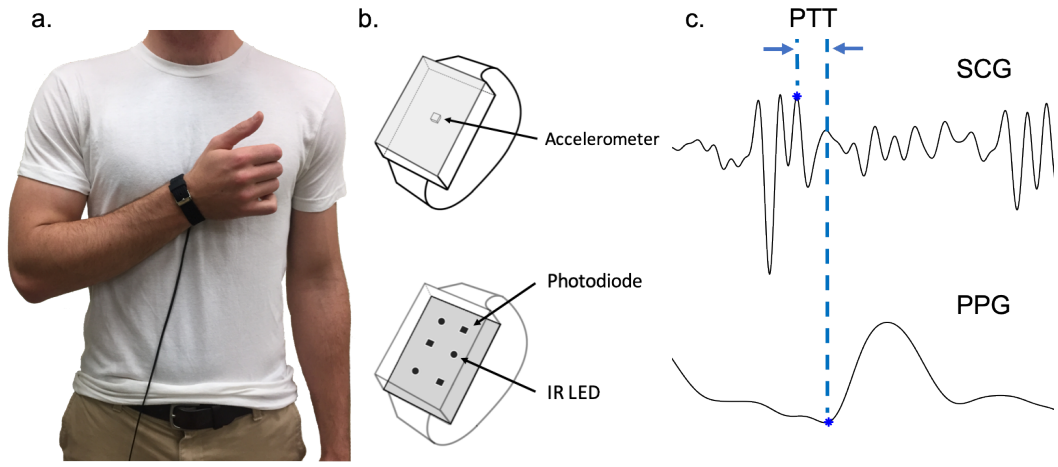

Figure 4.2: (a) Subject position to obtain seismocardiogram (SCG) and reflectance photoplethysmogram (PPG) recordings from the watch. (b) An accelerometer was placed in the inside of the watch and pairs of photodiodes and IR LEDs faced towards the wrist. (c) Representative SCG waveform from the sternum and PPG waveform from the wrist as the subject performed the maneuver. PTT was then calculated by using the AO point on the SCG and the foot of the PPG.

IR LEDs. The watch was tethered to an external box that housed the power supply and AFEs. The backside of the watch that made contact with the wrist included three cutouts approximately 1 cm apart to expose the pairs of photodiodes and LEDs. The spacing allowed for adequate coverage of the wrist and increased the chance of sensing the radial artery.

4.2.2 Human Subject Studies

To obtain a PTT measurement, the user first rotated the watch to the anterior portion of the wrist, ideally toward the lateral side. This positioned the LEDs above the radial artery. The user then placed the top face of the watch on the body of the sternum, above the xiphoid process. In this position, the accelerometer measured the low-frequency thoracic vibrations represented by the SCG while the PPG measured the pulse wave at the wrist. Consequently, the maneuver increased the contact pressure of the PPGs, improving the coupling between the PPGs and skin and increasing the signal quality.

We ran multiple studies to test the robustness and accuracy of the prototype. The Georgia Institute of Technology IRB approved all studies, and all subjects provided written informed consent before any studies were begun. In total, we recruited thirteen young and healthy subjects with no history of cardiovascular diseases (age: 23 ± 3; gender: 8 males, 5 females; weight: 68 ± 16 kg; height: 173 ± 10 cm). To acquire a timing reference for the start of a cardiac cycle, the subject wore standard gel electrodes and a wireless ECG module (BNEL50, Biopack Systems) to measure Lead II ECG. A finger-cuff BP sensor (ccNexfin, Edwards Lifesciences) placed on the hand contralateral to the watch acquired continuous beat-by-beat BP. An MP150 Data Acquisition system (Biopac Systems) sampled all sensors at 2 kHz and stored the data to a desktop computer for post-processing.

We performed three studies to test the device. For all the studies, we asked the subject to remove coats or other bulky clothing. The first study established a proof-of-concept and an ideal-case correlation between PTT and BP with all thirteen subjects participating. This protocol consisted of three sections: one-minute rest, one-minute exercise, and five-minute recovery. During the rest and recovery periods, the subject sat in a chair with the ccNexfin placed on the left index finger and the watch on the right wrist. During the exercise portion, we removed the watch to prevent damages, and the subject performed a stair stepping exercise.

Eight of the subjects returned for a follow-up study to test the multi-day repeatability of the PTT and BP correlations. This protocol consisted of two sections: one minute-rest and one-minute cold pressor. Cold pressor replaced exercise as the perturbation to test out the correlation curve under conditions that induced different physiological responses. Traditionally, a cold pressor test involves the subject immersing a hand in a bucket of cold water; however, to allow measurements on both hands and to prevent varying localized BP, each subject placed his / her foot in a bucket of cold water.

The final study tested the robustness of the SCG signal on five of the subjects for use in an at-home, unsupervised setting. We tested contact pressure and sensor location as

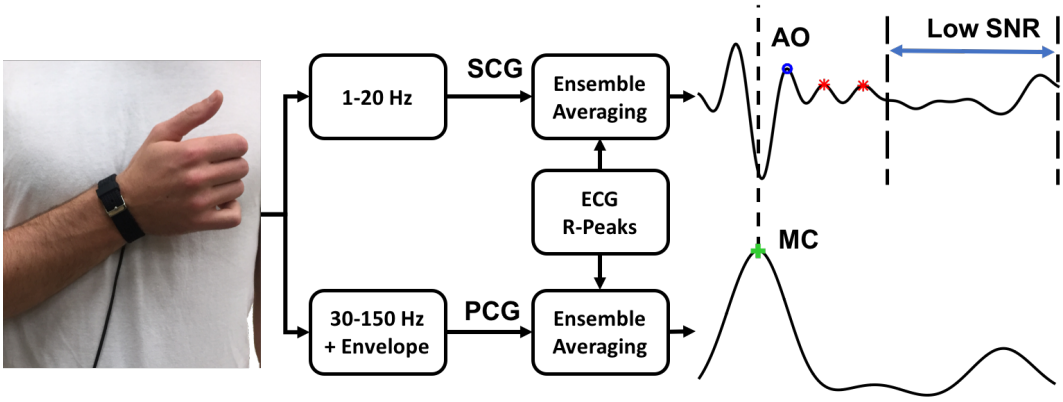

Figure 4.3: Block diagram of signal processing technique to extract the AO peak using both the SCG and the PCG signal.

they are possible sources of user errors that could occur in a home setting. The subject performed the maneuver and varied the amounts of contact pressures against the sternum, ranging from a light touch to a hard press. Then, the subject placed the device on varying locations on the chest while maintaining a constant pressure.

4.2.3 Signal Processing

Post-processing techniques on the accelerometer, PPG, and ECG extracted proximal and distal timing references for PTT. Note that the ECG was selected for its high signal quality and simply used in this study as a fiduciary point to validate the other sensor measurements and would not be required in the actual deployment of the device for home use. Similar techniques to the method used for the sole PPG, as described in Chapter 2, could extract the beats without the ECG. One of the technical challenges of the SCG signal is the variability in morphology between subjects and its susceptibility to motion artifacts and respiration-induced waveform distortions. Classical models of the SCG denote the AO as the highest peak immediately following the R-wave of the SCG [101]. However, by this simple method, the MC and AO can sometimes be confused with each other even in healthy subjects [102].

Figure 4.3 depicts the method of locating the AO in this work. To determine the correct waveform, we utilized both the SCG and the PCG from the accelerometer signal. A digital filter (BW = 0.8Hz - 30Hz) applied to the accelerometer signal extracted the SCG while a higher band filter (BW = 30Hz - 150Hz) extracted the PCG. Note that the PCG in this study was identical to the signal obtained using a digital stethoscope, as the accelerometer acted as a contact microphone. Spline interpolation of the local PCG peaks produced an amplitude envelope. Using the timing of the R-wave, we partitioned the SCG and the enveloped PCG into individual beats and ensemble averaged thirty beats together. Since the PCG is commonly used to identify the closing of the mitral valve, we considered the AO to be the first maximum of the SCG that follows the maximum PCG envelope point. We assumed the AO point to be the maximum that directly follows the MC. This technique can only be used during exercise, due to the shortening of PEP cause the MC and AO to occur in rapid succession. However, PEP should only move the timing of AO point and the waveform following the AO point, including the residual peaks, should be retained. To find the AO point in non-exercise signals, we first mapped out all peaks in the exercise signals and found the SNR of a 50 ms window around each peak. To find the SNR, we used the pre-ensembled average beats and the same technique as described in Chapter 2. We counted the number of peaks between the AO point and the first peak of low SNR. We applied this count to future SCG beats, counting backward from the first peak with low SNR, to determine the AO.

To extract the foot of the PPG for the distal timing reference, we first manually determined the highest quality PPG signal. A digital band-pass filter (BW = 0.8Hz - 15Hz) removed out of band noise. An average of thirty beats removed non-periodic noise. The intersecting tangent method then determined the foot of the PPG. The PTT was then simply the difference between the found AO of the SCG and the foot of the PPG.

Table 4.1: Subject Data

Subject	μDP [mmHg]	RMSE [mmHg]	R	e $<$ 5 mmHg	e $<$ 10 mmHg
1	80 ± 10	3.06	0.95	0.85	1.00
2	81 ± 4	2.29	0.77	1.00	1.00
3	76 ± 4	2.45	0.74	0.94	1.00
4	73 ± 5	2.73	0.80	0.94	1.00
5	80 ± 4	1.42	0.93	1.00	1.00
6	61 ± 3	1.56	0.69	1.00	1.00
7	60 ± 5	2.32	0.88	1.00	1.00
8	76 ± 3	1.41	0.89	1.00	1.00
9	85 ± 10	6.12	0.76	0.72	0.94
10	78 ± 5	1.71	0.92	1.00	1.00
11	73 ± 6	1.67	0.95	1.00	1.00
12	77 ± 6	3.37	0.81	0.83	1.00
13	88 ± 5	2.64	0.85	1.00	1.00
μ	76	2.52	0.84	0.95	1.00
σ	10	1.25	0.09	0.09	0.04

4.2.4 Results

1) Assessing Correlations Between Wearable PTT and BP

Figure 4.4 illustrates the correlation plot and Bland-Altman plots after a best-case calibration of BP based on PTT for MAP, DP, and SP. The RMSE was simply the root mean square of the difference between the PTT estimated BP and the measured BP. The group RMSE for MAP, DP, and SP was 3.2 mmHg, 2.9 mmHg, and 4.8 mmHg, respectively. DP estimations resulted in the best confidence interval (95%) at 5.8 mmHg. SP estimation proved to the least accurate, with the highest RMSE and a confidence interval at 9.7 mmHg. This result is consistent with physiological expectations since the foot of the PPG waveform represents distal pulse arrival which occurs during diastole rather than systole.

Table 4.1 summaries the individual results of the thirteen subjects when a best-case calibration curve converted PTT to BP. DP formed the lowest error and thus used for further evaluation. μDP was the average diastolic pressure, RMSE was the root mean square error,

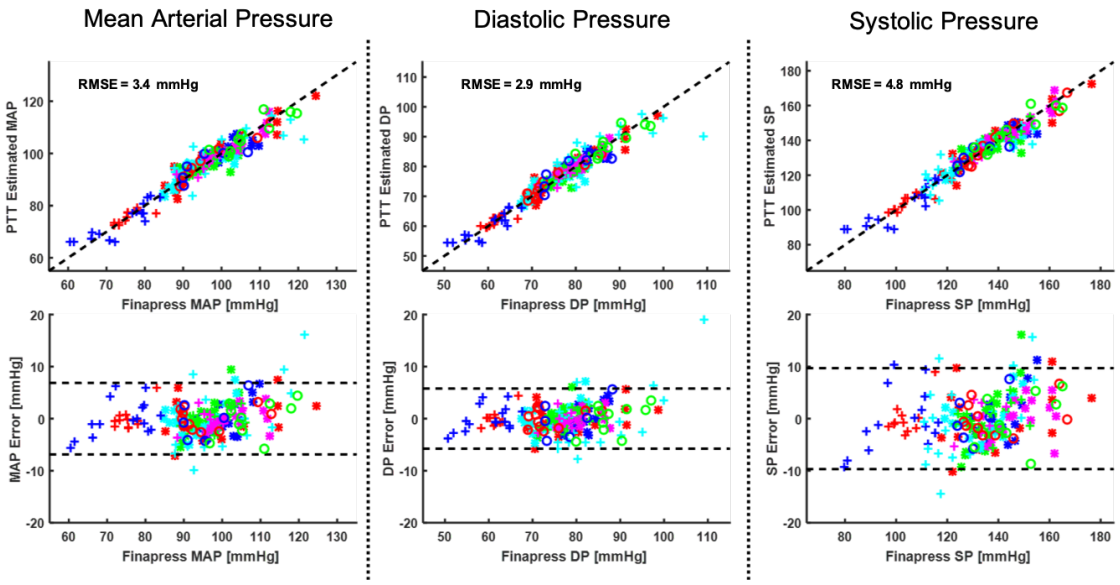

Figure 4.4: Correlation and Bland-Altman plots for mean arterial pressure (MAP), diastolic pressure (DP), and systolic pressure (SP)

R was the correlation coefficient, e $<$ 5 mmHg was the ratio between estimations less than 5 mmHg error to the total number of estimations, and e $<$ 10 mmHg was the same ratio but with 10 mmHg of error. Individual RMSE was less than 5 mmHG for twelve of the thirteen subjects. BP estimation errors were below 5 mmHg in eight subjects. Only one subject of the thirteen had a BP estimation error exceeding 10 mmHg.

2) Quantifying Day-to-Day Repeatablity in BP Estimation

Figure 4.5 depicts the follow-up study testing the day-to-day repeatability of the watch with MAP, DP, and SP estimated with PAT and with PTT. To note, we calculated the calibration curves of PTT and PAT to BP using data from the first protocol and applied the respective curves to PTT and PAT values measured during the follow-up study. During rest, PTT-based BP estimations significantly improved both MAP and DP when compared to PAT-based estimations ($p < 0.02$ and $p < 0.005$, respectively). During rest, BP estimations improved by an average of 12.3 mmHg when using PTT-based estimations over PAT-based estimations. All eight subjects had MAP and DP estimations within 5 mmHg

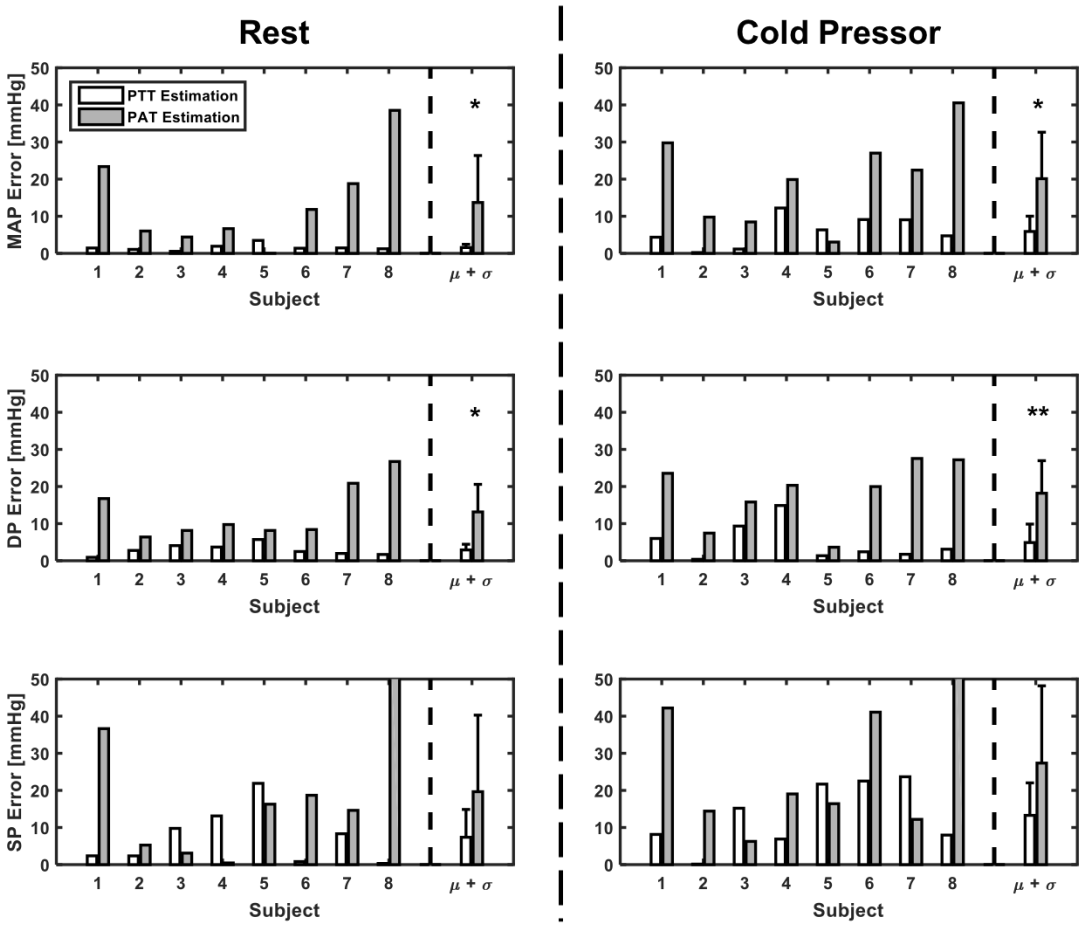

Figure 4.5: Comparison between PTT and PAT during both rest and cold pressor. * indicates $p < 0.05$, ** indicates $p < 0.01$

of their measured BP levels when using PTT. While the best-case BP using PAT produced less than 1.0 mmHg error, three of the eight estimations produced errors of more than 15 mmHg, rendering the measurements not sufficiently accurate for clinical use. DP had a similar comparison. BP estimations improved by an average of 13.9 mmHg with only one subject greater than 5 mmHg error (e = 5.7 mmHg). In contrast, SP estimations were poor. Though PTT calibration produced errors that were, on average, 12.3 mmHg lower than PAT estimation, no significant difference existed between the two estimations ($p > 0.05$).

During the cold pressor test, PTT significantly improved both MAP and DP estimations compared to PAT ($p < 0.01$ and $p < 0.005$, respectively). However, PTT-based BP estimations worsened when compared to rest values, averaging 6.3 ± 4.1 mmHg error for MAP

and 5.0 $\pm$ 5.0 mmHg error for DP. Though there was a decline in performance during this perturbation, BP estimation errors were still substantially lower than estimation using PAT which had an average error of 20.1 mmHg for MAP and 18.2 for DP. At the resting phase, the SP estimations were not within an acceptable error. Estimations yielded an average of 13.3 mmHg when using PTT and 27.4 mmHg when using PAT.

3) Determining Variability in SCG Signal Quality for Unsupervised Settings

Varying the watch in different locations and contact pressures tested the robustness and reliability of the watch in at-home scenarios when trained personnel are not available to supervise. The three contact pressures resulted in similar SCG signals, and the AO peaks only deviated an average of 3.2 ms, well within the normal variability of PEP. Qualitatively, the signal had similar morphology regardless of contact pressure, exhibiting comparable numbers and relative amplitudes of peaks and troughs. However, varying the locations affected the SCG, changing the morphology of the signal based on the location. When the contact area was at the bottom of the sternum, between the sternal angle and the xiphoid process, the signal was consistent and reliable. Positioning the watch above this section distorted the signal, and the AO peak deviated as much as 85%. Furthermore, locations away from the sternum, such as on the softer tissues of the pectoral muscles, resulted in a misclassification of the AO peak. To obtain a reliable SCG signal, the subject will need to place the watch face on the lower portion of the sternum, which should be feasible even in unsupervised settings. Fortunately, methods exist that use classification algorithms to automatically detect when SCG sensors are in any position other than the desired one. Users can be notified of improper placement and to change position [65]. Finally, the presence of light clothing seemed to have little effect on the quality of the signal as the direct skin contact and contact with a light clothing layer produced similar SCG signals.

4.2.5 Reliability of the Watch as a BP Monitor

This work presents a device that showed promise in being able to conveniently obtain BP measurements outside of clinical settings. A strong correlation between BP and PTT obtained from the timing references derived from an SCG and PPG existed for MAP and DP. While SP did not follow as strong of a trend, this is consistent with previous studies.

When compared to estimations using PAT, the watch showed a significant increase in accuracy. The addition of the accelerometer to measure SCG as the proximal timing reference for PTT proved to be superior to using the ECG as the proximal reference for PAT during rest. While ECG has the advantage of a higher SNR, the confounding effect of PEP negatively impacted MAP and DP estimation. In this study, exercise during the calibration phase had a large effect in shortening the PEP. After exercise, cardiac contractility returned to baseline while BP decreased relative to baseline due to exercise-induced vasodilation [103]. Thus, exercise recovery changed BP and PTT proportionally more than PEP. This corrupted the PAT-based calibration curve and led to an underestimation of BP during the follow-up study when BP and cardiac contractility returned to a baseline. In conditions that greatly vary BP but have little effect on PEP, BP estimation with PAT will be poor, and such conditions are common during normal daily living activities.

When analyzing the results, we found an increase in error for both PTT and PAT-based estimations during the cold pressor when compared to rest, presenting a potential limitation to the current system. SeismoWatch measured the pulse wave as it travels through the brachial artery, and the presence of smooth muscle in this arterial path could have accounted for the increase in error between rest and cold pressor. Cold pressor modulated vasomotor tone independent of blood pressure, changing the arterial stiffness and affecting PTT. Though this error occurred, current standards for blood pressure monitoring recommend subjects take measurements at room temperature. Abiding by these recommendations will minimize the impact of the vasomotor tone on PTT.

In this version of the SeismoWatch, the average power consumption was 360 mW.

While this would be difficult to sustain for long periods of time using an average smart watch battery, only a few seconds of measurements were sufficient to obtain a PTT. During the follow-up study, we only processed ten beats, resulting in an average recording time of 8.7 seconds. In future iterations, we were able to minimize power consumption by allowing the user to start the measurement. If there is a need for longer measurements, power consumption could be substantially improved by lowering the output intensity of the LEDs with varying current amplitude or duty cycles. Alternatively, the system could decide on the highest quality LED and turn the other two off.

Compared to a blood pressure cuff, SeismoWatch's form factor and measurement procedure were more convenient. During the study, we gave to the subject only basic instructions on how to operate the watch. We instructed them on the proper placement of the device before the protocol started, and they were successfully able to repeat the maneuver during the entire protocol. BP cuffs, on the other hand, are susceptible to positioning, cuff size, obesity level, and other user errors that would result in inaccurate readings [104].

Additionally, the subjects could perform the maneuver for five minutes while taking multiple consecutive readings ($>$10) without a loss of quality in either the SCG or PPG. The readings were independent of each other, with a measurement having little to no effect on PTT or BP. This would be difficult to achieve with a BP cuff since it is recommended to have one-minute in between successful measurement to prevent the inflation of the cuff, and subsequent occlusions of the artery, from changing the BP at the site of measurement. Thus, dynamic changes in BP in response to stressors such as exercise or mental stress can more readily be quantified with our approach.

4.2.6 Conclusion

This work explored the feasibility of using a watch-based wearable device to estimate BP based on PTT. We conducted a study to first establish a strong correlation between watch PTT and BP. A follow-up study tested the consistency of the device and compared the

watch PTT method to a PAT method that is commonly used. The results show a significant improvement while using SeismoWatch compared to the PAT method. This work established a method of extracting BP that is both convenient and robust enough for at-home usage.

4.3 Modification for Ambulatory Measurements

4.3.1 Hardware Design for Home Monitoring

A significant drawback to SeismoWatch was the lack of portability. In the design previously described, the various sensors in the watch needed to connect to an external AFE and a subsequent DAQ. Consequently, the watch was limited to lab studies, and home monitoring was not practical. To combat this limitation and allow the watch to be used outside the lab, we created SeismoWatch 2.0. This work was a collaborative effort between Venu Ganti, Brandi Nevius, and Caitlin Teague of the Georgia Institute of Technology and Alex Heller and Dr. Mozziyar Etemadi of Northwestern Medicine. The author of this thesis contributed to the structural design of the watch and the firmware, led the design and validation of the heardare, and planned and executed the initial tests.

We refined the design to incorporate all sensors inside the main body of the watch, removing any need for external components and including an on-board microcontroller, making the watch truly portable. Additionally, to allow for further assessment of cardiac health, we included an ECG, sternum PPG sensors, gyroscope, and environmental sensor. The ECG sensor allows for easy partitioning of the heart beats and can be used to assess the heart rate variability (HRV) to determine autonomic states [105]. To capture sternum PPG, we placed three additional PPG sensors to the top side of the watch to measure the sternum's pulse wave while the user performs the same maneuver needed to capture the SCG. The sternum PPGs will provide an additional timing reference for PTT calculations. We included a gyroscope to sense the gyrocardiogram (GCG) signal. Previous work noted a reduced error when using the GCG in combination with SCG to predict the PEP [106]. The

environment sensor measures the temperature, relative humidity, and barometric pressure, adding an aspect of activity context for improved physiological interpretations.

The complete design features three stacked printed circuit boards and a 150 mAh lithium-ion battery inside of a custom 3D printed case. From the backside of the watch—closer to the wrist when worn—to the topside, the boards and battery are stacked in the following order (Figure 4.6b): wrist PPG/ECG board, main board, battery, and finally, sternum PPG board. The case includes three slots on both the top and bottom portion to expose the PPG sensors.

For the microcontroller, we chose the ATSAM4LS8B (Microchip Technology, Chandler, AZ) for its large amount of storage (512kBytes Flash, 64kBytes RAM), high number of peripheral options (48 GPIOs, 4 USART), and ultra-low power consumption (1.5 μA sleep mode). We removed the custom AFEs used in the previous iteration and selected sensors with internal AFEs to reduce the number of components and power consumption. Additionally, we chose to not use on-board ADCs due to the relatively high noise and low bit conversion compared to external ADCs. Instead, we selected sensors that included an ADC. This allowed for a completely digital interface and allowed the sensors to independently make conversions, freeing up processor time on the microcontroller. We also chose sensors that interface via SPI, due to the fast clock speeds (12 MHz).

The various components on each of the boards can be seen in Figure 4.7. The main board contains much of the hardware for the watch, including the microcontroller. Additionally, the board includes the charging circuit, accelerometer, gyroscope, environmental sensor, SD card, and various connectors to the other components. For the accelerometer, we selected the digital version of the ADXL354, the ADXL355 (Analog Devices). The ADXL355 has a noise floor at 25 $\mu g/\sqrt{Hz}$, comparable to the 20 $\mu g/\sqrt{Hz}$ of the ADXL355. Additionally, the ADXL355 has a 20 bit ADC with a full-scale range of 3.3V, a drastic improvement over the MP150's 16 bit ADC over a 20V range. To measure the GCG, we chose the BMG250 (Bosch) due to the low output noise (0.007 $^\circ/\mathrm{s}/\sqrt{Hz}$. The

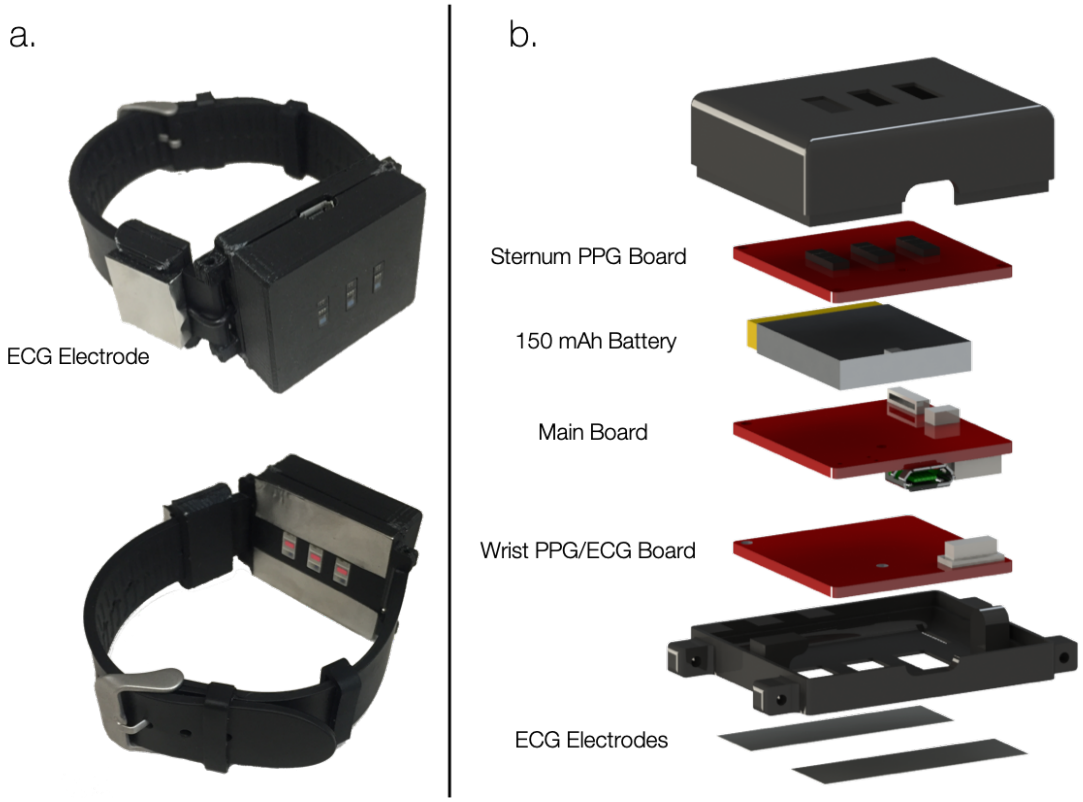

Figure 4.6: (a) SeismoWatch 2.0. (b) The inside of the watch contains three PCBs and a 150 mAh lithium-ion battery. A stack connector connects the main board to the wrist PPG/ECG board. The sternum PPG board and the wrist PPG/ECG board snap into the 3D printed case. Stainless steel electrodes placed on the back of the watch and the wristband allow for ECG measurements.

main board also includes the BME280 (Bosch) that features a small package size (2.5mm x 2.5mm), low current consumption (3.6 μA), and low noise floor of the pressure sensor (0.2 Pa RMS). The microcontroller stores data on an on-board SD card at a write speed of 12MB/s.

The wrist PPG/ECG board, as the name implies, contains both the wrist PPG and ECG circuit. On the back side of the board are three SFH7072s (Osram, Munich, Germany) with each containing a green, red, and infrared LED and two photodiodes. One of the photodiodes blocks red and IR wavelength, improving the detection of a green wavelength, while the second photodiode has a peak sensitivity around the red and IR wavelength. Measurements of PTT would utilize the red and infrared detectors to monitor the deeper arteries.

The high-SNR green detector could constantly measure heart rate when the user is not taking a PTT measurement and indicate physiological states between PTT measurement. Each SFH7072 interfaces with a MAX86141 (Maxim Integrated, San Jose, CA) to drive the LEDs and to read the current output of the photodiodes. This board also includes the ECG circuitry where we selected the ADS1291 (Texas Instruments, Dallas, TX) due to the low-noise (8 μV_{pp}) and high-resolution ADC (24 bit). The ADS1291 connects to three dry stainless steel electrodes. For the negative reference and the right leg drive, two electrodes are placed on the backside of the watch to make contact with the wrist. We placed a third electrode for the positive reference on the outside of the wristband. The user simply touches the electrode with the opposite hand while taking a measurement. Additionally, the ADS1291 includes a lead-off detection that constantly monitors the connection to the body. This feature allows the user to initiate a measurement by touching the wristband electrode.

The remaining board, the sternum PPG board, contains three pairs of SFH7060s (Osram) and MAX86140s (Maxim Integrated). We selected the SFH7060 over the SFH7072 due to the increased area of the photodiodes, increasing the total sensitivity and compensating for the decreased perfusion at the sternum when compared to the wrist. Since the SFH7060 only includes a single photodiode, we selected the one-channel MAX86140.

The ECG is sampled at 1kHz, the accelerometer and gyroscope are sampled at 500 Hz, the enviromental sensor is sampled at 33 Hz, and each PPG sensor is sampled at 333Hz, and the data is temporarily saved to the SD card. The watch interfaces with the computer through a microUSB port on the main board and is accessible through a cut-out in the case. The HeartPulse App (Department of Anesthesiology, Northwestern Medical, Chicago, IL) communicates with the microcontroller to pull and subsequently delete data on the SD card, freeing up space for future measurements. Additionally, the inserted microUSB interfaces with a battery charger (BQ24232RGTR, Texas Instruments) to charge the battery.

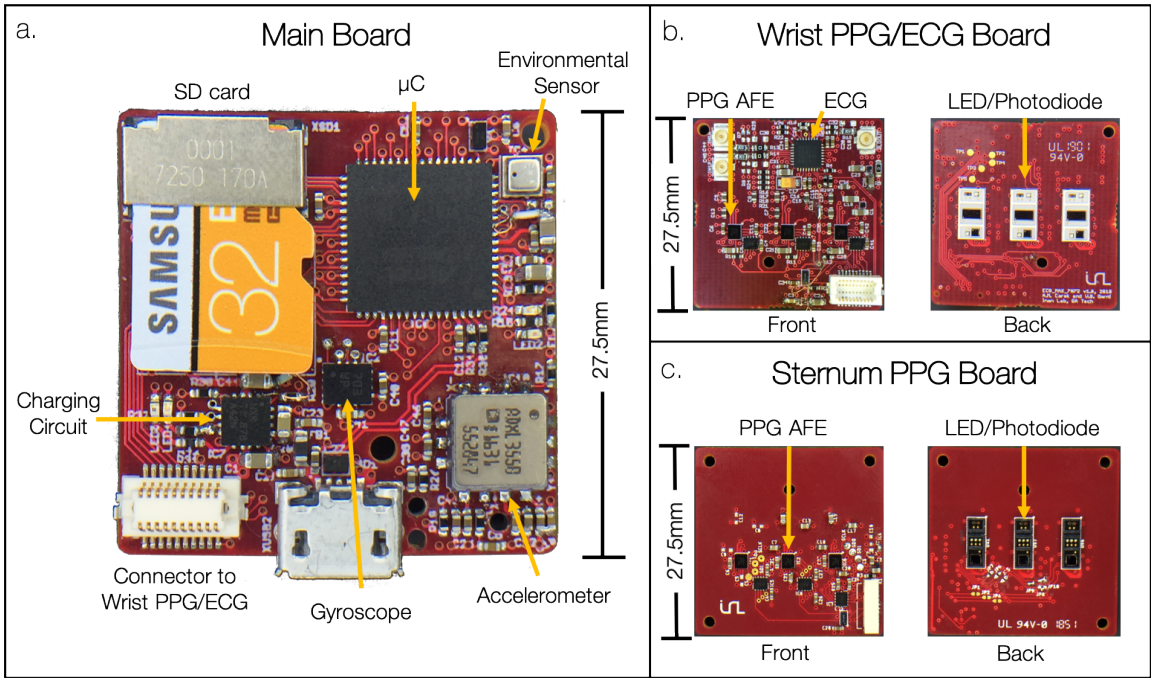

Figure 4.7: (a) Main board that includes the ATSAM4LS8B microcontroller, ADXL355 accelerometer, BMG250 gyroscope, BME280 environmental sensor, SD card, charging circuit, and connectors to the daughter boards. An on-board microUSB port allows for data transfer and battery charging. (b) The wrist PPG/ECG board with three pairs of SFH7072 photodiodes/LEDs and MAX86141 AFEs and the ADS1291 ECG AFE. (c) Sternum PPG board with three pair of SFH7060 photodiodes/LEDs and MAX86140.

4.3.2 Device Operations

We designed the watch to operate in three modes: standby, continuous, and PTT measurement mode. During standby mode, all sensors on the device are shut down except for a PPG on the wrist, and the watch waits for an interrupt from a PPG which was configured to act as a proximity sensor. When an object approaches the sensor, as when the user places the watch on the wrist (Figure 4.8b), an interrupt flag is set, and the watch transitions to continuous mode. During this mode, the green PPGs, accelerometer, and gyroscope are active and sample at 125Hz. The environmental sensor is also turned on and samples at 4 Hz. The lower sample rate saves power while providing enough context for activity classification.

The watch transitions to PTT measurement mode when the ECG senses a lead-on event. When wearing the watch on the wrist, the user will need to touch the wrist-band electrode

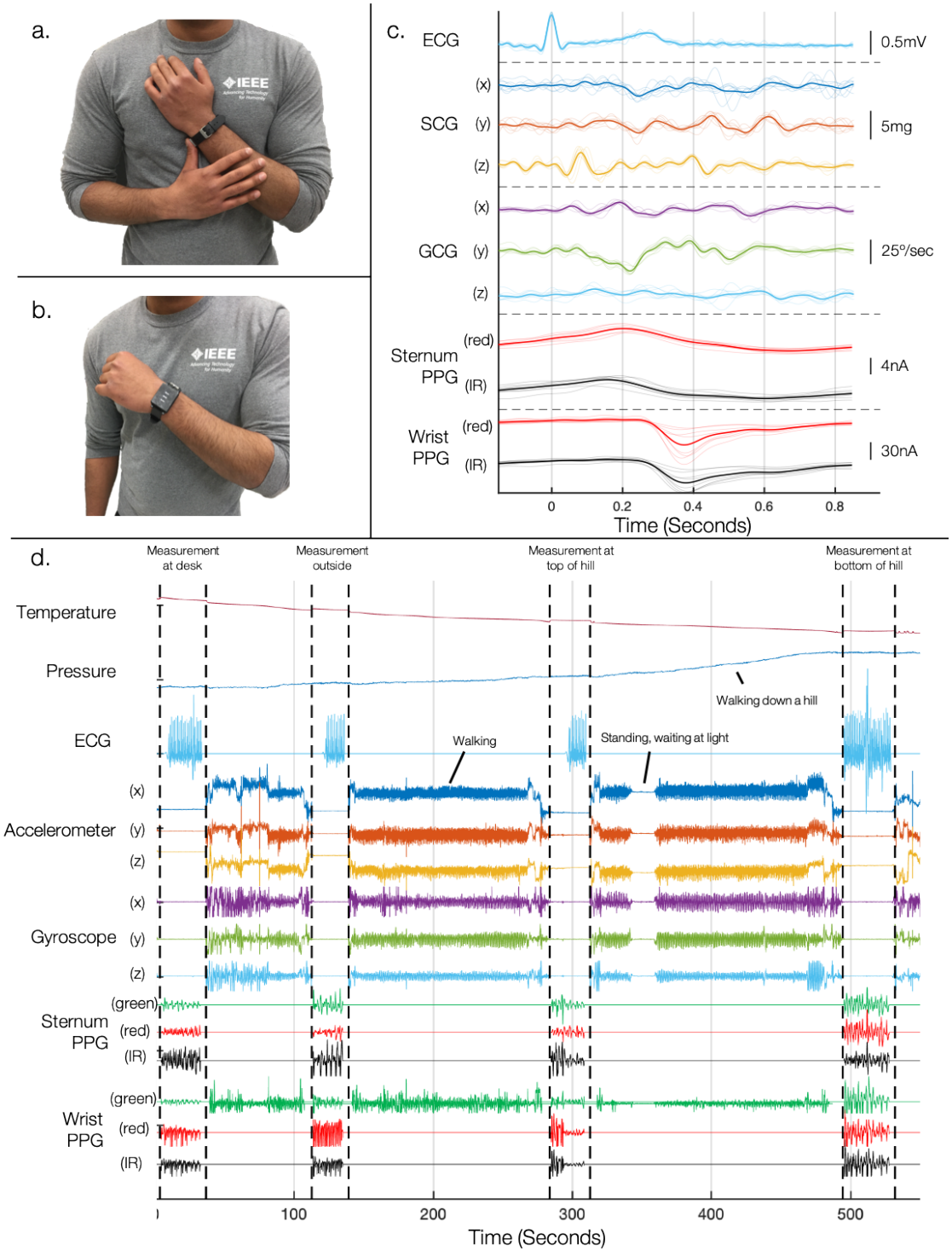

Figure 4.8: (a) To take a complete measurement, subjects place a finger or thumb on the wrist electrode. (b) When there is no contact with the electrode and watch is on the wrist, the watch reduces power by lowering the sample rate and only turning on certain sensors. (c) Ensemble averaged waveforms from a single 30-second recording. (d) Recordings during a 10-minute walk outside where 30-second measurements were taken four times.

with hand contralateral to the watch (as seen in Figure 4.8a). During this mode, all sensors are sampled at the full rate as previously described. Figure 4.8c shows the ensemble average of the ECG, SCG, GCG, and PPG, during a 30-second recording while the watch was operating in the PTT measurement mode.

Figure 4.8d shows the recordings of all sensors during a 10-minute walk outdoors. When the user touched the wrist electrode, the watch successfully transitioned to PTT measurement mode, increasing the sample rate and sampling from all sensors. When the finger was removed, the watch returned to continuous mode, decreasing the sample rate and only sensing from sensors that give activity context for determining physiological states. Configuring the watch to transition between these modes reduces power consumption, reduces memory needs, and indicates timings of PTT measurements.

4.4 Conclusion and Future Work

In this chapter, we developed a watch-based system to measure PTT after recording the SCG at the sternum and PPG at the wrist during a simple maneuver. We tested the device over different days and showed an improvement in BP estimation over wrist-based PAT methods. We then modified the design, including additional sensors for improved hemodynamic tracking during normal daily living activities. We removed the need for external components and made SeismoWatch completely portable with a similar form factor to commercially available smart watches.

The primary limitation of the SeismoWatch is the need for a cuff-based BP measurement for calibration during the first use and periodical updates to account for slow changes in arterial stiffness. Potentially, a solution would be to leverage posture-induced changes in hydrostatic pressure to calibrate the watch. The subjects would adjust their arms to a specific height above and below the heart, varying the hydrostatic pressure in the arteries. Both BP and PTT would change, and calibration would be possible. This method requires an ECG and SCG to measure PEP which would be assumed to remain constant during the

remaining maneuvers. Then, by measuring the PAT at various levels using the ECG and PPG, it is possible to derive changes in BP and PTT for calibration. A BP cuff reading would still be necessary for the initial calibration. Future work will be needed to validate this proposed work.

Another drawback is that the user is constrained to perform the maneuver while static. The system requires direct contact to the sternum by the watch due to the SCG's low signal and poor coupling to the rest of the body. This factor prevents the user from continuously monitoring PTT during sports or other high motion activities. However, current cuff-based systems are also constrained in the same way to static measurements only. Though PTT cannot be constantly monitored, the green wrist PPGs and inertial sensors can continuously record heart rate and activity levels. These sensors would determine the optimal time to take a measurement, such as periods of high heart rate or high activity, and the watch can indicate to the user to take a reading.

Future work will also be needed to validate SeimsoWatch 2.0. First, lab-based studies should determine the impact of adding the gyroscope in the detection of the AO. Using data from multiple days and various perturbations, supervised learning techniques could estimate the AO based on features of the accelerometer and gyroscope [106]. Furthermore, improvements in the portability enable studies in subjects during normal activities of daily living that are necessary to assess the robustness and the ability to measure PTT in an unsupervised setting.

CHAPTER 5
CONCLUSION AND FUTURE WORK

5.1 Conclusion

Hypertension is a major health care concern afflicting nearly half of the US population. To exacerbate matters, hypertension is the leading risk factors for cardiovascular diseases, the number one cause of death worldwide. Cuff-less home monitoring solutions for estimating BP would potentially allow for improved detection and management of hypertension. Physicians would then be able to properly identify the patient's needs and develop patient specific strategies to combat the disease.

In this thesis, we developed techniques to measure PTT, a potential alternative to the cuff. We first modified a scale to measure PTT. We validated the BCG as a proximal timing reference and created sensors to extract the distal timing reference at the foot. We refined the distal sensor to extract multiple pulse signals and automatically select the signal of larger arteries that are more correlated to BP. We established scale PTT as a improvement over PAT-based systems at estimating BP. We then developed a PTT monitoring device in a watch form factor. We showed that the watch is able to extract timing references by simultaneously measuring the SCG and PPG at the wrist. We again showed an improvement of this system over conventional PAT-based systems. We improved this device, allowing for portable at-home measurements to be taken in future studies. Both these systems provide a convenient means for extracting PTT at home, thus allowing for the tracking of BP. More importantly, these devices utilized methods that were physiology-based to improve the estimation of BP over current timing-based methods. In sum, this work established methods that are convenient and robust enough for out-of-clinic monitoring, potentially improving the control of cardiovascular diseases.

5.2 Future Work

Various future research directions could stem from this work. Both the watch and scale include multiple sensors that could be extended to more hemodynamic parameters other than just PTT. For example, SeismoWatch could be used to measure the left ventricular ejection time (LVET) and provide a measurement of cardiac contractility. Additionally, algorithms could be developed to extract a more comprehensive set of features from the various sensors and be used to improve the estimations of BP.

The major limitation of PTT that will need to be addressed in future work is the need for calibration. In our studies, we altered BP and PTT through various intervention and measured the change. By using a clinical BP monitor, we were able to capture continuous BP measurement, allowing for a relatively large amount of data points to develop a reliable calibration curve between PTT and BP. Additionally, the continuous measurement gave us direct feedback of BP during the study to ensure that the interventions were having the desired effect and that we were able to make subtle changes—such as asking the subject to increase effort during exercise. In an unsupervised setting outside the lab, it may be difficult to establish a wide range and large set of BP and PTT values in a convenient manner.

Future work should attempt to reduce the burden of calibration while using the devices developed in this work [107]. One method could be to develop convenient techniques to vary BP and thus PTT. This could be as simple as taking both BP and PTT measurements at different times during the day, ideally over multiple days. BP typically peaks around mid-morning and decreases as the day goes on [107], potentially creating a large enough range to create a calibration curve. To increase the convenience, wearable sensors could indicate optimal times to take a BP and PTT measurements, ensuring a large range of values. Another method is to attempt to only perform single point calibration, and utilize the features from all cardiac sensors to determine the "state" of BP compared to the single measurement (elevated, reduced, etc.). Potentially the most exhaustive method is to eliminate

the need for calibration by assessing the CVD risk factors associated with relative changes in PTT. Thus, by providing changes in PTT values could indicate hemodynamic status to physician. This would be beneficial in scenarios where traditional BP readings are difficult to obtain, such as during sleep. While PTT may not be able to completely replace BP as the gold standard for continuous monitoring, it could potentially complement BP readings and provide a more complete understanding of a patient's cardiovascular health.

REFERENCES

[1] D. Williams and E. Burgess, "34 - hypertension," in *Scientific Foundations of Biochemistry in Clinical Practice (Second Edition)*, D. L. Williams and V. Marks, Eds., Second Edition, Butterworth-Heinemann, 1994, pp. 585 –600, ISBN: 978-0-7506-0167-2.

[2] W. Mercer, "Build and Blood Pressure Study, 1959. Volume 1," *Journal of the American Medical Association*, vol. 172, no. 6, pp. 633–633, Feb. 1960. eprint: https://jamanetwork.com/journals/jama/articlepdf/327575/jama_172_6_033.pdf.

[3] "Age-specific relevance of usual blood pressure to vascular mortality: A meta-analysis of individual data for one million adults in 61 prospective studies," *The Lancet*, vol. 360, no. 9349, pp. 1903 –1913, 2002.

[4] "Report of the joint national committee on detection, evaluation, and treatment of high blood pressure," *JAMA*, vol. 237, no. 3, pp. 255–261, Jan. 1977. eprint: https://jamanetwork.com/journals/jama/articlepdf/350859/jama_237_3_008.pdf.

[5] P. K. Whelton, R. M. Carey, W. S. Aronow, D. E. Casey, K. J. Collins, C. D. Himmelfarb, S. M. DePalma, S. Gidding, K. A. Jamerson, D. W. Jones, E. J. MacLaughlin, P. Muntner, B. Ovbiagele, S. C. Smith, C. C. Spencer, R. S. Stafford, S. J. Taler, R. J. Thomas, K. A. Williams, J. D. Williamson, and J. T. Wright, "2017 acc/aha/aapa/abc/acpm/ags/apha/ash/aspc/nma/pcna guideline for the prevention, detection, evaluation, and management of high blood pressure in adults: Executive summary: A report of the american college of cardiology/american heart association task force on clinical practice guidelines," *Hypertension*, vol. 71, no. 6, pp. 1269–1324, 2018.

[6] X. Guo, X. Zhang, L. Guo, Z. Li, L. Zheng, S. Yu, H. Yang, X. Zhou, X. Zhang, Z. Sun, *et al.*, "Association between pre-hypertension and cardiovascular outcomes: A systematic review and meta-analysis of prospective studies," *Current Hypertension Reports*, vol. 15, no. 6, pp. 703–716, 2013.

[7] A. P. Carson, G. Howard, G. L. Burke, S. Shea, E. B. Levitan, and P. Muntner, "Ethnic differences in hypertension incidence among middle-aged and older adults: The multi-ethnic study of atherosclerosis," *Hypertension*, HYPERTENSIONAHA–110, 2011.

[8] J. Mayet and A. Hughes, "Cardiac and vascular pathophysiology in hypertension," *Heart*, vol. 89, no. 9, pp. 1104–1109, 2003.

[9] R. Ross, "The pathogenesis of atherosclerosis: A perspective for the 1990s," *Nature*, vol. 362, no. 6423, p. 801, 1993.

[10] R. E. Schmieder, "End organ damage in hypertension," *Deutsches Ärzteblatt International*, vol. 107, no. 49, p. 866, 2010.

[11] P Lund-Johansen, *Haemodynamics in essential hypertension*, 1980.

[12] W. J. Elliott and H. R. Black, "Prehypertension," *Nature Clinical Practice.Cardiovascular Medicine*, vol. 4, no. 10, pp. 538–548, Oct. 2007, Copyright - Copyright Nature Publishing Group Oct 2007; Last updated - 2017-06-14.

[13] M. D. Sinha, J. A. Gilg, L. Kerecuk, C. J. Reid, and B. A. for Paediatric Nephrology, "Progression to hypertension in non-hypertensive children following renal transplantation," *Nephrology Dialysis Transplantation*, vol. 27, no. 7, pp. 2990–2996, 2012.

[14] W. H. Organization, *The world health report 2002: reducing risks, promoting healthy life*. World Health Organization, 2002.

[15] G. Parati, S. Mendis, D. Abegunde, R. Asmar, S. Mieke, A. Murray, B. Shengelia, G. Steenvoorden, G. Van Montfrans, and E. O'brien, "Recommendations for blood pressure measuring devices for office/clinic use in low resource settings," *Blood Pressure Monitoring*, vol. 10, no. 1, pp. 3–10, 2005.

[16] P. E. Drawz, M. Abdalla, and M. Rahman, "Blood pressure measurement: Clinic, home, ambulatory, and beyond," *American Journal of Kidney Diseases*, vol. 60, no. 3, pp. 449 –462, 2012.

[17] Y. Imai, T. Ohkubo, M. Kikuya, and J. Hashimoto, "Practical aspect of monitoring hypertension based on self-measured blood pressure at home," *Internal Medicine*, vol. 43, no. 9, pp. 771–778, 2004.

[18] T. Pickering, "Recommendations for the use of home (self) and ambulatory blood pressure monitoring," *American Journal of Hypertension*, vol. 9, no. 1, pp. 1 –11, 1996.

[19] T J Niiranen, A M Jula, I. Kantola, H. Karanko, and A Reunanen, "Home-measured blood pressure is more strongly associated with electrocardiographic left ventricular hypertrophy than is clinic blood pressure: The finn-home study," *Journal of Human Hypertension*, vol. 21, pp. 788–94, Nov. 2007.

[20] H. B. Bosworth, M. K. Olsen, T. Dudley, M. Orr, A. Neary, M. Harrelson, M. Adams, L. P. Svetkey, R. J. Dolor, and E. Z. Oddone, "The take control of your blood pressure (tcyb) study: Study design and methodology," *Contemporary Clinical Trials*, vol. 28, no. 1, pp. 33–47, 2007.

[21] F. P. Cappuccio, S. M. Kerry, L. Forbes, and A. Donald, "Blood pressure control by home monitoring: Meta-analysis of randomised trials," *BMJ*, vol. 329, no. 7458, p. 145, 2004. eprint: `https://www.bmj.com/content/329/7458/145.full.pdf`.

[22] B. H. McGhee and E. J. Bridges, "Monitoring arterial blood pressure: What you may not know," *Critical Care Nurse*, vol. 22, no. 2, pp. 60–79, 2002.

[23] B. B. Green, A. J. Cook, J. D. Ralston, P. A. Fishman, S. L. Catz, J. Carlson, D. Carrell, L. Tyll, E. B. Larson, and R. S. Thompson, "Effectiveness of home blood pressure monitoring, web communication, and pharmacist care on hypertension control: A randomized controlled trial," *JAMA*, vol. 299, no. 24, pp. 2857–2867, 2008.

[24] M. Kikuya, K. Chonan, Y. Imai, E. Goto, M. Ishii, *et al.*, "Accuracy and reliability of wrist-cuff devices for self-measurement of blood pressure," *Journal of Hypertension*, vol. 20, no. 4, pp. 629–638, 2002.

[25] M. Forouzanfar, S. Ahmad, I. Batkin, H. R. Dajani, V. Z. Groza, and M. Bolic, "Coefficient-free blood pressure estimation based on pulse transit time–cuff pressure dependence," *IEEE Transactions on Biomedical Engineering*, vol. 60, no. 7, pp. 1814–1824, 2013.

[26] A. M. Zakrzewski, A. Y. Huang, R. Zubajlo, and B. W. Anthony, "Real-time blood pressure estimation from force-measured ultrasound," *IEEE Transactions on Biomedical Engineering*, vol. 65, no. 11, pp. 2405–2416, 2018.

[27] C. Wang, X. Li, H. Hu, L. Zhang, Z. Huang, M. Lin, Z. Zhang, Z. Yin, B. Huang, H. Gong, *et al.*, "Monitoring of the central blood pressure waveform via a conformal ultrasonic device," *Nature Biomedical Engineering*, vol. 2, no. 9, p. 687, 2018.

[28] R. Mukkamala, J. Hahn, O. T. Inan, L. K. Mestha, C. Kim, H. Toreyin, and S. Kyal, "Toward ubiquitous blood pressure monitoring via pulse transit time: Theory and practice," *IEEE Transactions on Biomedical Engineering*, vol. 62, no. 8, pp. 1879–1901, 2015.

[29] G. Langewouters, K. Wesseling, and W. Goedhard, "The static elastic properties of 45 human thoracic and 20 abdominal aortas in vitro and the parameters of a new model," *Journal of Biomechanics*, vol. 17, no. 6, pp. 425–435, 1984.

[30] D. Hughes, C. F. Babbs, L. Geddes, and J. Bourland, "Measurements of young's modulus of elasticity of the canine aorta with ultrasound," *Ultrasonic Imaging*, vol. 1, no. 4, pp. 356–367, 1979.

[31] A. U. Ferrari, A. Radaelli, and M. Centola, "Invited review: Aging and the cardiovascular system," *Journal of Applied Physiology*, vol. 95, no. 6, pp. 2591–2597, 2003.

[32] R. H. Cox, "Regional variation of series elasticity in canine arterial smooth muscles," *American Journal of Physiology-Heart and Circulatory Physiology*, vol. 234, no. 5, H542–H551, 1978, PMID: 645919.

[33] S. S. Thomas, V. Nathan, C. Zong, E. Akinbola, A. L. P. Aroul, L. Philipose, K. Soundarapandian, X. Shi, and R. Jafari, "Biowatch - a wristwatch based signal acquisition system for physiological signals including blood pressure," in *Engineering in Medicine and Biology Society (EMBC), 2014 36th Annual International Conference of the IEEE*, 2014, pp. 2286–2289.

[34] Y. t. Zhang, C. C. Y. Poon, C. h. Chan, M. W. W. Tsang, and K. f. Wu, "A healthshirt using e-textile materials for the continuous and cuffless monitoring of arterial blood pressure," in *2006 3rd IEEE/EMBS International Summer School on Medical Devices and Biosensors*, 2006, pp. 86–89.

[35] Z. Tang, T. Tamura, M. Sekine, M. Huang, W. Chen, M. Yoshida, K. Sakatani, H. Kobayashi, and S. Kanaya, "A chair-based unobtrusive cuffless blood pressure monitoring system based on pulse arrival time," *IEEE Journal of Biomedical and Health Informatics*, vol. 21, no. 5, pp. 1194–1205, 2017.

[36] A. F. Parisi, B. P. Hamilton, C. N. Thomas, and E. L. Mazzaferri, "The short cardiac pre-ejection period: An index to thyrotoxicosis," *Circulation*, vol. 49, no. 5, pp. 900–904, 1974.

[37] D. B. Newlin and R. W. Levenson, "Pre-ejection period: Measuring beta-adrenergic influences upon the heart," *Psychophysiology*, vol. 16, no. 6, pp. 546–552, 1979.

[38] J Ross Jr and B. Sobel, "Regulation of cardiac contraction," *Annual Review of Physiology*, vol. 34, no. 1, pp. 47–90, 1972.

[39] R. Payne, C. Symeonides, D. Webb, and S. Maxwell, "Pulse transit time measured from the ecg: An unreliable marker of beat-to-beat blood pressure," *Journal of Applied Physiology*, vol. 100, no. 1, pp. 136–141, 2006.

[40] A Eriksson, E Greiff, T Loupas, M Persson, and P Pesque, "Arterial pulse wave velocity with tissue doppler imaging," *Ultrasound in Medicine and Biology*, vol. 28, no. 5, pp. 571 –580, 2002.

[41] B. Jiang, B. Liu, K. L. McNeill, and P. J. Chowienczyk, "Measurement of pulse wave velocity using pulse wave doppler ultrasound: Comparison with arterial tonometry," *Ultrasound in Medicine and Biology*, vol. 34, no. 3, pp. 509 –512, 2008.

[42] P. V. Vaitkevicius, J. L. Fleg, J. H. Engel, F. C. O'connor, J. G. Wright, L. E. Lakatta, F. C. Yin, and E. G. Lakatta, "Effects of age and aerobic capacity on arterial stiffness in healthy adults.," *Circulation*, vol. 88, no. 4, pp. 1456–1462, 1993.

[43] T. Tamura, Y. Maeda, M. Sekine, and M. Yoshida, "Wearable photoplethysmographic sensors–past and present," *Electronics*, vol. 3, no. 2, pp. 282–302, 2014.

[44] Y. Zheng, T. C. H. Wong, B. H. K. Leung, and C. C. Y. Poon, "Unobtrusive and multimodal wearable sensing to quantify anxiety," *IEEE Sensors Journal*, vol. 16, no. 10, pp. 3689–3696, 2016.

[45] K. Lydon, B. Y. Su, L. Rosales, M. Enayati, K Ho, M. Rantz, and M. Skubic, "Robust heartbeat detection from in-home ballistocardiogram signals of older adults using a bed sensor," Aug. 2015.

[46] M. D. Rienzo, P. Meriggi, F. Rizzo, E. Vaini, A. Faini, G. Merati, G. Parati, and P. Castiglioni, "A wearable system for the seismocardiogram assessment in daily life conditions," in *2011 Annual International Conference of the IEEE Engineering in Medicine and Biology Society*, 2011, pp. 4263–4266.

[47] M. Elgendi, "On the analysis of fingertip photoplethysmogram signals," *Current Cardiology Reviews*, vol. 8, no. 1, pp. 14–25, 2012.

[48] A. Visvanathan, A. Sinha, and A. Pal, "Estimation of blood pressure levels from reflective photoplethysmograph using smart phones," in *13th IEEE International Conference on BioInformatics and BioEngineering*, 2013, pp. 1–5.

[49] X. Xing and M. Sun, "Optical blood pressure estimation with photoplethysmography and fft-based neural networks," *Biomedical optics express*, vol. 7, no. 8, pp. 3007–3020, 2016.

[50] G. Natalini, A. Rosano, M. E Franceschetti, P. Facchetti, and A. Bernardini, "Variations in arterial blood pressure and photoplethysmography during mechanical ventilation," *Anesthesia and Analgesia*, vol. 103, pp. 1182–8, Nov. 2006.

[51] J. Allen, "Photoplethysmography and its application in clinical physiological measurement," *Physiological measurement*, vol. 28, no. 3, R1, 2007.

[52] Y. Maeda, M. Sekine, and T. Tamura, "Relationship between measurement site and motion artifacts in wearable reflected photoplethysmography," *Journal of Medical Systems*, vol. 35, no. 5, pp. 969–976, 2011.

[53] J. Lee, K. Matsumura, K.-i. Yamakoshi, P. Rolfe, S. Tanaka, and T. Yamakoshi, "Comparison between red, green and blue light reflection photoplethysmography for heart rate monitoring during motion," in *Engineering in Medicine and Biology Society (EMBC), 2013 35th Annual International Conference of the IEEE*, IEEE, 2013, pp. 1724–1727.

[54] J. Gordon, "Certain molar movements of the human body produced by the circulation of the blood," *Journal of Anatomy and Physiology*, vol. 11, no. Pt 3, p. 533, 1877.

[55] L. Giovangrandi, O. T. Inan, R. M. Wiard, M. Etemadi, and G. T. A. Kovacs, "Ballistocardiography - a method worth revisiting," in *2011 Annual International Conference of the IEEE Engineering in Medicine and Biology Society*, 2011, pp. 4279–4282.

[56] C.-S. Kim, S. L. Ober, M. S. McMurtry, B. A. Finegan, O. T. Inan, R. Mukkamala, and J.-O. Hahn, "Ballistocardiogram, mechanism and potential for unobtrusive cardiovascular health monitoring," *Scientific Reports*, vol. 6, p. 31 297, 2016.

[57] O. T. Inan, P.-F. Migeotte, K.-S. Park, M. Etemadi, K. Tavakolian, R. Casanella, J. M. Zanetti, J. Tank, I. Funtova, G. K. Prisk, *et al.*, "Ballistocardiography and seismocardiography: A review of recent advances.," *IEEE J. Biomedical and Health Informatics*, vol. 19, no. 4, pp. 1414–1427, 2015.

[58] H. J. Baek, G. S. Chung, K. K. Kim, and K. S. Park, "A smart health monitoring chair for nonintrusive measurement of biological signals," *IEEE Transactions on Information Technology in Biomedicine*, vol. 16, no. 1, pp. 150–158, 2012.

[59] C. Bruser, K. Stadlthanner, S. de Waele, and S. Leonhardt, "Adaptive beat-to-beat heart rate estimation in ballistocardiograms," *IEEE Transactions on Information Technology in Biomedicine*, vol. 15, no. 5, pp. 778–786, 2011.

[60] A. D. Wiens and O. T. Inan, "A novel system identification technique for improved wearable hemodynamics assessment," *IEEE Transactions on Biomedical Engineering*, vol. 62, no. 5, pp. 1345–1354, 2015.

[61] R. M. Rangayyan and R. J. Lehner, "Phonocardiogram signal analysis, a review," *Critical Reviews in Biomedical Engineering*, vol. 15, no. 3, pp. 211–236, 1987.

[62] J. M. Zanetti and K. Tavakolian, "Seismocardiography, past, present and future," in *Engineering in Medicine and Biology Society (EMBC), 2013 35th Annual International Conference of the IEEE*, IEEE, 2013, pp. 7004–7007.

[63] J. M. Zanetti and D. M. Salerno, "Seismocardiography: A technique for recording precordial acceleration," in *Computer-Based Medical Systems-Proceedings of the Fourth Annual IEEE Symposium*, IEEE, 1991, pp. 4–9.

[64] Y. Chuo, M. Marzencki, B. Hung, C. Jaggernauth, K. Tavakolian, P. Lin, and B. Kaminska, "Mechanically flexible wireless multisensor platform for human physical activity and vitals monitoring," *Biomedical Circuits and Systems, IEEE Transactions on*, vol. 4, pp. 281 –294, Nov. 2010.

[65] H. Ashouri and O. T. Inan, "Automatic detection of seismocardiogram sensor misplacement for robust pre-ejection period estimation in unsupervised settings," *IEEE Sensors Journal*, vol. 17, no. 12, pp. 3805–3813, 2017.

[66] R. Patterson, "Fundamentals of impedance cardiography," *IEEE Engineering in Medicine and Biology Magazine*, vol. 8, no. 1, pp. 35–38, 1989.

[67] A. Sherwood, M. T. Allen, J. Fahrenberg, R. M. Kelsey, W. R. Lovallo, and L. J. Van Doornen, "Methodological guidelines for impedance cardiography," *Psychophysiology*, vol. 27, no. 1, pp. 1–23, 1990.

[68] M. Ulbrich, J. Mhlsteff, A. Sipil, M. Kamppi, A. Koskela, M. Myry, T. Wan, S. Leonhardt, and M. Walter, "The IMPACT shirt: Textile integrated and portable impedance cardiography," *Physiological Measurement*, vol. 35, no. 6, pp. 1181–1196, 2014.

[69] R. González-Landaeta, O. Casas, and R. Pallàs-Areny, "Heart rate detection from plantar bioimpedance measurements," *IEEE Transactions on Biomedical Engineering*, vol. 55, no. 3, pp. 1163–1167, 2008.

[70] J. Gomez-Clapers, R. Casanella, and R. Pallas-Areny, "A novel method to obtain proximal plethysmographic information from distal measurements using the impedance plethysmogram," *Journal of Electrical Bioimpedance*, vol. 6, no. 1, pp. 44–48, 2015.

[71] T. H. Huynh, R. Jafari, and W.-Y. Chung, "Noninvasive cuffless blood pressure estimation using pulse transit time and impedance plethysmography," *IEEE Transactions on Biomedical Engineering*, 2018.

[72] L. Critchley, "Impedance cardiographythe impact of new technology," *Anaesthesia*, vol. 53, no. 7, pp. 677–684, 1998.

[73] D. M. Steinberg, D. F. Tate, G. G. Bennett, S. Ennett, C. Samuel-Hodge, and D. S. Ward, "The efficacy of a daily self-weighing weight loss intervention using smart scales and e-mail," *Obesity*, vol. 21, no. 9, pp. 1789–1797, 2013.

[74] K. Dickstein, A. F. Members, A. Cohen-Solal, G. Filippatos, J. J. McMurray, P. Ponikowski, P. A. Poole-Wilson, A. Strmberg, D. J. van Veldhuisen, D. Atar, A. W. Hoes, A. Keren, A. Mebazaa, M. Nieminen, S. G. Priori, K. Swedberg, A. Vahanian, E. C. for Practice Guidelines (CPG), J. Camm, R. De Caterina, V. Dean, K. Dickstein, G. Filippatos, C. Funck-Brentano, I. Hellemans, S. D. Kristensen, K. McGregor, U. Sechtem, S. Silber, M. Tendera, P. Widimsky, J. L. Zamorano, M. Tendera, D. Reviewers, A. Auricchio, J. Bax, M. Bhm, U. Corr, P. della Bella, P. M. Elliott, F. Follath, M. Gheorghiade, Y. Hasin, A. Hernborg, T. Jaarsma, M. Komajda, R. Kornowski, M. Piepoli, B. Prendergast, L. Tavazzi, J.-L. Vachiery, F. W. A. Verheugt, J. L. Zamorano, and F. Zannad, "Esc guidelines for the diagnosis and treatment of acute and chronic heart failure 2008," *European Journal of Heart Failure*, vol. 10, no. 10, pp. 933–989, 2008.

[75] O. Inan, M Etemadi, A Paloma, L Giovangrandi, and G. Kovacs, "Non-invasive cardiac output trending during exercise recovery on a bathroom-scale-based ballistocardiograph," *Physiological Measurement*, vol. 30, no. 3, p. 261, 2009.

[76] A. Lindqvist, K Pihlajamäki, J Jalonen, V Laaksonen, and J Alihanka, "Static-charge-sensitive bed ballistocardiography in cardiovascular monitoring," *Clinical Physiology*, vol. 16, no. 1, pp. 23–30, 1996.

[77] M. Etemadi, O. T. Inan, L. Giovangrandi, and G. T. A. Kovacs, "Rapid assessment of cardiac contractility on a home bathroom scale," *IEEE Transactions on Information Technology in Biomedicine*, vol. 15, no. 6, pp. 864–869, 2011.

[78] N. Gaddum, J Alastruey, P Beerbaum, P Chowienczyk, and T Schaeffter, "A technical assessment of pulse wave velocity algorithms applied to non-invasive arterial waveforms," *Annals of Biomedical Engineering*, vol. 41, no. 12, pp. 2617–2629, 2013.

[79] P. A. Obrist, K. C. Light, J. A. McCubbin, J. S. Hutcheson, and J. L. Hoffer, "Pulse transit time: Relationship to blood pressure and myocardial performance," *Psychophysiology*, vol. 16, no. 3, pp. 292–301, 1979.

[80] G. V. Marie, C. Lo, J Van Jones, and D. W. Johnston, "The relationship between arterial blood pressure and pulse transit time during dynamic and static exercise," *Psychophysiology*, vol. 21, no. 5, pp. 521–527, 1984.

[81] J. D. Lane, L. Greenstadt, D. Shapiro, and E. Rubinstein, "Pulse transit time and blood pressure: An intensive analysis," *Psychophysiology*, vol. 20, no. 1, pp. 45–49, 1983.

[82] L. M. Van Bortel, S. Laurent, P. Boutouyrie, P. Chowienczyk, J. Cruickshank, T. De Backer, J. Filipovsky, S. Huybrechts, F. U. Mattace-Raso, A. D. Protogerou, *et al.*, "Expert consensus document on the measurement of aortic stiffness in daily prac-

tice using carotid-femoral pulse wave velocity," *Journal of Hypertension*, vol. 30, no. 3, pp. 445–448, 2012.

[83] B. Paliakaitė, S. Daukantas, A. Sakalauskas, and V. Marozas, "Estimation of pulse arrival time using impedance plethysmogram from body composition scales," in *Sensors Applications Symposium (SAS), 2015 IEEE*, IEEE, 2015, pp. 1–4.

[84] A. Grabovskis, Z. Marcinkevics, U. Rubins, and E. Kviesis-Kipge, "Effect of probe contact pressure on the photoplethysmographic assessment of conduit artery stiffness," *Journal of Biomedical Optics*, vol. 18, no. 2, p. 027 004, 2013.

[85] B. A. Fallow, T. Tarumi, and H. Tanaka, "Influence of skin type and wavelength on light wave reflectance," *Journal of Clinical Monitoring and Computing*, vol. 27, no. 3, pp. 313–317, 2013.

[86] A. Johansson, C Ahlstrom, T Lanne, and P. Ask, "Pulse wave transit time for monitoring respiration rate," *Medical and Biological Engineering and Computing*, vol. 44, no. 6, pp. 471–478, 2006.

[87] R. P. Smith, D. Veale, J.-L. Pépin, and P. A. Lévy, "Obstructive sleep apnoea and the autonomic nervous system," *Sleep Medicine Reviews*, vol. 2, no. 2, pp. 69–92, 1998.

[88] M. J. Drinnan, J. Allen, and A. Murray, "Relation between heart rate and pulse transit time during paced respiration," *Physiological Measurement*, vol. 22, no. 3, p. 425, 2001.

[89] T Ma and Y.-T. Zhang, "A correlation study on the variabilities in pulse transit time, blood pressure, and heart rate recorded simultaneously from healthy subjects," in *2005 IEEE Engineering in Medicine and Biology 27th Annual Conference*, IEEE, 2006, pp. 996–999.

[90] D. Pitson, A Sandell, R Van den Hout, *et al.*, "Use of pulse transit time as a measure of inspiratory effort in patients with obstructive sleep apnoea," *European Respiratory Journal*, vol. 8, no. 10, pp. 1669–1674, 1995.

[91] M. Al'Absi, S. Bongard, T. Buchanan, G. A. Pincomb, J. Licinio, and W. R. Lovallo, "Cardiovascular and neuroendocrine adjustment to public speaking and mental arithmetic stressors," *Psychophysiology*, vol. 34, no. 3, pp. 266–275, 1997.

[92] E. A. Hines and G. E. Brown, "The cold pressor test for measuring the reactibility of the blood pressure: Data concerning 571 normal and hypertensive subjects," *American Heart Journal*, vol. 11, no. 1, pp. 1–9, 1936.

[93] O. T. Inan, G. T. A. Kovacs, and L. Giovangrandi, "Evaluating the lower-body electromyogram signal acquired from the feet as a noise reference for standing ballistocardiogram measurements," *IEEE Transactions on Information Technology in Biomedicine*, vol. 14, no. 5, pp. 1188–1196, 2010.

[94] S. Laurent, J. Cockcroft, L. Van Bortel, P. Boutouyrie, C. Giannattasio, D. Hayoz, B. Pannier, C. Vlachopoulos, I. Wilkinson, and H. Struijker-Boudier, "Expert consensus document on arterial stiffness: Methodological issues and clinical applications," *European Heart Journal*, vol. 27, no. 21, pp. 2588–2605, 2006.

[95] T. Sugiura and E. D. Freis, "Pressure pulse in small arteries," *Circulation Research*, vol. 11, no. 5, pp. 838–842, 1962.

[96] C. S. Roy and J. G. Brown, "The blood-pressure and its variations in the arterioles, capillaries and smaller veins," *The Journal of Physiology*, vol. 2, no. 5-6, pp. 323–446, 1880.

[97] L. Yan, S. Hu, A. Alzahrani, S. Alharbi, and P. Blanos, "A multi-wavelength optoelectronic patch sensor to effectively detect physiological changes against human skin types," *Biosensors*, vol. 7, no. 2, p. 22, 2017.

[98] F. W. Tsai, N. Tulsyan, D. N. Jones, N. Abdel-Al, J. J. Castronuovo Jr, and S. A. Carter, "Skin perfusion pressure of the foot is a good substitute for toe pressure in the assessment of limb ischemia," *Journal of Vascular Surgery*, vol. 32, no. 1, pp. 32–36, 2000.

[99] P. R. Cavanagh, M. M. Rodgers, and A. liboshi, "Pressure distribution under symptom-free feet during barefoot standing," *Foot & Ankle*, vol. 7, no. 5, pp. 262–278, 1987, PMID: 3583160.

[100] A. M. Carek, J. Conant, A. Joshi, H. Kang, and O. T. Inan, "Seismowatch: Wearable cuffless blood pressure monitoring using pulse transit time," *Proc. ACM Interact. Mob. Wearable Ubiquitous Technol.*, vol. 1, no. 3, 40:1–40:16, Sep. 2017.

[101] P. Castiglioni, A. Faini, G. Parati, and M. Di Rienzo, "Wearable seismocardiography," in *Engineering in Medicine and Biology Society 29th Annual International Conference*, IEEE, 2007, pp. 3954–3957.

[102] F. Khosrow-Khavar, K. Tavakolian, A. P. Blaber, J. M. Zanetti, R. Fazel-Rezai, and C. Menon, "Automatic annotation of seismocardiogram with high-frequency precordial accelerations," *IEEE Journal of Biomedical and Health Informatics*, vol. 19, no. 4, pp. 1428–1434, 2015.

[103] A. Maiorana, G. O'Driscoll, R. Taylor, and D. Green, "Exercise and the nitric oxide vasodilator system," *Sports Medicine*, vol. 33, no. 14, pp. 1013–1035, 2003.

[104] T. G. Pickering, J. E. Hall, L. J. Appel, B. E. Falkner, J. Graves, M. N. Hill, D. W. Jones, T. Kurtz, S. G. Sheps, and E. J. Roccella, "Recommendations for blood pressure measurement in humans and experimental animals," *Circulation*, vol. 111, no. 5, pp. 697–716, 2005.

[105] G. G. Berntson, J. T. Bigger, D. L. Eckberg, P. Grossman, P. G. Kaufmann, M. Malik, H. N. Nagaraja, S. W. Porges, J. P. Saul, P. H. Stone, *et al.*, "Heart rate variability: Origins, methods, and interpretive caveats," *Psychophysiology*, vol. 34, no. 6, pp. 623–648, 1997.

[106] M. M. H. Shandhi, B. Semiz, S. Hersek, N. Goller, F. Ayazi, and O. T. Inan, "Performance analysis of gyroscope and accelerometer sensors for seismocardiography-based wearable pre-ejection period estimation," *IEEE Journal of Biomedical and Health Informatics*, pp. 1–1, 2019.

[107] M. Millar-Craig, C. Bishop, and E. Raftery, "Circadian variation of blood-pressure," *The Lancet*, vol. 311, no. 8068, pp. 795–797, 1978.